



UDESC

**SANTA CATARINA STATE UNIVERSITY - UDESC
COLLEGE OF TECHNOLOGICAL SCIENCE - CCT
MASTER IN MECHANICAL ENGINEERING - PPGEM**

MASTER THESIS

**ON THE USE OF FRACTIONAL DERIVATIVES
FOR MODELING NONLINEAR VISCOELASTICITY**

THAIS CLARA DA COSTA HAVEROTH

JOINVILLE, 2015

THAIS CLARA DA COSTA HAVEROTH

**ON THE USE OF FRACTIONAL DERIVATIVES FOR
MODELING NONLINEAR VISCOELASTICITY**

Master thesis presented to the Mechanical Engineering Department at the College of Technological Science of the Santa Catarina State University, in fulfillment of the partial requirement for the degree of Master in Mechanical Engineering.

Advisor:

Prof. Dr. Pablo Andrés Muñoz Rojas

Co-advisor:

Prof. Dr. Fernando Deeke Sasse

**JOINVILLE, SC
2015**

H387o

Haveroth, Thais Clara da Costa

On the use o fractional derivatives for modeling nonlinear viscoelasticity/ Thais Clara da Costa Haveroth. – 2015.

145 p. : il. ; 21cm

Advisor: Pablo Andrés Muñoz Rojas

Co-advisor: Fernando Deeke Sasse

Bibliography: p. 115-124

Masther thesis (master) - Santa Catarina State University, College o Technological Science, Post Graduation Program in Mechanical Engineering, Joinville, 2015.

1. Viscoelasticity 2. Fractional derivatives. 3. Time-stress equivalence principle. 4. Modified superposition principle. 5. HDPE. I. Rojas, Pablo Andrés Muñoz-Rojas. II. Sasse, Fernando Deeke. III. Santa Catarina State University. Post Graduation Program in Mechanical Engineering. IV. On the use o fractional derivatives or modeling nonlinear viscoelasticity.

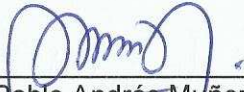
CDD 620.1 – 23. ed.

THAIS CLARA DA COSTA HAVEROTH
SOBRE O USO DE DERIVADAS FRACIONÁRIAS PARA
MODELAMENTO DE VISCOELASTICIDADE NÃO-LINEAR

Dissertação apresentada ao Curso de Mestrado Acadêmico em Engenharia Mecânica como requisito parcial para obtenção do título de Mestre em Engenharia Mecânica na área de concentração "Modelagem e Simulação Numérica".

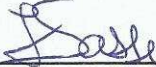
Banca Examinadora

Orientador:



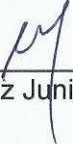
Prof. Dr. Pablo Andrés Muñoz Rojas
CCT/UESC

Coorientador:

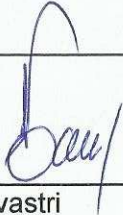


Prof. Dr. Fernando Deeke Sasse
CCT/UESC

Membros



Prof. Dr. Miguel Vaz Junior
CCT/UESC



Prof. Dr. Carlos Alberto Bavastri
UFPR



Prof. Dr. Paulo de Tarso Rocha de Mendonça
UFSC

Joinville, SC, 26 de outubro de 2015.

This is for you, Geovane.

Thanks for the encouragement and endless support.

ACKNOWLEDGEMENTS

I would like to extend my deepest gratitude to the following persons who in one way or another have contributed in making this study possible.

I wish to thank my advisor, Dr. Pablo Andrés Muños Rojas, for the support and guidance throughout this project. I am also grateful to my co-advisor Dr. Fernando Deeke Sasse for his assistance and encouragement.

To all my professors who has been a constant source of knowledge and inspiration.

To the Mechanical Engineering Department of the Santa Catarina State University for the opportunity to carry through this research.

To UDESC/PROMOP for the concession of a Master's scholarship.

To my husband Geovane for his continued and unflinching love and comforting words that accompanied my growth both academic and personal.

To my parents Leori and Vanir, whose dedication allowed my comprehension that true success is built upon determination and that learning has a value which can not be measured.

Thank you everyone!

RESUMO

Dentre a vasta gama de polímeros estruturais atualmente disponíveis no mercado, este trabalho está particularmente voltado ao estudo do polietileno de alta densidade. Embora este material já tenha sido investigado por diversos autores, seu típico comportamento viscoelástico não-linear apresenta dificuldades na modelagem. Visando uma nova contribuição, este trabalho propõe a descrição de tal comportamento utilizando uma abordagem baseada em derivadas fracionárias. Esta formulação produz equações constitutivas fracionais que resultam em boas propriedades de ajuste de curvas com menos parâmetros a serem identificados que nos métodos tradicionais. Neste sentido, os resultados experimentais de fluência para o polietileno de alta densidade, avaliados em diferentes níveis de tensão, são ajustados por este esquema. Para estimar a deformação à níveis de tensão que não tenham sido medidos experimentalmente, o princípio da equivalência tensão-tempo é utilizado e os resultados são comparados com aqueles apresentados por uma interpolação linear dos parâmetros. Além disso, o princípio da superposição modificado é aplicado para prever o comportamento de materiais sujeitos a níveis de tensão que mudam abruptamente ao longo do tempo. Embora a abordagem fracionária simplifique o problema de otimização inversa subjacente, é observado um grande aumento no esforço computacional. Assim, alguns algoritmos que objetivam economia computacional, são estudados. Conclui-se que, quando a acurácia é necessária ou quando um modelo de séries Prony requer um número muito grande de parâmetros, a abordagem fracionária pode ser uma opção interessante.

Palavras-chave: Viscoelasticidade. Derivadas fracionárias. Princípio da equivalência tensão-tempo. Princípio da superposição modificada. PEAD.

ABSTRACT

Among the wide range of structural polymers currently available in the market, this work is concerned particularly with high density polyethylene. The typical nonlinear viscoelastic behavior presented by this material is not trivial to model, and has already been investigated by many authors in the past. Aiming at a further contribution, this work proposes modeling this material behavior using an approach based on fractional derivatives. This formulation produces fractional constitutive equations that result in good curve-fitting properties with less parameters to be identified when compared to traditional methods. In this regard, experimental creep results of high density polyethylene evaluated at different stress levels are fitted by this scheme. To estimate creep at stress levels that have not been measured experimentally, the time-stress equivalence principle is used and the results are compared with those presented by a linear interpolation of the parameters. Furthermore, the modified superposition principle is applied to predict the strain for materials subject to stress levels which change abruptly from time to time. Some comparative results are presented showing that the fractional approach proposed in this work leads to better results in relation to traditional formulations described in the literature. Although the fractional approach simplifies the underlying inverse optimization problem, a major increase in computational effort is observed. Hence, some algorithms that show computational cost reduction, are studied. It is concluded that when high accuracy is mandatory or when a Prony series model requires a very large number of parameters, the fractional approach may be an interesting option.

Key-words: Viscoelasticity. Fractional derivatives. Time-stress equivalence principle. Modified superposition principle. HDPE.

LIST OF FIGURES

Figure 1	– HDPE pipelines installation in storm drain project in Mexico.	31
Figure 2	– GL coefficients for $\alpha = 0.1$	45
Figure 3	– Time line representing the G1 algorithm. The red range is the whole fractional derivatives history.	45
Figure 4	– Time line illustrating the P2 algorithm. The red range is the calculated history and the black one is the disregarded history.	47
Figure 5	– Time line representing the SG algorithm.	48
Figure 6	– Strain and stress behavior in the creep-compliance phenomenon.	53
Figure 7	– Stress and strain behavior in the stress relaxation phenomenon.	54
Figure 8	– Representation of the spring.	55
Figure 9	– Representation of the dashpot.	55
Figure 10	– Traditional rheological models of viscoelasticity: Maxwell, Kelvin and the two equivalent representations of the Zener model.	56
Figure 11	– Generalized Kelvin model.	57
Figure 12	– Generalized Maxwell model.	57
Figure 13	– Representation of the fractional element.	61
Figure 14	– Fractional rheological models of viscoelasticity: Maxwell, Kelvin and the two equivalent representations of the Zener model.	62
Figure 15	– Zener fractional model used to deriving the fractional constitutive relationship strain-stress in this work.	63
Figure 16	– Example of an unsuccessful material parameter interpolation.	68
Figure 17	– TSEP master curve formation for the horizontal shift ϕ_σ . In this example, σ_1 is the reference stress level.	72

Figure 18 – Two-step loading effect.	74
Figure 19 – Experimental data obtained from Liu’s work.	79
Figure 20 – Sample used in Kühl’s experimental procedure: (a) Extraction; (b) Sample of HDPE PE80 extracted from water transport pipes.	80
Figure 21 – Experimental data obtained by Kühl (2014).	80
Figure 22 – PSO behavior after n iterations in a three-dimensional space.	83
Figure 23 – PSO updating of the best positions towards to the optimum value in a three-dimensional space.	86
Figure 24 – Fractional fitting obtained for Liu’s experimental data in Case 1 (a) and in Case 2 (b).	90
Figure 25 – Fractional Zener and generalized Kelvin fittings for Kühl’s experimental data.	93
Figure 26 – Linear interpolation approach for Liu’s experimen- tal data: (a) 5.97 MPa; (b) 7.71 MPa; (c) 10.31 MPa.	96
Figure 27 – Linear interpolation approach for Kühl’s experi- mental data: (a) 5.5 MPa; (b) 7.2 MPa; (c) 9.1 MPa; (d) 11 MPa.	97
Figure 28 – Master curve fitting in the TSEP for Liu’s data: (a) log-log scale; (b) linear scale.	99
Figure 29 – Fitting of the shifts values for Liu’s data: (a) hor- izontal shift (ϕ_σ); (b) vertical shift (δ_σ).	99
Figure 30 – TSEP results for Liu’s experimental data.	101
Figure 31 – Master curve fitting in the TSEP for Kühl’s data: (a) log-log scale; (b) linear scale.	102
Figure 32 – Fitting of the shifts values for Kühl’s data.	102
Figure 33 – TSEP results for Kühl’s’s experimental data.	103
Figure 34 – Increasing two-step loading: (a) changing from 5.25 to 8.31 MPa at $t_1 \approx 16000$ s; (b) changing from 5.33 to 10.55 MPa at $t_1 \approx 18000$ s. Decreas- ing two-step loading: (c) changing from 10.59 to 5.35 MPa at $t_1 \approx 17000$ s; (d) changing from 8.36 to 5.29 MPa at $t_1 \approx 13000$ s.	105

Figure 35 – (a) Application of P2 algorithm in contrast with the G1 algorithm for some values of N_{\max} ; (b) Emphasis on the interest region X.	106
Figure 36 – ℓ^2 norm of the relative error for P2 algorithm in contrast with the CPU time: (a) linear scale; (b) logarithm scale.	107
Figure 37 – Ratio (Δ time/ Δ error) of P2 algorithm in relation to the truncation value.	108
Figure 38 – (a) Application of the SG algorithm in contrast with the G1 algorithm for some values of $i = k$; (b) Emphasis on the interest region X.	109
Figure 39 – ℓ_2 norm of the relative error for SG algorithm in contrast with the CPU time: (a) linear scale; (b) logarithm scale.	109
Figure 40 – Ratio (Δ time/ Δ error) of SG algorithm in relation to the parameters $i = k$	110
Figure 41 – Gamma function, $\Gamma(x)$	127
Figure 42 – Ratio $R_{f_r}, r = 2, \dots, 5$ in comparison with R_1 according to Eq. (2.24).	130
Figure 43 – Transfer function T_n in relation to the Eqs. (2.25) and (2.23).	131
Figure 44 – Relative error in T_n given by Eq. (2.25) and the actual T_n given by Eq. (2.23).	132
Figure 45 – Rods of polyoxymethylene (POM), also known as polyacetal.	133
Figure 46 – Schematized polyacetal rod.	133
Figure 47 – Fractional viscoelastic model for polyacetal: two fractional Maxwell models and a spring in parallel.	134
Figure 48 – Discretized viscoelastic rod.	136
Figure 49 – Evaluation of the $S_{m\varepsilon}$ and $S_{m\sigma}$. The actual time calculation uses the overall variable history.	138
Figure 50 – Displacement in the node $i = 30$ for the polyacetal rod.	143
Figure 51 – Strain in the node $i = 30$ for the polyacetal rod.	143

Figure 52 – Stress in the node $i = 30$ for the polyacetal rod. . 144
Figure 53 – Displacement in the node $i = 30$ for an instantaneous initial load. 144

LIST OF TABLES

Table 1	– Identified Prony series parameters by Liu, Polak and Penlidis (2008).	78
Table 2	– Identified Prony series parameters by Kühl (2014).	81
Table 3	– Identified fractional parameters for Liu’s experimental data (Case 1).	90
Table 4	– Identified fractional parameters for Liu’s experimental data (Case 2).	91
Table 5	– ℓ^2 norm of the relative error between the experimental strains and the fractional fitting in Case 1 and 2.	91
Table 6	– Identified fractional parameters obtained for Kühl’s experimental data (Case 1).	92
Table 7	– ℓ^2 norm of the relative error between the experimental strains and both, the fractional fitting and the Prony series fitting.	94
Table 8	– Identified fractional parameters to model the polyacetal rod.	141

LIST OF SYMBOLS

General Symbols:

A	Material constant in the Doolittle's equation
A_{m+1}	Grünwald-Letnikov coefficient for $m + 1$
\mathbf{a}	Optimum solution for the particle swarm optimization method
a	Material constant in the fractional derivative
B	Material constant in the Doolittle's equation
\mathbf{b}	Fractional parameters vector
b_i	Fractional derivative parameter in the position i
b^{\min}	Inferior limiting in the minimization procedure
b^{\max}	Superior limiting in the minimization procedure
C_1, C_2, C_3	Material constants in the time-stress equivalence principle
c_1, c_2	Material constants in the fractional derivative
D_1, D_2	Material constants in the time-stress equivalence principle
E	Spring stiffness constant
E_i	Spring stiffness constant for the i -th rheological block

f	Free volume fraction
f_0	Free volume fraction in the reference state
G	Relaxation function
g	Best know position of the entire swarm (particle swarm optimization method)
i	Factor considered in the algorithm SG
J	Creep-compliance function
\tilde{J}	Master curve creep
J_{Prony}	Creep-compliance in the Prony series formulation
J^φ	Time independent component for creep
J^χ	Time dependent component for creep
k	Factor considered in the algorithm SG
l	Counter in the Prony series
m	Counter in the fractional derivative definition
\mathbb{N}	Set of natural numbers
N	Number of divisions in the time interval
N_{max}	Truncation value for the G1 algorithm
\tilde{N}	Number of stress changes in the Modified Superposition Principle
n_g	Number of generations (particle swarm optimization method)

n_p	Number of particles in the swarm (particle swarm optimization method)
$npts$	Number of sampled experimental points in the optimization procedure
\mathbf{p}_i	Best know position for the i -th particle
p	Proportionality fractional constant in the fractional derivative
q	Number of rheological blocks in the Kelvin (or Maxwell) model
\mathbb{R}	Set of real numbers
\mathbb{R}^n	Real coordinate space of n dimensions
R_f	Ratio considered in the SG algorithm to interpolate the time in the function f
r	Minimum value between N and N_{\max}
S_A	Summation in the fractional derivative for the GL coefficients
S_J	Summation in the fractional derivative for the creep-compliance
S_ε	Summation in the fractional derivative for strain
S_σ	Summation in the fractional derivative for stress
s	Constant in the Laplace transform
T	Temperature

T_0	Reference temperature in the time-stress equivalence principle
T_n	Transfer function for n
T_n^1	Transfer function for n evaluated in $f(t) = 1$
T_∞	Transfer function in the limiting value
T_∞^1	Transfer function in the limiting value evaluated in $f(t) = 1$
t	Time
t_1	Inferior limit in the derivation interval
t_2	Superior limit in the derivation interval
t_a	Actual time in the SG algorithm
t_c	Truncation time in the P2 algorithm
t_I	Time for the SG algorithm
t_i	Arbitrary time value in the interval $[t_1, t_2]$
V	Search space for the velocity in the particle swarm optimization problem
V	Total volume in the time-equivalence principle
V_f	Free volume in the time-equivalence principle
v_i	Velocity of the i -th particle in the particle swarm optimization method

X	Search space for the optimum point in the particle swarm optimization method
\mathbf{x}_i	Position of the i -th particle in the particle swarm optimization method
\mathbb{Z}_-^*	Set of negative integers numbers
α	Fractional order of the derivative operator
γ_T	Thermal expansion coefficient
γ_σ	Stress expansion coefficient
Δt	Time-step increment
δ_σ	Vertical shift factor
ε	Strain
ε_c	Constant strain
ε_{exp}	Experimental strain
ε_{Prony}	Strain in the Prony series formulation
ε_s	Spring strain
ε_{sp}	Spring-pot strain
η	Viscosity constant
ξ	Reduced time in the time-stress equivalence principle
ρ	Density
σ	Stress
σ_0	Reference stress level in the time-stress equivalence principle

σ_c	Constant stress
τ	Relaxation time in the Prony series
ϕ_σ	Horizontal shift factor for σ
$\phi_{T,\sigma}$	Temperature-stress shift factor
ϕ_σ^T	Shift factor at constant temperature
ϕ_σ^T	Shift factor at constant stress
φ_p	Constant in the PSO method
φ_g	Constant in the PSO method
ω	Constant in the PSO method
ℓ	Length
ℓ^2	Norm

Operators and Functions:

$\frac{d^n}{dx^n}(\cdot)$	Derivative operator of order n
${}_{t_1}D_{t_2}^\alpha(\cdot)$	Derivative operator of order α in the interval $[t_1, t_2]$
${}_0D_{t_2}^\alpha(\cdot), D^\alpha(\cdot)$	Derivative operator of α order in the interval $[0, t_2]$
$\Gamma(\cdot)$	Gamma function
$\mathcal{L}\{\cdot\}$	Laplace Transform

LIST OF ACRONYMS AND ALGORITHMS

Acronyms:

TSEP Time-stress equivalence principle

MSP Modified superposition principle

GL Grünwald-Letnikov

Algorithms:

G1 Referential algorithm of fractional derivation

P2 Algorithm of fractional derivation with truncation time

SG Algorithm of fractional derivation with interpolated time

CONTENTS

1	INTRODUCTION	31
1.1	Objectives	33
1.2	Outline of the Thesis	34
2	FRACTIONAL DERIVATIVES	37
2.1	BRIEF HISTORICAL OVERVIEW	37
2.2	GRÜNWALD-LETNIKOV DERIVATIVES	39
2.2.1	Definition of Grünwald-Letnikov	39
2.2.2	Numerical Grünwald-Letnikov Fractional Derivatives	42
3	VISCOELASTICITY	51
3.1	VISCOELASTIC BEHAVIOR	51
3.1.1	Creep-Compliance	52
3.1.2	Stress Relaxation	53
3.2	TRADITIONAL VISCOELASTIC MODEL- ING	54
3.2.1	Generalized Chains	56
3.2.2	Prony Series Formulation	58
3.3	FRACTIONAL VISCOELASTIC MODELING	59
3.3.1	Fractional Zener model	61
3.3.2	Grünwald-Letnikov Definition for the Zener Model	64
3.4	CREEP AT INTERMEDIATE STRESS LEV- ELS	66
3.4.1	Linear Interpolation Scheme	67
3.4.2	Time-Stress Equivalence Principle (TSEP)	68
3.5	MODIFIED SUPERPOSITION PRINCIPLE (MSP)	72
4	CREEP EXPERIMENTS AND OPTIMIZA- TION PROBLEM	77

4.1	CREEP EXPERIMENTS	77
4.1.1	Experiments Conducted by Liu, Polak and Penlidis (2008)	77
4.1.2	Experiments Conducted by Kühl (2014)	78
4.2	OPTIMIZATION PROBLEM	81
4.2.1	Particle Swarm Optimization (PSO)	82
4.2.2	Optimization Procedure	86
5	APPLICATIONS, RESULTS AND DISCUSSIONS	89
5.1	CURVE FITTING	89
5.1.1	Curve Fitting for Experimental Data Obtained by Liu, Polak and Penlidis (2008)	89
5.1.2	Curve Fitting for Experimental Data obtained by Kühl (2014)	92
5.2	CREEP AT INTERMEDIATE STRESS LEVELS	94
5.2.1	Results for Linear Interpolation	94
5.2.2	Results for Time-Stress Equivalence Principle	98
5.3	RESPONSE TO MULTIPLE LOADING STEPS	100
5.4	LONG-TERM CREEP TESTS	104
5.4.1	Results for the P2 algorithm	104
5.4.2	Results for the SG algorithm	107
6	CONCLUSIONS	111
	REFERENCES	115
	APPENDIX A – SOME DEFINITIONS OF FRACTIONAL DERIVATIVES	125
	APPENDIX B – GAMMA FUNCTION	127

	APPENDIX C – ANALYSIS OF THE SG ALGORITHM	129
	APPENDIX D – AN EXAMPLE FOR VAL- IDATION OF THE FRAC- TIONAL VISCOELASTIC IMPLEMENTATION . .	133
D.1	FINITE DIFERENCE SCHEME	135
D.2	DISCUSSION AND RESULTS	142
	APPENDIX E – LAPLACE TRANSFORM OF THE FRACTIONAL DERIVATIVE	145

1 INTRODUCTION

Polymers have been used increasingly in the industry in the last decades. Especially in engineering, it has been ever more frequently applied as a lighter and cheaper substitute of metallic materials. One of the most currently used type of polymer is the high density polyethylene (HDPE). Due to its favorable chemical and physical properties, it has gained wide use in structural applications. Among these properties, chemical inertness and good ratio stiffness/weight have turned HDPE into one of the preferred materials for manufacturing pipes for gas and water distribution (see Fig. 1).

Figure 1 – HDPE pipelines installation in storm drain project in Mexico.



©Tomas Castelazo

Structural use implies that the HDPE-made components are subjected to non-negligible stress conditions, which should be predicted in order to avoid failure in service. Like other polymers, HDPE shows a time-dependent material response and viscoelastic properties, which must be considered when checking satisfaction of these failure criteria. Viscoelastic behavior can be represented by a constitutive equation that specifies the relationship between stress, strain and their respective time rates

(TSCHOEGL, 1989). If the constitutive equation can be expressed as a linear differential equation with constant coefficients, the material is said linear viscoelastic, otherwise the material shows nonlinear viscoelasticity. Boltzmann superposition principle describes the response for deformations under linear behavior. However, nonlinear behavior is much more complex, requiring more elaborate constitutive models (WINEMAN; RAJAGOPAL, 2000; DEALY; WISSBRUN, 1999). In spite of substantial work on nonlinear time-dependent analysis has been done, researchers have considerable difficulty finding an accurate and easy way to simulate structural problems which captures nonlinear effects of polymeric materials (LIU; POLAK; PENLIDIS, 2008).

Literature shows no consensus whether HDPE presents linear viscoelastic behavior at any stress range. For instance, while Elleuch and Taktak (2006) report linear viscoelastic behavior for this material in both tensile and compressive creep tests in the range of 3 to 10 MPa, most researchers have found that HDPE shows nonlinear viscoelastic behavior up to nearly vanishing stresses (LAI; BAKKER, 1995). This implies that the mechanical behaviour of HDPE cannot be described by the Boltzmann superposition principle. Different constitutive models have been developed for this purpose [e.g., Schapery (1969), Krishnaswamy et al. (2006), Liu, Polak and Penlidis (2008)]. In particular, Liu, Polak and Penlidis (2008) developed a practical method for constitutive modeling that includes time and nonlinear effects with an accuracy acceptable for structural analysis. Their formulation adopts the generalized rheological Kelvin model, described by Prony series, to fit experimental results of creep tests at given stress levels. Thereafter, a simple linear interpolation is performed to estimate the corresponding creep coefficients at intermediate stresses. Muñoz-Rojas and Kühl (2011) proposed a slight modification in Liu's interpolation procedure, resulting in better agreement with experimental results. The

work presented here consists of an extension of such method, where the generalized Kelvin model, expressed in terms of Prony series, has been replaced by a simple rheological Zener model described by fractional derivatives.

The application of fractional derivatives in viscoelastic problems has been studied substantially by many authors, [e.g., Bagley and Torvik (1983b), Lion (1997), Friedrich, Schissel and Blumen (1999), Glockle and Nonnenmacher (1991)]. This approach results in fractional-order differential stress-strain relations that provide good curve-fitting properties and require fewer parameters than traditional methods (PADOVAN, 1987). In this regard, the present work proposes the evaluation of the HDPE creep behavior using fractional derivatives in four different and complementary steps. Firstly, the fractional Zener model is used to fit results from creep tests. Secondly, a different approach based on the time-stress equivalence principle in association with the fractional derivatives is employed to predict the strain at intermediate stress levels, different from those experimentally measured. Thirdly, the modified superposition principle is used to describe the uniaxial response of HDPE bars subjected to complex (non-constant stress) loadings. Finally, some economic schemes are studied in order to improve the efficiency in numerical evaluation of fractional derivatives used to fit the nonlinear behavior of HDPE.

1.1 Objectives

The objectives of this work are:

1. To use the fractional derivatives formulations in order to fit experimental creep results provided by Kühn (2014) and Liu, Polak and Penlidis (2008);

2. To approximate the creep behavior of HDPE in stress levels, different from those experimentally measured, using a linear interpolation of the material parameters and the time-stress equivalence principle;
3. To estimate the strain behavior of HDPE when subject to non-constant stress levels, using the modified superposition principle;
4. To implement the numerical fractional derivative formulations G1, P2 and SG and compare the results provided by them regarding to accuracy and computational effort.

It is important emphasize that to the author's knowledge, there are not precedents in the literature for the applications proposed in the items 2 and 3. In this sense this part of the study is an original contribution.

1.2 Outline of the Thesis

Chapter 2 provides background information on fractional derivatives. A brief historical overview around this subject is carried out followed by the presentation of the Grünwald-Letnikov (GL) definition. Some aspects concerning such definition are discussed leading to numerical extensions of the GL fractional derivative: the algorithm G1, that is used as referential in the proposed applications; and the economy schemes P2 and SG, which are introduced aiming to reduce the computational effort associated with the fractional derivatives evaluation.

In Chapter 3 a literature review is presented, covering topics such as viscoelastic behaviour and modeling. The basic traditional viscoelastic models are presented, along with a discussion concerning the Prony series formulation. The extension of the

traditional approach to the fractional counterpart, through the introduction of the rheological element called spring-pot is given. Both these approaches, using Prony series and fractional derivatives, are used to fit results from experimental creep tests. Two procedures to approximate the creep behavior at intermediate stress levels are used, namely, a linear interpolation of the material parameters and the time-stress equivalence principle (TSEP). Finally, the modified superposition principle (MSP) is used in order to estimate the strain resulting for stress levels which change over the time.

Chapter 4 expose the obtaining of experimental data used to test the fractional approach. Such data is divided in two groups: the first one is provided by Liu, Polak and Penlidis (2008) and the second is given by Kühn (2014). Additionally, the particle swarm optimization method (PSO), that is chosen to solve the underlying inverse optimization problem associated with the curves fitting, is detailed.

In Chapter 5 the fitting and interpolation results are presented. Moreover the application of the modified superposition principle is employed for some cases of stress which change in a stepwise pattern. It additionally describes the outcome of numerical schemes G1, P2 and SG, used in the fractional derivatives modeling.

2 FUNDAMENTALS OF FRACTIONAL DERIVATIVES

In this chapter some aspects of the fractional derivative are discussed. First, the historical background around the origin of this concept is briefly summarized. Afterwards, the particular kind of fractional derivative, chosen to be used in this work, is discussed in the framework of its analytical definition and the resulting numerical extensions.

2.1 BRIEF HISTORICAL OVERVIEW

The origin of fractional derivatives is as old as the definition of the usual derivative. Indeed, it can be said that it refers to the year 1695, when Leibniz created the following notation to characterize the derivative:

$$\frac{d^n}{dx^n}(\cdot).$$

After being advised of such notation, Marquis de L'Hôpital initiated a discussion around the "nature" of the factor n . He sent a letter to Leibniz saying: "*Your notation for derivatives pleases me... however, I have a doubt. What is the mathematical interpretation when n is $1/2$, $1/3$, $2/5$, and so forth?*" Leibniz answered to L'Hospital as follows: "*An apparent paradox, from which one day useful consequences will be drawn.*" (LOVERRO, 2004). These words would be the starting point for a discussion that led to the first definitions of non-natural order derivatives and giving rise to fractional derivatives (NISHIMOTO, 1991).

In the eighteenth century, Euler and Lagrange considered some issues involving fractional derivatives, but it was only in the nineteenth century that more relevant works began to be published. In 1812, Laplace proposed a formulation to fractional derivatives, but it was Lacroix who first used the term derivative

of arbitrary order, followed by Fourier who presented a generalization of the derivative definition. Pursuant to, other mathematicians such as Riemann, Liouville, Abel, Hargrave, Holmgren, Heaviside, Marchaud, among others, also have devoted time to study this subject (SAMKO; KILBAS; MARICHEV, 1987).

Until the late nineteenth century, the development of fractional derivatives occurred strictly in the field of pure mathematics, without major applications in other areas. However, with the twentieth century awakening intriguing leaps in engineering start to be linked to the development of the fractional derivatives. This fact lead to the change of some mathematical concepts to meet the requirements of physical reality. In 1969, Caputo reformulated the definition of Riemann-Liouville for fractional derivatives in order to use integer order initial conditions to solve fractional order differential equations. More recently, Kolowankar and Gangal (1996) reformulated again the Riemann-Liouville fractional derivative in order to study fractal functions.

The authors mentioned have sought, using their own notations and methodologies, definitions for the concept of fractional order derivatives. Currently, the number of definitions is as large as the amount of people who have studied the subject, so that there is no uniqueness of definitions and, in many cases, not even equivalence between them. For instance, in the work of Oliveira and Machado (2014) it can be found more than thirty definitions for fractional derivatives. In Appendix A, one can see the most famous fractional derivatives definitions. Such concepts are, in most cases, variations of Riemann-Liouville and Grünwald-Letnikov definitions, which are the most widely accept and disseminated definitions.

Considering the studies over the past 300 years, Leibniz's response to L'Hôpital has proven right with some caveats. The physical meaning of this subject is certainly difficult, or even impossible to interpret (LOVERRO, 2004). On the other hand,

numerous applications and physical manifestations of fractional derivatives have been found and the mathematical background underlying fractional derivatives is nowadays no more rigorous than the integer order counterparts.

2.2 ASPECTS OF GRÜNWARD-LETNIKOV FRACTIONAL DERIVATIVES

Different definitions of fractional differential derivatives may lead to different mathematical and physical results, making it difficult to establish a systematic theory. Although in a purely mathematical viewpoint it is legitimate accept or even use one or all, from the standpoint of applications the situation is different. Only the definitions that may lead to a theory consistent with usual practice can be accepted.

In the study that follows, the Grünwald-Letnikov definition for fractional derivatives is used to formulate the proposed applications of viscoelasticity. Therefore, the meaning of the notation that will be common in the text is established: following Davis (2008) notation, the derivative of arbitrary real order α is denoted by ${}_{t_1}D_{t_2}^\alpha(\cdot)$, where the subscripts t_1 and t_2 are the two limits related to the operation of fractional derivation.

2.2.1 Definition of Grünwald-Letnikov

The Grunwald-Letnikov (GL) definition stems from the generalization of the incremental ratio used in the natural order derivatives. According to the usual definition, the first order derivative in terms of the backward quotient of the function $f(t)$, in the time interval $[t_1, t_2]$, is defined by

$${}_{t_1}D_{t_2}f(t) = \lim_{\Delta t \rightarrow 0} \frac{f(t) - f(t - \Delta t)}{\Delta t}, \quad (2.1)$$

when Δt is the time-step increment. Applying successively the above equation one obtains higher order derivatives. For instance

$${}_{t_1}D_{t_2}^2 f(t) = \lim_{\Delta t \rightarrow 0} \frac{f(t) - 2f(t - \Delta t) + f(t - 2\Delta t)}{\Delta t^2}. \quad (2.2)$$

To the n -th derivative, this procedure is consolidated by induction:

$${}_{t_1}D_{t_2}^n f(t) = \lim_{\Delta t \rightarrow 0} \Delta t^{-n} \sum_{m=0}^n (-1)^m \binom{n}{m} f(t - m\Delta t), \quad (2.3)$$

with $n \in \mathbb{N}$ and

$$\binom{n}{m} = \begin{cases} \frac{n!}{m!(n-m)!}, & \text{for } 0 \leq m \leq n, \\ 0, & \text{for } 0 \leq n < m. \end{cases} \quad (2.4)$$

If $\Delta t = t/N$, such that $N = 1, 2, 3, \dots$, then

$${}_{t_1}D_{t_2}^n f(t) = \lim_{N \rightarrow \infty} \Delta t^{-n} \sum_{m=0}^{N-1} (-1)^m \binom{n}{m} f(t - m\Delta t), \quad (2.5)$$

with $n \in \mathbb{N}$. The upper limit of the sum $N - 1$ seems to be somewhat arbitrary. However, it derives from defining the lower limit of an integral, when Eq. (2.5) is used to define integrals as a limit of the Riemann sum. More details can be found in Oldham and Spanier (1974).

Although the subscripts t_1 and t_2 in the notation ${}_{t_1}D_{t_2}^n(\cdot)$, are not compulsorily required for $n \in \mathbb{N}$, they are included to construct a link between the usual definition and the fractional counterpart. In order to deduce a formulation that is valid for any real order derivative, one can use the extended definition of the binomial coefficient

$$\binom{n}{m} = \begin{cases} \frac{n(n-1)\dots(n-m-1)}{m!}, & \text{for } m > 0, \\ 1, & \text{for } m = 0. \end{cases} \quad (2.6)$$

Thus, for $m > 0$

$$\begin{aligned}
 (-1)^m \binom{n}{m} &= \frac{(-1)^m}{m!} \prod_{k=1}^m (n - k + 1) \\
 &= \frac{1}{m!} \prod_{k=1}^m (m - n - k) \\
 &= \binom{m - n - 1}{m} \\
 &= \frac{\Gamma(m - n)}{\Gamma(-n)\Gamma(m + 1)}, \tag{2.7}
 \end{aligned}$$

such that Γ is the usual gamma function (see Appendix B) and $n \in \mathbb{Z}_-^*$ due to gamma function definition. Replacing the above equation into Eq. (2.5), one obtains

$${}_{t_1}D_{t_2}^n f(t) = \lim_{N \rightarrow \infty} (\Delta t)^{-n} \sum_{m=0}^{N-1} \frac{\Gamma(m - n)}{\Gamma(-n)\Gamma(m + 1)} f(t - m\Delta t), \tag{2.8}$$

which is valid for all $n \in \mathbb{Z}_-^*$. Removing the restriction that n should be an integer, one may assume the following generalization for Eq. (2.8).

$${}_{t_1}D_{t_2}^\alpha f(t) = \lim_{N \rightarrow \infty} (\Delta t)^{-\alpha} \sum_{m=0}^{N-1} A_{m+1} f_m, \tag{2.9}$$

where $\alpha \in \mathbb{R} - \mathbb{N}$, $f_m = f(t - m\Delta t)$ and

$$A_{m+1} = \frac{\Gamma(m - \alpha)}{\Gamma(-\alpha)\Gamma(m + 1)}. \tag{2.10}$$

Eq. (2.9) is said generalized form of the GL and A_{m+1} are the GL coefficients.

Note that in this context, all the GL coefficients A_{m+1} are different from zero as long as the derivative order α is not a

natural number. If, e.g. $\alpha = -1$, then $A_{m+1} = 1$ for all m . For α being a natural number n , only the first $n + 1$ GL coefficients are non-zero, indicating a local operator¹. Conversely, since for any positive non-integer number all coefficients A_{m+1} are non-zero, fractional derivatives are non-local operator (SCHMIDT; GAUL, 2002). Regarding to the form of the sum in Eq. (2.9), the first factor ($m = 0$) is $A_1 f(t)$ and the last ($m = N - 1$) is

$$A_N f \left(t - \frac{N-1}{N} t \right) = A_N f \left(\frac{t}{N} \right). \quad (2.11)$$

2.2.2 Numerical Calculation of the Grünwald-Letnikov Fractional Derivatives

The GL definition has been considered naturally appropriate for numerical and incremental computations by many authors, e.g., Sousa (2012) and Akil, Muniandy and Lim (2012). On account of this feature, the numerical extensions of the GL definition are present in this section. Additionally some aspects of the GL coefficients are discussed.

2.2.2.1 Behavior of the Grünwald-Letnikov Coefficients

In the calculation of GL coefficients by Eq. (2.10), some numerical issues can arise if α is close to a natural number or if large values of m occur. Accordingly, the calculation of such

¹ The definition of fractional derivative is a non-local operator for non-positive integers because it is defined on an interval. In other words, calculating time-fractional derivative of a function $f(t)$ defined in the interval $[t_1, t_2]$ at some time $t_1 \leq t_i \leq t_2$ requires all the previous history, i.e., all $f(t)$ from $t = t_1$ to t_i .

coefficients should be accomplished by the recursive relationship

$$\begin{aligned}
 A_{m+1} &= \frac{\Gamma(m - \alpha)}{\Gamma(-\alpha)\Gamma(m + 1)} \\
 &= \frac{(m - 1 - \alpha)\Gamma(m - 1 - \alpha)}{\Gamma(-\alpha)\Gamma(m + 1)} \\
 &= \frac{(m - 1 - \alpha)}{m} \frac{\Gamma(m - 1 - \alpha)}{\Gamma(-\alpha)\Gamma(m)} \\
 &= \frac{(m - 1 - \alpha)}{m} A_m. \tag{2.12}
 \end{aligned}$$

In the above equation, Γ satisfies the property established in Eq. (B.2) (see Appendix B). From (2.12) it follows that

$$\begin{aligned}
 |A_{m+1}| &= \left| \frac{m - 1 - \alpha}{m} \right| |A_m| \\
 &\leq |A_m|, \quad m > \alpha, \alpha > 0, \tag{2.13}
 \end{aligned}$$

since

$$\left| \frac{m - 1 - \alpha}{m} \right| < 1. \tag{2.14}$$

It means that the sequence given by the absolute value of the GL coefficients is strictly monotonic and decreasing for $\alpha > -1$ if $m > \alpha$. When $m \rightarrow \infty$ one obtains

$$\begin{aligned}
 \lim_{m \rightarrow \infty} |A_{m+1}| &= \left| \frac{1}{\Gamma(-\alpha)} \right| \lim_{m \rightarrow \infty} \left| \frac{\Gamma(m - \alpha)}{\Gamma(m + 1)} \right| \\
 &< \left| \frac{1}{\Gamma(-\alpha)} \right| \lim_{m \rightarrow \infty} \left| \frac{\Gamma(m)}{\Gamma(m + 1)} \right|, \tag{2.15}
 \end{aligned}$$

as long as $m > \alpha + 2$, since the Gamma function is strictly non-decreasing for values greater than two. Considering that $m \in \mathbb{N}$,

then $\Gamma(m + 1) = m!$ and

$$\begin{aligned} \lim_{m \rightarrow \infty} |A_{m+1}| &< \left| \frac{1}{\Gamma(-\alpha)} \right| \lim_{m \rightarrow \infty} \left| \frac{(m-1)!}{m!} \right| \\ &= \left| \frac{1}{\Gamma(-\alpha)} \right| \lim_{m \rightarrow \infty} \left| \frac{1}{m} \right| \\ &= 0. \end{aligned} \tag{2.16}$$

Equation (2.16) can be interpreted in the example presented in Fig. 2, where the GL coefficients are shown for $\alpha = 0.1$ (for other α values the behavior is similar). The value of A_{m+1} tends to zero when $m > \alpha$. The behavior that A_{m+1} assumes when m is close to the α value is not relevant in this work, since $m \in \mathbb{N}$, such that A_{m+1} is discrete. The GL coefficients are weighting functions values that are situated farther in the past with growing m . In other words, the influence of the past is faded out as time elapses. This property is called “fading memory”² and is used in the numerical fractional derivatives schemes presented in the next sections. In the following text, the fractional derivative operator for $f(t)$ in the interval $[t_1, t_2]$ assumes $t_1 = 0$, such that the notation becomes ${}_0D_{t_2}^\alpha(\cdot)$, or simply $D^\alpha(\cdot)$.

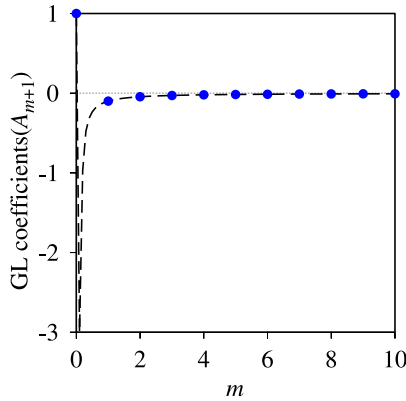
2.2.2.2 Algorithm G1

Oldham and Spanier (1974) presented the algorithm G1, which results from Eq. (2.9), by taking just N terms in the summation

$${}_0D_{t_2}^\alpha f(t) \simeq \Delta t^{-\alpha} \sum_{m=0}^{N-1} A_{m+1} f_m, \tag{2.17}$$

where $\Delta t = t/N$ is the time increment. The time interval $[0, t_2]$ is divided into N equally spaced sections of size Δt . Thus, at

² The property of fading memory is also called weak memory or logarithmic memory (DENG, 2007) and is largely discussed by Podlubny (1999).

Figure 2 – GL coefficients for $\alpha = 0.1$.

the N -th step, the summation in Eq. (2.17) requires $N - 1$ operations if the GL coefficients are given. The whole time-integration process requires N^2 operations. In this algorithm, all the fractional derivatives must be evaluated at each increment in time, and every time the whole variable history must be accounted for. Thus, as time evolves, the computational effort and storage requirement grow considerably and the process slows down significantly (SCHMIDT; GAUL, 2002). This algorithm is illustrated in Fig. 3, where the red line represents the fractional derivative calculated history.

Figure 3 – Time line representing the G1 algorithm. The red range is the whole fractional derivatives history.



2.2.2.3 Algorithm P2

The algorithm called P2 by Padovan (1987) uses the fading memory property. This means that, as long as the order of the derivative satisfies $\alpha > -1$, the GL coefficients A_{m+1} , which are the weighting factors of the function values at different times, tend to zero when m increases. Thus, since the influence of any value fades out as time elapses, it is reasonable to truncate the series, considering only the newest part of the historical variables in the evaluation of fractional derivative. This can be expressed mathematically as

$${}_0D_{t_2}^{-\alpha} f(t) \simeq \Delta t^\alpha \sum_{m=0}^r A_{m+1} f_m, \quad (2.18)$$

where $r = \min\{N, N_{\max}\}$, $N_{\max} = t_c/\Delta t$ is the truncation value and t_c is the truncation time, i.e., the time-step increment where the economic process begins. According to Eq. (2.18), only function values associated to the last N_{\max} are taken into account. This can be visualized by a time slot: the influence of all functions outside the time slot simply drops out. The numerical effort is the same as for G1 algorithm as long as the number N of time steps satisfies $N \leq N_{\max}$. If $N > N_{\max}$, the number of operations is constant and equal to $2N_{\max} - 1$. For the whole time integration consisting of $N > N_{\max}$ time steps, $N(2N_{\max} - 1) - N_{\max}(N_{\max} - 1)$ operations must be performed to evaluate the sum in Eq. (2.18) (SCHMIDT; GAUL, 2002). Note that this expression is linear in N in contrast to the G1. The algorithm P2 is illustrate in the Fig. 4, where the black range represents the neglected history and the red one represents the considered history.

Figure 4 – Time line illustrating the P2 algorithm. The red range is the calculated history and the black one is the disregarded history.



2.2.2.4 Algorithm SG

The basic idea of the SG algorithm (SCHMIDT; GAUL, 2002) is to reduce the numerical effort by considering the information of the farther past only approximately through a cheap interpolation scheme. The fractional derivative of the function $f(t)$, evaluated at the actual time t_a , can be written as

$${}_0D_{t_a}^\alpha f(t) = {}_0D_{t_I}^\alpha f(t) + {}_{t_I}D_{t_a}^\alpha f(t), \quad (2.19)$$

Using the G1 algorithm one obtains

$${}_0D_{t_I}^\alpha f(t) \simeq \Delta t^{-\alpha} \sum_{m=i}^{i+k-1} A_{m+1} f_m, \quad (2.20)$$

and

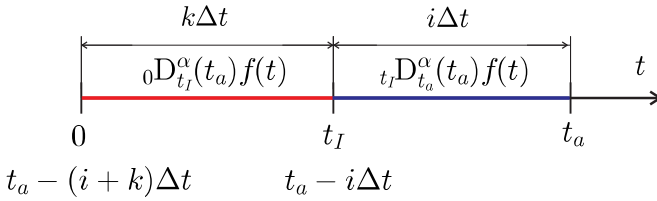
$${}_{t_I}D_{t_a}^\alpha f(t) \simeq \Delta t^{-\alpha} \sum_{m=0}^{i-1} A_{m+1} f_m. \quad (2.21)$$

Equation (2.20) represents the contribution of the old part of the function's fractional derivative history. According to this idea, the interval will be kept constant during further time integration (i.e., $i, k = \text{constant}$) as shown in Fig. 5.

After n time steps one obtains

$$\begin{aligned} {}_0D_{t_I}^\alpha (t_a + n\Delta t) f(t) &\simeq \Delta t^{-\alpha} \sum_{m=i}^{i+k-1} A_{m+n+1} f_m \\ &= \Delta t^{-\alpha} A_{i+n+1} T_n, \end{aligned} \quad (2.22)$$

Figure 5 – Time line representing the SG algorithm.



where T_n is a transfer function defined by

$$\begin{aligned}
 T_n = & f_i + \left(\frac{i+n-\alpha}{i+n+1}\right)f_{i+1} + \left(\frac{i+n-\alpha}{i+n+1}\right) \\
 & \left(\frac{i+n-\alpha+1}{i+n+2}\right)f_{i+2} + \dots + \left(\frac{i+n-\alpha}{i+n+1}\right) \\
 & \left(\frac{i+n-\alpha+1}{i+n+2}\right) \dots \left(\frac{i+n+k-2-\alpha}{i+n+k-1}\right)f_{i+k-1}.
 \end{aligned} \tag{2.23}$$

In order to reduce the numerical costs, the factor T_n , which includes the contribution of k function values, is approximated as one single contribution to the fractional derivative. This is done by calculating the starting value T_0 according to Eq. (2.23) at the time t_a and the limiting value

$$T_\infty = f_i + f_{i+1} + f_{i+2} + \dots + f_{i+k-1}.$$

From Eq. (2.23) it can be seen that all the weighting factors multiplied by f_m , $m = i, \dots, (i+k-1)$ are positive, but less or equal to one. In addition, as time elapses these factors increase monotonically and tend to unity. Therefore, the following expression can be defined

$$R_f = \frac{T_n - T_0}{T_\infty - T_0} \approx R_1 = \frac{T_n^1 - T_0^1}{T_\infty^1 - T_0^1} \xrightarrow{t \rightarrow \infty} 1, \tag{2.24}$$

where R_f is the ratio corresponding to any function f and the index 1 denotes that the respective ratio is calculated using the test function $f(t) = 1$. From Eq. (2.24), it results

$$\begin{aligned} T_n &\approx T_0 + \frac{T_n^1 - T_0^1}{T_\infty^1 - T_0^1} (T_\infty - T_0) \\ &= T_0 + R_1 (T_\infty - T_0), \quad R_1 \in [0, 1]. \end{aligned} \quad (2.25)$$

In the above equation it is possible to see that the transfer function associated to any function $f(t)$ can be interpolated at any given point between T_0 and T_∞ , using the ratio R_1 . The approximation given by Eq. (2.25) replaces Eq. (2.23) in this algorithm. Thus, Eq. (2.19) can be rewritten as

$$\begin{aligned} {}_0D_{t_a}^\alpha (t_a) f(t) &\simeq \Delta t^{-\alpha} A_{i+n+1} [T_0 + R_1 (T_\infty - T_0)] + \\ &\quad + \Delta t^{-\alpha} \sum_{m=0}^{i-1} A_{m+1} f_m. \end{aligned} \quad (2.26)$$

Equation (2.26) reduces the numerical effort needed to calculate T_n , since the whole history previous to the i -th increment is approximated using only one contribution to the fractional derivative. So, instead of processing and storing all the functions with their historical values at each time step, only two values, T_0 and T_∞ are used for each interval. In addition, the oldest history of variables needs not to be taken into account, contrary to what happens in the P2 algorithm. A study concerning the results provided by the SG scheme is proposed by Gaul and Schmidt (2007) and shown in detail in Appendix C.

A preliminary investigation on the behavior of the GL fractional derivative applied to viscoelastic modeling preceded the drafting of the present work. A problem proposed by Gaul and Schmidt (2007) was implemented and solved following the suggestion of this authors. The employed formulation in such a

problem is given in Appendix D. More details can be found in Costa Haveroth (2015).

Regarding the applications that will be shown later in this work, the numerical algorithm G1 is taken as referential for evaluating the fractional derivatives. Furthermore, a comparison between the results supplied by the algorithms G1, P2 and SG about the efficiency and accuracy intended for computational cost reduction, is also discussed in Section 5.4.

3 FRACTIONAL DERIVATIVES IN VISCOELASTICITY

In this chapter the fractional derivatives are discussed in the framework of viscoelasticity analysis. Such discussion starts with a description of the viscoelastic behavior followed by the presentation of the traditional method to model this phenomenon, which is based on the use of Prony series. Furthermore, the fractional counterpart is presented. Both these formulations are presented aiming at the description of creep-compliance for HDPE.

In order to predict the strain behavior of HDPE at non-experimentally measured stress levels, two different schemes are proposed, namely, a linear interpolation of the material parameters (LIU; POLAK; PENLIDIS, 2008) and the time-stress equivalence principle (LUO; YANG; AN, 2001). It additionally describes the modified superposition principle to approximate the strain behavior at non-constant stress levels.

3.1 VISCOELASTIC BEHAVIOR

In general, materials can be classified by their behavior when subjected to strain. If the material deforms under stress but returns instantaneously to its original state (size and shape) when the load is removed, it is said to show *elastic response*. On the other hand, when a material deforms continuously under constant tension, it is said to present *viscous behavior* (RIANDE et al., 1999). However, certain materials, called *viscoelastic*, exhibit a partially viscous and partially elastic behavior. In this case, the time dependence can be represented by constitutive equations between stresses, strains and their respective time rates. Depending on the relation between the strain rate and stress, the viscoelasticity can be categorized as linear or nonlinear. If the stress is linearly proportional to the strain rate this material

is said linear viscoelastic (Newtonian) (MEYERS; CHAWLA, 2009). Conversely, if the material exhibits non-linear stress response for the strain rate, then it is said nonlinear viscoelastic (non-Newtonian). For many materials, the linear viscoelasticity exists only at very small strains, where the response is independent of the strain (LIU; POLAK; PENLIDIS, 2008). In view of that, nonlinearity must be considered in most structural applications.

Polymers are a classic example of viscoelastic material. They are susceptible to changes as a result of environmental conditions, applied loading and aging over time. While the environmental conditions and aging are related to a time-dependent degradation process, the influence of the applied load can be attributed to a viscoelastic behavior that is manifested mainly in two ways: creep-compliance and stress relaxation, as described next.

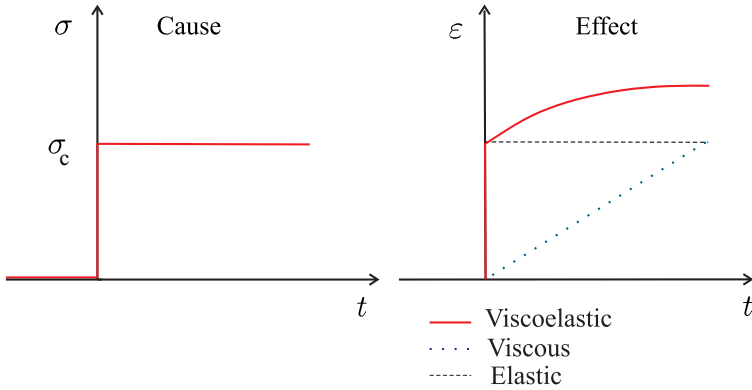
3.1.1 Creep-Compliance

The phenomenon called creep-compliance (or creep) is associated with an instantaneous elastic initial strain, followed by a time dependent strain (Fig. 6). The creep-compliance response, $J(t)$, for a constant stress level σ_c is

$$J(t) = \frac{\varepsilon(t)}{\sigma_c}. \quad (3.1)$$

According to Dasappa, Lee-Sullivan and Xiao (2010), creep tests are a good alternative to characterize the viscoelastic behavior, due to their experimental relative ease. Furthermore, the material creep behavior must be accounted for design and manufacturing, since this has a great impact on the end product (MUI, 2008).

Figure 6 – Strain and stress behavior in the creep-compliance phenomenon.



3.1.2 Stress Relaxation

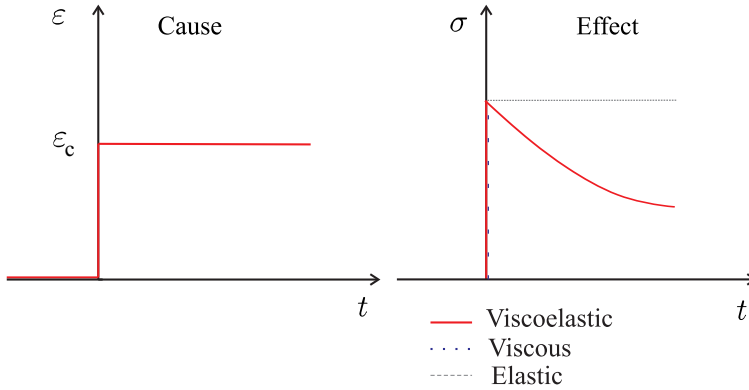
Another phenomenon that results from time-dependent material behavior is stress relaxation, where the stress in the material decreases over the time while subjected to a constant strain (MUI, 2008). The relaxation $G(t)$, for a constant strain level ε_c is

$$G(t) = \sigma(t)/\varepsilon_c. \quad (3.2)$$

Figure 7 illustrates the typical stress response of a material undergoing relaxation.

Many authors have studied the stress relaxation for polymers [e.g., Ayoub et al. (2010) and Hodge and Huvard (1983)]. The current study focuses mainly on creep behavior.

Figure 7 – Stress and strain behavior in the stress relaxation phenomenon.



3.2 TRADITIONAL VISCOELASTIC MODELING

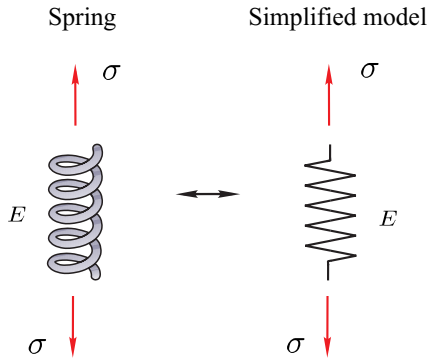
Models based on mechanical analogues have been created to approximate the viscoelastic constitutive equations (FINDLEY; DAVIS, 2013). Such models are based on the duality of the viscoelastic behavior: elastic solid + viscous fluid = viscoelastic solid. Usually, the material elastic behavior is represented by springs (see Fig. 8). The equation that describes the stress-strain relationship in this component is given by Hooke's Law

$$\begin{aligned}\sigma(t) &= E\varepsilon(t) \\ &= ED^0\varepsilon(t),\end{aligned}\quad (3.3)$$

where E denotes the spring stiffness constant and D^0 denotes the derivative operator of order zero. Equation (3.3) shows that for an abrupt loading, the spring responds with an instantaneous strain, and when the loading is removed it responds instantaneously once again, recovering the original dimensions.

The dashpot is used to model the viscous behavior and

Figure 8 – Representation of the spring.

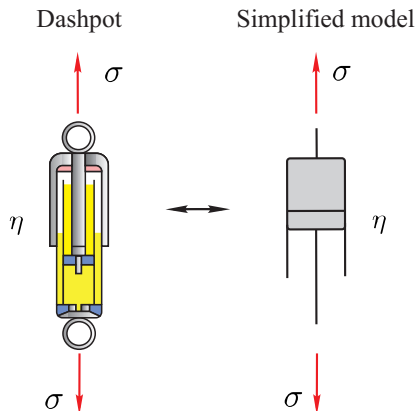


the equation that describes this element is

$$\begin{aligned}\sigma(t) &= \eta D\varepsilon(t) \\ &= \eta D^1\varepsilon(t),\end{aligned}\tag{3.4}$$

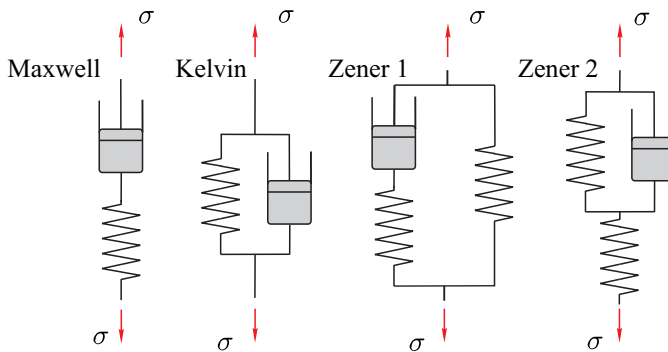
where η denotes a viscous constant. Figure 9 depicts the symbol for the dashpot.

Figure 9 – Representation of the dashpot.



A wide variety of viscoelastic materials, including HDPE, can be modeled using combinations of springs and dashpots. Such combinations are known as rheological viscoelastic models, and although purely phenomenological, they are particularly useful for predicting the material response under creep (constant stress) or relaxation (constant strain) conditions. The most famous rheological models are Maxwell, Kelvin and Zener which are shown in Fig. 10.

Figure 10 – Traditional rheological models of viscoelasticity: Maxwell, Kelvin and the two equivalent representations of the Zener model.



3.2.1 Generalized Chains

One way to systematically construct complex rheological models is combining Kelvin or Maxwell models¹, creating generalized chains. In the case of the Kelvin model, the generalization is done connecting a certain number of blocks in series, and optionally allowing for the inclusion of an additional spring

¹ The generalized Maxwell and Kelvin models are the most extensively used ones, however, there are other types of generalized chains as it can be seen in the work of Schiessel et al. (1995).

or dashpot in series (see Fig 11). The presence of the additional spring gives the model instantaneous response, while the presence of the dashpot results in viscous behavior. For the Maxwell model, some blocks can be connected in parallel, according to Fig. 12. Similarly to the Kelvin model, the additional spring or dashpot gives to the model instantaneous elastic response or fluid behavior.

Figure 11 – Generalized Kelvin model.

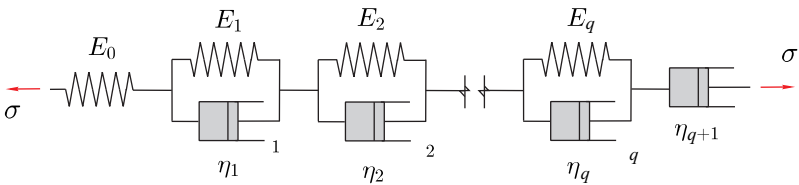
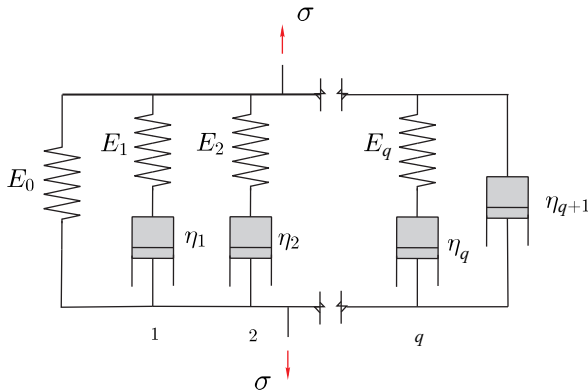


Figure 12 – Generalized Maxwell model.



In particular, this work uses extensively the traditional generalized Kelvin model described by Prony series as referential to construct comparisons with the fractional model that will be shown later. Both these models, will be used to model the HDPE viscoelastic behavior.

3.2.2 Prony Series Formulation

The Prony series scheme is used to represent the generalized Kelvin model (see Fig. 11). In such formulation the resulting strain is

$$\varepsilon_{\text{Prony}}(t) = \frac{\sigma(t)}{E_0(\sigma)} + \sum_{l=1}^q \frac{\sigma(t)}{E_l(\sigma)} \left[1 - \exp\left(-\frac{t}{\tau_l}\right) \right]. \quad (3.5)$$

where $\tau_l(\sigma) = \eta_l(\sigma)/E_l(\sigma)$, $l = 1, \dots, q$ are the relaxation times. If $\sigma(t) = \sigma_c$ is constant, then the creep-compliance can be given by

$$J_{\text{Prony}}(\sigma_c, t) = \frac{1}{E_0(\sigma_c)} + \sum_{l=1}^q \frac{1}{E_l(\sigma_c)} \left[1 - \exp\left(-\frac{t}{\tau_l}\right) \right], \quad (3.6)$$

where $E_l(\sigma_c)$, $l = 0, \dots, q$ denote the material parameter at a given stress level σ_c . Equivalently, one can rewrite Eq. (3.6) in the form

$$J_{\text{Prony}}(\sigma_c, t) = J_{\text{Prony}}^{\varphi}(\sigma_c) + J_{\text{Prony}}^{\chi}(\sigma_c, t), \quad (3.7)$$

where

$$J_{\text{Prony}}^{\varphi}(\sigma_c) = \frac{1}{E_0(\sigma_c)}, \quad (3.8)$$

and

$$J_{\text{Prony}}^{\chi}(\sigma_c, t) = \sum_{l=1}^q \frac{1}{E_l(\sigma_c)} \left[1 - \exp\left(-\frac{t}{\tau_l}\right) \right]. \quad (3.9)$$

Here, $J_{\text{Prony}}^{\varphi}$ is the time independent component and J_{Prony}^{χ} the time dependent component of the creep compliance. For more details about the Prony series formulation see Park and Schapery (1999) or Kühl (2014).

3.3 FRACTIONAL VISCOELASTIC MODELING

Using the generalized models described in the previous section, it is possible to establish approaches for modeling the viscoelastic behavior. Nonetheless, such models require identification of many parameters in the constitutive equation, since various springs and dashpots must be involved. Modifications in these models can be obtained proposing a formulation that uses fractional derivatives (MAINARDI, 2010).

Models of arbitrary order aiming to describe the viscoelastic behavior have proven to be useful to model many materials (LION, 1997; FRIEDRICH; SCHISSEL; BLUMEN, 1999; BAGLEY; TORVIK, 1983b; GLOCKLE; NONNENMACHER, 1991). According to Welch, Rorre and Duren (1999), the use of a fractional derivative operator typically demands fewer rheological elements, providing more flexibility to the models.

Indeed, in spite that the relationship between viscoelasticity and fractional derivatives begun to be treated only after 1930, nowadays viscoelastic analysis is definitely the field of the most extensive applications of fractional derivatives. This fact can be attributed to its ability to model hereditary phenomena with long memory (MAINARDI, 2012). The pioneers in the application of this approach were Gemant [(GEMANT, 1936; GEMANT, 1938)] and Scott-Blair [(SCOTT-BLAIR, 1944a; SCOTT-BLAIR, 1944b)], who showed the possibility of using fractional differential operators to find the relaxation curves of some viscoelastic fluids. Thereafter, Rabotnov (1948) and Gerasimov (1948) also used this concept.

In the second half of the twentieth century Caputo (CAPUTO, 1966; CAPUTO, 1967) and later Caputo and Mainardi (CAPUTO; MAINARDI, 1971a; CAPUTO; MAINARDI, 1971b) proposed using this approach to fit experimental creep curves. A great advance for the grounding of modeling by fractional deriva-

tives was done in the work of Bagley and Torvik (1983b), who presented a physical justification for such procedure. They developed a study on the relationship between the molecular theory (that describes the microscopic behavior of certain viscoelastic materials) and empirical viscoelastic models. These authors proved that when viscoelasticity is described by fractional derivatives, it presents results equivalent to those obtained in the molecular theory.

Koeller (1984) showed the link between fractional derivatives and the usual viscoelastic formulation through the generalization of the traditional models. This author presented expressions to creep and relaxation in terms of fractional parameters. The resulting constitutive equations are used to describe materials with time dependent behavior (memory materials).

More recently, important contributions in this sense have been done by Schmidt and Gaul (2001) and Jia, Shen and Hua (2007), who performed comparisons between classical models and their fractional counterpart, showing that the latter presents better representations in the curve fitting properties. Other authors also have studied concepts in this regard [e.g., Rossikhin and Shitikova (2010) and Mainardi and Spada (2011)].

Basically, the procedure to convert the classical models of viscoelasticity into fractional ones is to replace the dashpot by a rheological element that allows a continuous transition between viscous and elastic states. This element was named spring-pot² by Koeller (1984) and is represented by a rhombus, as shown in Fig. 13. The resulting fractional constitutive equation for that element is given by

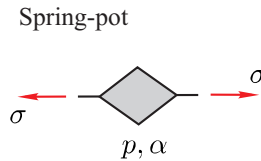
$$\sigma = pD^\alpha \varepsilon, \quad (3.10)$$

where p is a proportionality factor, D^α denotes the fractional

² Many authors [e.g., Mainardi and Spada (2011) and Mainardi (2010)] refer to the spring-pot as Scott-Blair element.

derivative operator and α is the order of the fractional derivative, which is commonly taken into the interval $[0, 1]$ to describe viscoelasticity. If $\alpha = 0$, Eq. (3.10) describes the behavior of a spring, where p specifies the spring stiffness. For $\alpha = 1$, Eq. (3.10) defines the constitutive equation of a dashpot, in which p defines the viscosity. Thus, Eq. (3.10) represents an element that behaves partly as a spring and partly as a dashpot.

Figure 13 – Representation of the fractional element.



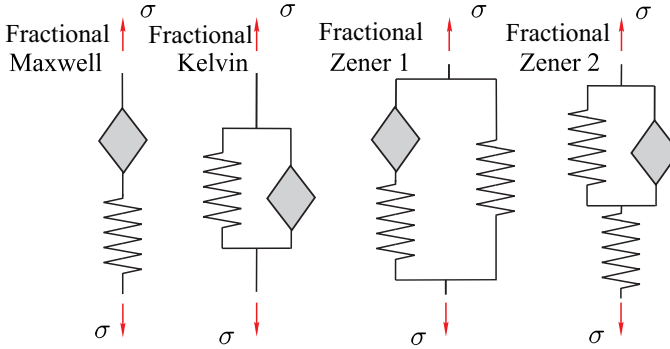
The combination of a spring-pot with the classic spring yields fractional viscoelastic rheological models whose constitutive equations are represented by fractional differential equations. Such rheological arrangements can be constructed from modifications in the classical models presented previously just replacing the dashpot by a spring-pot, according to the Fig. 14.

3.3.1 Fractional Zener model

The fractional model chosen to describe the HDPE viscoelastic behavior in this work is the fractional Zener one. The motivation for such a choice has its basis in previous applications found in the literature. According to Gaul and Schmidt (2007) and Bagley and Torvik (1983a) this model which has only four material parameters is able to show all phenomena related to viscoelasticity.

The fractional Zener rheological model consists of a fractional Maxwell model and a spring in parallel, or a fractional

Figure 14 – Fractional rheological models of viscoelasticity: Maxwell, Kelvin and the two equivalent representations of the Zener model.



Kelvin model and a spring in series (see Fig. 14). Both models lead to the same constitutive equation involving stress, strain and time (WINEMAN; RAJAGOPAL, 2000). In what follows, the fractional Maxwell model with a spring in parallel is adopted for deriving the formulation.

The strain in the spring E_0 , shown in Fig. 15, is represented by

$$\varepsilon_2(t) = \frac{\sigma_2(t)}{E_0}, \quad \Rightarrow \quad \sigma_2(t) = E_0 \varepsilon_2(t), \quad (3.11 - 3.12)$$

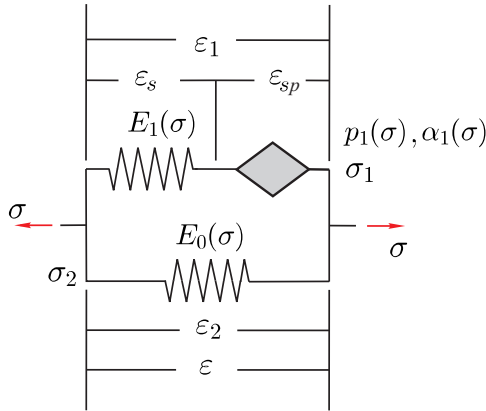
and the equation for the fractional Maxwell model is

$$\begin{aligned} \varepsilon_1(t) &= \varepsilon_s(t) + \varepsilon_{sp}(t) \\ D^\alpha \varepsilon_1(t) &= D^\alpha \varepsilon_s(t) + D^\alpha \varepsilon_{sp}(t) \\ D^\alpha \varepsilon_1(t) &= \frac{1}{E_1} D^\alpha \sigma_1(t) + \frac{\sigma_1(t)}{p_1}. \end{aligned} \quad (3.13)$$

Considering null initial conditions and applying the Laplace transform (see Appendix E) in Eqs. (3.11) and (3.13), one obtains

$$\mathcal{L}[\sigma_2(t)] = E_0 \mathcal{L}[\varepsilon_2(t)], \quad (3.14)$$

Figure 15 – Zener fractional model used to deriving the fractional constitutive relationship strain-stress in this work.



and

$$s^\alpha \mathcal{L}[\varepsilon_1(t)] = \frac{1}{p_1} \mathcal{L}[\sigma_1(t)] + \frac{s^\alpha}{E_1} \mathcal{L}[\sigma_1(t)], \quad (3.15)$$

respectively.

According to Fig. 15, it is possible to consider

$$\varepsilon(t) = \varepsilon_1(t) = \varepsilon_2(t), \quad \Rightarrow \quad \mathcal{L}[\varepsilon(t)] = \mathcal{L}[\varepsilon_1(t)] = \mathcal{L}[\varepsilon_2(t)], \quad (3.16 - 3.17)$$

and

$$\sigma(t) = \sigma_1(t) + \sigma_2(t), \quad \Rightarrow \quad \mathcal{L}[\sigma(t)] = \mathcal{L}[\sigma_1(t)] + \mathcal{L}[\sigma_2(t)], \quad (3.18 - 3.19)$$

Replacing Eq. (3.14) and (3.15) into Eq. (3.19) yields

$$\begin{aligned} \mathcal{L}[\sigma(t)] &= \mathcal{L}[\sigma_1(t)] + \mathcal{L}[\sigma_2(t)] \\ &= \mathcal{L}[\varepsilon_1(t)] \left(\frac{p_1 E_1 s^\alpha}{E_1 + p_1 s^\alpha} \right) + E_0 \mathcal{L}[\varepsilon_2(t)]. \end{aligned} \quad (3.20)$$

Using Eq. (3.17) in the above equation, it comes out that

$$\mathcal{L}[\sigma(t)] = \mathcal{L}[\varepsilon(t)] \left(\frac{p_1 E_1 s^\alpha}{E_1 + p_1 s^\alpha} \right) + E_0 \mathcal{L}[\varepsilon(t)]. \quad (3.21)$$

Finally, applying the inverse Laplace transform in Eq. (3.21), it can be rewritten as

$$E_1 \sigma(t) + p_1 D^\alpha \sigma(t) - E_0 E_1 \varepsilon(t) - E_0 p_1 D^\alpha \varepsilon(t) = p_1 E_1 D^\alpha \varepsilon(t). \quad (3.22)$$

The standard form of Eq. (3.22) is

$$\sigma(t) + \frac{p_1}{E_1} D^\alpha \sigma(t) = p_1 \left(\frac{E_0 + E_1}{E_1} \right) D^\alpha \varepsilon(t) + E_0 \varepsilon(t), \quad (3.23)$$

which is the one-dimensional constitutive equation for the fractional Zener model where the material parameters are α , p_1 , E_0 and E_1 .

3.3.2 Grünwald-Letnikov Definition for the Zener Model

The GL definition, presented in Section 2.2, can be used in order to solve numerically the constitutive equation for Zener model. Considering Eq. (3.23) and replacing the referential algorithm G1, represented by the Eq. (2.17), into Eq. (3.23), one obtains

$$\begin{aligned} \sigma(t) + \frac{p_1}{E_1} \Delta t^{-\alpha} \sum_{m=0}^{N-1} A_{m+1} \sigma_m &= E_0 \varepsilon(t) + \\ p_1 \left(\frac{E_0 + E_1}{E_1} \right) \Delta t^{-\alpha} \sum_{m=0}^{N-1} A_{m+1} \varepsilon_m. & \end{aligned} \quad (3.24)$$

Considering

$$\sum_{m=0}^{N-1} A_{m+1} \sigma_m = \sigma_0 + \sum_{m=1}^{N-1} A_{m+1} \sigma_m, \quad (3.25)$$

and

$$\sum_{m=0}^{N-1} A_{m+1} \varepsilon_m = \varepsilon_0 + \sum_{m=1}^{N-1} A_{m+1} \varepsilon_m, \quad (3.26)$$

with $\varepsilon_0 = \varepsilon(t)$, one can rewrite Eq. (3.24) in the form

$$\begin{aligned} \sigma(t) \left(1 + \frac{p_1}{E_1} \Delta t^{-\alpha} \right) + \frac{p_1}{E_1} \Delta t^{-\alpha} \sum_{m=1}^{N-1} A_{m+1} \sigma_m = \\ \varepsilon(t) \left(E_0 + p_1 \frac{E_0 + E_1}{E_1} \Delta t^{-\alpha} \right) + \\ + p_1 \frac{E_0 + E_1}{E_1} \Delta t^{-\alpha} \sum_{m=1}^{N-1} A_{m+1} \varepsilon_m, \end{aligned} \quad (3.27)$$

or equivalently

$$\sigma(t)(1 + a) + a S_\sigma = \varepsilon(t)[E_0 + b] + b S_\varepsilon, \quad (3.28)$$

where

$$a = \frac{p_1}{E_1} \Delta t^{-\alpha_1}, \quad b = a[E_0 + E_1], \quad (3.29 - 3.30)$$

$$S_\sigma = \sum_{m=1}^{N-1} A_{m+1} \sigma_m, \quad S_\varepsilon = \sum_{m=1}^{N-1} A_{m+1} \varepsilon_m. \quad (3.31 - 3.32)$$

Solving for $\varepsilon(t)$ in Eq. (3.28), gives

$$\varepsilon(t) = \sigma c_1 + \frac{a}{c_2} S_\sigma - \frac{b}{c_2} S_\varepsilon, \quad (3.33)$$

with

$$c_1 = \frac{1 + a}{c_2}, \quad c_2 = E_0 + b. \quad (3.34 - 3.35)$$

Similarly, if $\sigma(t) = \sigma_c$ constant, the creep compliance $J(t) = \varepsilon(t)/\sigma_c$ associated with the applied stress σ_c is given by

$$\begin{aligned} J(t) &= c_1 + \frac{a}{c_2} S_A - \frac{b}{c_2} S_J \\ &= J^\varphi(\sigma_c) + J^X(\sigma_c, t), \end{aligned} \quad (3.36)$$

where

$$S_A = \sum_{m=1}^{n-1} A_{m+1}, \quad S_J = \sum_{m=1}^{n-1} A_{m+1} J_m, \quad (3.37 - 3.38)$$

with $J_m = J(t - m\Delta t)$ and

$$J^\varphi(\sigma) = c_1, \quad J^X(\sigma, t) = \frac{a}{c_2} S_A - \frac{b}{c_2} S_J. \quad (3.39 - 3.40)$$

In the above equation, $J^\varphi(\sigma_c)$ represents the time-independent part of the creep-compliance and $J^X(\sigma_c, t)$ represents the time-dependent component.

In a similar way is possible to solve Eq. (3.23) using the algorithms P2 and SG through Eqs. (2.18) and (2.26), respectively.

Equations (3.33) and (3.36) describe the strain behavior along time and are used to fit experimental results obtained in creep tests for the HDPE, as will be explained later. For analysis of the strain behavior in stress levels different from those experimentally measured or in situations of non-constant stress levels, a modification in the above formulation should be done. For this purpose, two principles are presented in the next sections.

3.4 CREEP AT INTERMEDIATE STRESS LEVELS

The theoretical background of two different approaches which aim to approximate the creep behavior at intermediate

stress levels, are presented in this section. The first one is based in a simple linear interpolation of the material parameters, and the second is grounded on the concept of time-stress equivalence principle. It is important to emphasize that in a creep analysis the stress level remains constant along time. Hence in the following derivations it is considered that $\sigma(t) = \sigma_c$. Moreover, the material parameters associated with each formulation correspond to the considered stress level.

3.4.1 Linear Interpolation Scheme

Liu, Polak and Penlidis (2008) propose the application of Eq. (3.5) to identify the HDPE material parameters E_i , at different stress levels, using three rheological blocks ($q = 3$, $l = 0, \dots, q$). Pursuant to, they use the identified parameters to estimate the strain behavior at intermediate stress levels, according to the following linear interpolation scheme:

$$E_0(\sigma) = E_0(\sigma_m) + \frac{\sigma - \sigma_m}{\sigma_n - \sigma_m} [E_0(\sigma_n) - E_0(\sigma_m)], \quad (3.41)$$

and

$$\frac{1}{E_l(\sigma)} = \frac{1}{E_l(\sigma_m)} + \frac{\sigma - \sigma_m}{\sigma_n - \sigma_m} \left[\frac{1}{E_l(\sigma_n)} - \frac{1}{E_l(\sigma_m)} \right], \quad (3.42)$$

where $\sigma_m \leq \sigma \leq \sigma_n$ and $l = 1, 2, 3$. Adopting a similar procedure for the interpolation of the fractional parameters in the Eq. (3.33), one obtains

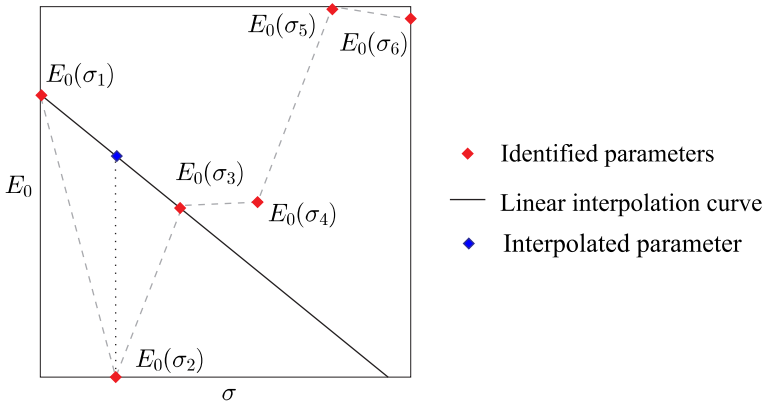
$$\mathbf{b}_i(\sigma) = \mathbf{b}_i(\sigma_m) + \frac{\sigma - \sigma_m}{\sigma_n - \sigma_m} [\mathbf{b}_i(\sigma_n) - \mathbf{b}_i(\sigma_m)], \quad (3.43)$$

where $\mathbf{b} = [\alpha, p, E_0, E_1]$ is the fractional parameters vector.

According to Liu, Polak and Penlidis (2008), the presented linear interpolation yields in acceptable accuracy for structural analysis. On the other hand, in the work of Costa Haveroth

et al. (2015), it is shown that if the individual parameters are not well behaved (in the sense that a monotonic change of parameters should occur when the stress levels are monotonically increased) the interpolation scheme does not give useful approximations. This situation is illustrated in an example in Fig. 16, where the parameter E_0 does not present a monotonic change with the increase of the stress levels, yielding in an unrealistic approximation in the interpolation. In the next section, an approach less dependent of the material parameters behavior is presented.

Figure 16 – Example of an unsuccessful material parameter interpolation.



3.4.2 Time-Stress Equivalence Principle (TSEP)

The time-temperature-stress equivalence principle can be deduced from the free volume theory that refers to a small amount of unfilled volume associated with the end of a polymer chain (PETERS, 2013; LUO; YANG; AN, 2001). According to this theory, the viscosity of the material η , which is associated with the material's intrinsic time, can be related to the free volume

fraction, f , via Doolittle's equation (AKLONIS; MACKNIGHT, 1983):

$$\ln \eta = \ln A + B \frac{V - V_f}{V_f}, \quad (3.44)$$

where V is the total volume, V_f is the free volume, and A and B are material constants. Defining the fractional free volume as

$$f = \frac{V_f}{V}, \quad (3.45)$$

Doolittle's equation becomes,

$$\ln \eta = \ln A + B \left(\frac{1}{f} - 1 \right). \quad (3.46)$$

The change in the free volume fraction that results from a change in temperature is usually assumed to depend linearly on the temperature change. It is further assumed that the stress has a similar effect, so that the change in the free volume fraction resulting from a change in the stress depends linearly on the stress change (LUO; YANG; AN, 2001). When the combined effect of temperature and stress on the free volume fraction of viscoelastic materials is considered, the free volume fraction can be expressed as

$$f = f_0 + \gamma_T(T - T_0) + \gamma_\sigma(\sigma - \sigma_0), \quad (3.47)$$

where γ_T is the thermal expansion coefficient of the free volume fraction, γ_σ refers to the stress-induced expansion coefficient, and f_0 is the free volume fraction in the reference state (TALLA et al., 2014; AKLONIS; MACKNIGHT, 1983). Replacing (3.47) into Eq. (3.46) yields

$$\ln \eta(T, \sigma) = \ln A + B \left(\frac{1}{f_0 + \gamma_T(T - T_0) + \gamma_\sigma(\sigma - \sigma_0)} - 1 \right). \quad (3.48)$$

The natural logarithm of the viscosity ratio at any temperature and stress divided by the viscosity at the temperature T_0 and stress σ_0 will give, after simplification

$$\ln \frac{\eta(T, \sigma)}{\eta(T_0, \sigma_0)} = B \left(\frac{1}{f_0 + \gamma_T(T - T_0) + \gamma_\sigma(\sigma - \sigma_0)} - \frac{1}{f_0} \right). \quad (3.49)$$

Converting the above equation to base 10 logarithm and supposing that there exists a temperature-stress shift factor $\phi_{T,\sigma}$ satisfying the relation

$$\phi_{T,\sigma} = \frac{\eta(T, \sigma)}{\eta(T_0, \sigma_0)},$$

one obtains

$$\log \phi_{T,\sigma} = -C_1 \left[\frac{C_3(T - T_0) + C_2(\sigma - \sigma_0)}{C_2 C_3 + C_3(T - T_0) + C_2(\sigma - \sigma_0)} \right], \quad (3.50)$$

where $C_1 = B/(2.303f_0)$, $C_2 = f_0/\gamma_T$ and $C_3 = f_0/\gamma_\sigma$ (BRINSON; BRINSON, 2015). Equation (3.50) reduces to the Williams-Landel-Ferry equation at a single stress level if there is no stress difference.

The stress shift factor at constant temperature, ϕ_σ^T , and the temperature shift factor at constant stress ϕ_T^σ , may be defined such that

$$\begin{aligned} \eta(T, \sigma) &= \eta(T, \sigma_0) \phi_\sigma^T = \eta(T_0, \sigma_0) \phi_T^{\sigma_0} \phi_\sigma^T \\ &= \eta(T_0, \sigma) \phi_T^\sigma = \eta(T_0, \sigma_0) \phi_T^{\sigma_0} \phi_T^\sigma. \end{aligned} \quad (3.51)$$

Equation (3.51) leads to

$$\phi_{T,\sigma} = \phi_T^{\sigma_0} \phi_\sigma^T = \phi_\sigma^{T_0} \phi_T^\sigma. \quad (3.52)$$

From Equation (3.52) it can be seen that the viscoelastic behavior at different stress levels and temperatures can be shifted along the time scale by constructing a master curve at a reference

stress level, σ_0 and a reference temperature, T_0 . It may be done at one time via temperature-stress shift factor, $\phi_{T,\sigma}$, or in two steps by combining the shift factor at a constant temperature, ϕ_σ^T and the temperature shift factor at constant stress level ϕ_T^σ (LUO; YANG; AN, 2001). This allows the evaluation of the viscoelastic behavior at convenient time scales.

By choosing the reference temperature, T_0 , Eq. (3.50) reduces to

$$\begin{aligned} \log \phi_\sigma &= -\frac{B}{2.303f_0} \left(\frac{\sigma - \sigma_0}{f_0/\gamma_\sigma + \sigma - \sigma_0} \right) \\ &= \frac{-C_1(\sigma - \sigma_0)}{C_3 + (\sigma - \sigma_0)}, \end{aligned} \quad (3.53)$$

where ϕ_σ denotes the stress shift, also called horizontal shift. Such equation characterizes the time-stress equivalence principle (TSEP).

The creep compliance curves at different stress levels can be related to each other by the reduced time $\xi = t/\phi_\sigma$, (see Fig. 17):

$$J(\sigma, t) = \tilde{J}(\sigma_0, \xi) = \delta_\sigma J(\sigma_0, \xi), \quad (3.54)$$

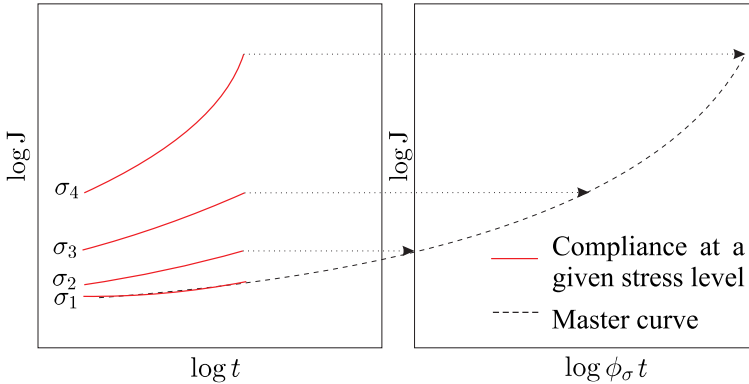
with $\tilde{J}(\sigma_0, \xi)$ the master curve creep at the stress level σ_0 and δ_σ the vertical shift factor along the creep compliance axis, that has the form similar to the horizontal shift factor:

$$\log \delta_\sigma = -\frac{D_1(\sigma - \sigma_0)}{D_2 + (\sigma - \sigma_0)}, \quad (3.55)$$

with D_1 and D_2 material constants.

It must be emphasized that temperature and stress shifts are only allowed for thermorheologically and piezorheologically simple materials, respectively (MUÑOZ-ROJAS; KÜHL, 2011). HDPE is a semicrystalline polymer, and thus not thermorheologically simple, so time-temperature equivalence cannot rigorously be applied. In spite of that, successful application of the

Figure 17 – TSEP master curve formation for the horizontal shift ϕ_σ .
In this example, σ_1 is the reference stress level.



Edited from Brinson and Brinson (2015).

TSEP has been reported in some references (LAI; BAKKER, 1995; LUO; YANG; AN, 2001). According to Barbero (2010) and Brinson and Brinson (2015), the TSEP is frequently used to predict long term viscoelastic behavior from short term experimental data, but in this work it is used to approximate the creep behavior at non-experimentally measured stress levels from data obtained in tested levels. One advantage in using this method for this purpose is the possibility of obtaining a unique set of parameters, through the master curve fitting, with is able to approximate the strain or creep-compliance in any stress level in a preset range.

3.5 MODIFIED SUPERPOSITION PRINCIPLE (MSP)

The modified superposition principle (MSP) was introduced by (FINDLEY; LAI, 1967) and consists of relaxing the requirement of linearity to describe the nonlinear time behavior

for stress levels which change abruptly from time to time. The strain response in such a case will be considered the sum of the strain due to the first loading and the strain response due to each change of stress (FINDLEY; LAI, 1967). Namely, the stress σ_1 is applied instantaneously at time t_0 and held constant until the time t_1 . At time t_1 , the strain is equal to

$$\varepsilon_1 = \sigma_1 J^\varphi(\sigma_1) + \sigma_1 J^X(\sigma_1, t_1 - t_0), \quad (3.56)$$

where J^φ and J^X are respectively the time independent and the time-dependent components of the creep-compliance. In the case of the Prony series formulation these components are shown in Eqs. (3.8) and (3.9). For the fractional formulation the same components are given by Eqs. (3.39 - 3.40).

If in time t_1 a new stress σ_2 is applied in a step and held constant until time t_2 , the stresses σ_1 and σ_2 are considered independent and the calculation of strain at time t_2 includes strain recovery from time t_1 to t_2 :

$$\begin{aligned} \varepsilon_2 = & \sigma_2 J^\varphi(\sigma_2) + \sigma_1 J^X(\sigma_1, t_2 - t_0) + \sigma_2 J^X(\sigma_2, t_2 - t_1) \\ & - \sigma_1 J^X(\sigma_1, t_2 - t_1). \end{aligned} \quad (3.57)$$

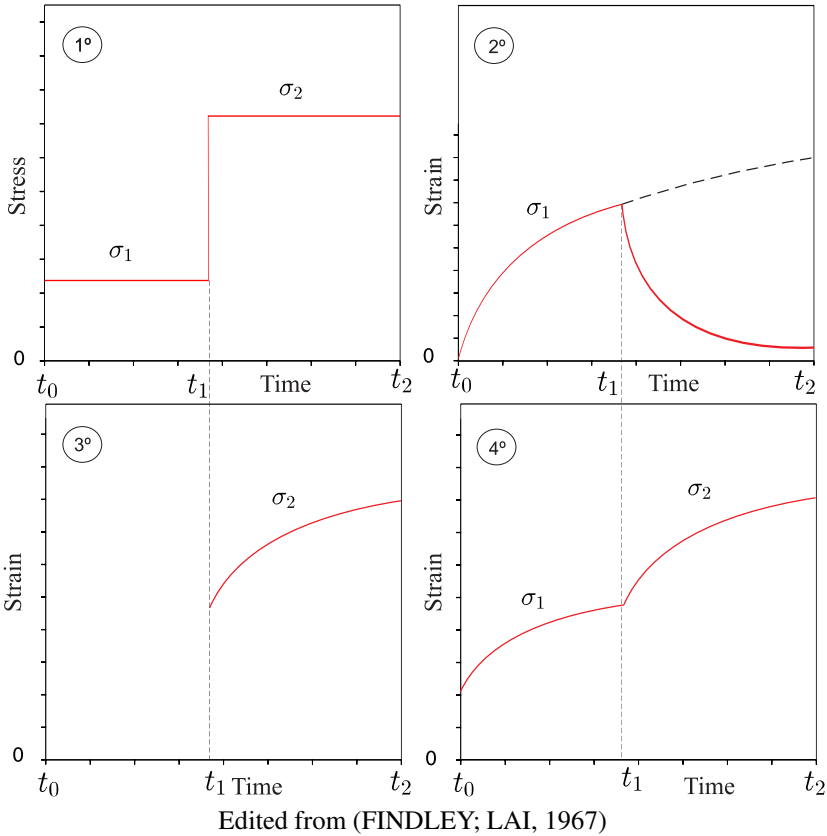
Figure 18 shows a two-step loading and the resulting strain according to Eq. (3.57).

In the same manner, one obtains the strain response when the state of stress changes \tilde{N} times, as follows:

$$\begin{aligned} \varepsilon_{\tilde{N}} = & \sigma_{\tilde{N}} J^\varphi(\sigma_{\tilde{N}}) + \sum_{w=1}^{\tilde{N}} \left[\sigma_w J^X(\sigma_w, t_{\tilde{N}} - t_{w-1}) \right. \\ & \left. - \sigma_{w-1} J^X(\sigma_{w-1}, t_{\tilde{N}} - t_{w-1}) \right], \end{aligned} \quad (3.58)$$

in which the total time t is divided into \tilde{N} discrete intervals. Equation (3.58) shows that the time-dependent part of the strain

Figure 18 – Two-step loading effect.



depends on both stress state and stress history, while the time independent part depends only on the current state of stress.

FINDLEY and LAI (1967) have investigated many ways to introduce the MSP. However the results provided by these other formulations are not as satisfactory as those obtained using the approach presented here. The application of the theory described above to model nonlinear viscoelasticity is done as follows: initially the Prony series formulation is used in associa-

tion with the linear interpolation procedure shown in the Section 3.4.1; thereafter, the fractional formulation proposed in the Section 3.3, is applied in association with the linear interpolation and the TSEP. Both approaches are compared with the experimental results provided by Liu, Polak and Penlidis (2008).

4 CREEP EXPERIMENTS AND OPTIMIZATION PROBLEM

The experimental data employed to corroborate the numerical procedures proposed herein are presented in this chapter. Also, a detailed presentation of the optimization algorithm used for curve fitting is given.

4.1 CREEP EXPERIMENTS

The creep experimental data used are obtained from two different fonts, as explained below.

4.1.1 Experiments Conducted by Liu, Polak and Penlidis (2008)

Liu, Polak and Penlidis (2008) obtained experimental data for creep testing samples extracted from HDPE pipes at 2.97, 5.97, 7.71, 10.31, and 12.19 MPa¹. They also perform some step loading tests. These authors fitted the experimental data to the generalized Kelvin model [see Eq. (3.5)] adopting three rheological blocks in the Prony series formulation with preset relaxation times $\tau_1 = 500$, $\tau_2 = 1000$ and $\tau_3 = 200000$ s. For step loading cases, the same procedure to fit each individual stress level is posed in association with the modified superposition principle (MSP) to evaluate hereditary effects in the behavior of HDPE.

In this work, sampled points from the creep curves identified by Liu, Polak and Penlidis (2008) (Tab. 1) are used to simulate the actual experimental values to be matched. The resulting curves in such a case are depict in Fig. 19. Afterwards,

¹ The reader interest in details about experimental conditions and setup is referred to Liu's original work.

an estimate of the stress behavior at intermediate stress levels is done via linear interpolation of the parameters and via time-stress equivalence principle (TSEP). The results are compared with those obtained by Liu's linear interpolation of the Prony series material parameters. The MSP is applied in association with the fractional derivatives to approximate some cases of step loading creep.

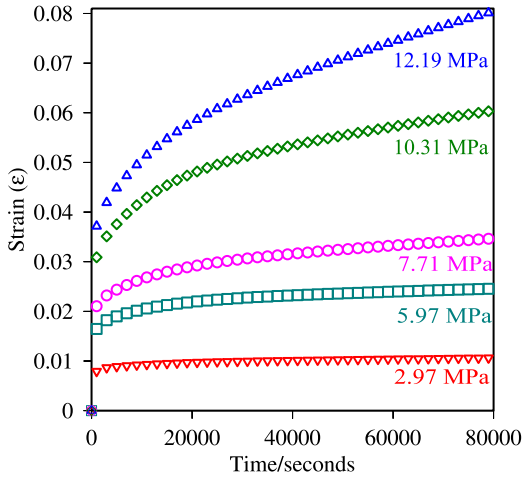
Table 1 – Identified Prony series parameters by Liu, Polak and Penlidis (2008).

Stress (MPa)	Prony series parameters			
	$E_0(\text{N/m}^2)$	$E_1(\text{N/m}^2)$	$E_2(\text{N/m}^2)$	$E_3(\text{N/m}^2)$
2.97	650	797.3889	2320.3566	925.0882
5.97	580	913.5936	1212.2605	695.0461
7.71	520	1224.7911	1104.9922	385.8572
10.31	500	1034.2045	694.1084	226.4555
12.19	470	1128.4448	806.0972	140.6875

4.1.2 Experiments Conducted by Kühl (2014)

In the creep experiments developed by Kühl (2014), material samples of HDPE – PE80 were extracted from water transport pipes using mechanical pressure according to the NBR 96-22 Brazilian norm [see Figs. 20(a) and 20(b)]. The samples were kept at controlled constant temperature of 20°C and subjected to axial loading dead during approximately 22 hours (80000 seconds). The creep tests were performed at six different stress levels: 3.6, 5.5, 7.2, 9.1, 11 and 13 MPa. The resulting strains were

Figure 19 – Experimental data obtained from Liu’s work.

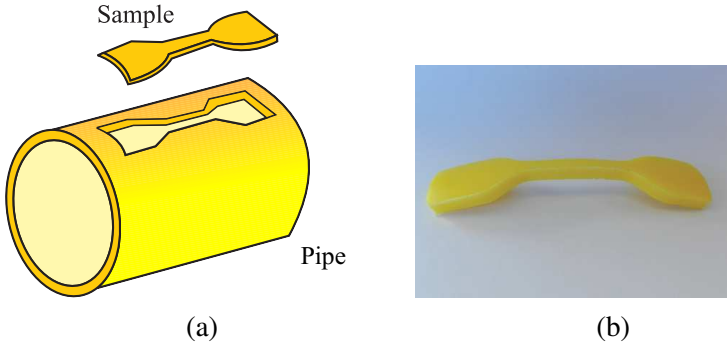


measured with a strain gage and the loading was monitored using a load cell. A data acquisition system was used to measure and store the strain history. The time interval between each of the experimental data was 1000 seconds, resulting in 80 experimental points, as schematized in Fig 21.

Kühl (2014) also employed the traditional Kelvin model described by Prony series with two rheological blocks in order to fit the experimental data shown in Fig. 21. The parameters identified by this author are presented in Tab. 2 and the resulting fitting is shown later in section 5.1.2, where a comparison with the fractional fitting proposed in this work is performed.

In this case, the actual experimental data is used to test the fractional formulation. The material parameters are identified using the Zener fractional model and an estimate of the stress behavior at intermediate stress levels is done via linear interpolation of the material parameters, and via TSEP.

Figure 20 – Sample used in Küh1’s experimental procedure: (a) Extraction; (b) Sample of HDPE PE80 extracted from water transport pipes.



Font: Edited from Küh1 (2014)

Figure 21 – Experimental data obtained by Küh1 (2014).

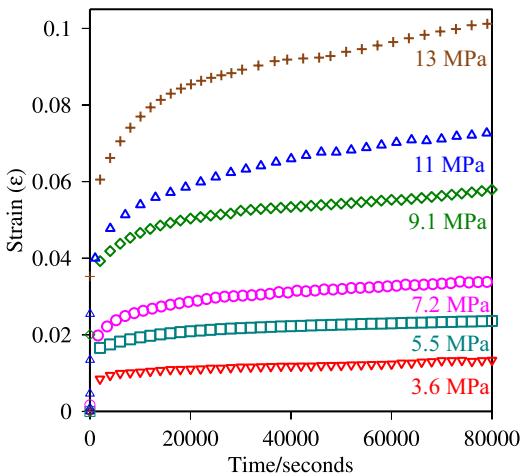


Table 2 – Identified Prony series parameters by Kühl (2014).

Stress (MPa)	Prony series parameters		
	$E_0(\text{N/m}^2)$	$E_1(\text{N/m}^2)$	$E_2(\text{N/m}^2)$
3,6	1038.55	664.60	1335.50
5.5	986.98	840.13	632.55
7.2	1086.73	4120.26	333.63
9.1	459.19	550.15	589.98
11.0	420.09	1275.85	353.47
13.0	370.96	1582.65	275.45

4.2 OPTIMIZATION PROBLEM

An optimization algorithm is employed for curve fitting data obtained in the creep tests (described in the previous section) by the problem:

$$\text{Minimize } f : \mathbb{R}^n \rightarrow \mathbb{R}, \quad (4.1)$$

with

$$f(\mathbf{b}) = \sqrt{\sum_{n=1}^{npts} |\varepsilon_{exp}^n - \varepsilon^n(\mathbf{b})|^2}, \quad (4.2)$$

subject to

$$\mathbf{b}_i^{\min} \leq \mathbf{b} \leq \mathbf{b}_i^{\max}, \quad (4.3)$$

where ε_{exp}^n is the experimental strain, $npts$ is the number of sampled experimental points (here $npts = 80$), ε^n is the strain obtained by fractional derivatives modeling (see Eq. (3.33)), and the design variable vector is $\mathbf{b} = [\alpha, p, E_0, E_1]$.

The chosen optimization algorithm is the PSO, which is described below.

4.2.1 Particle Swarm Optimization (PSO)

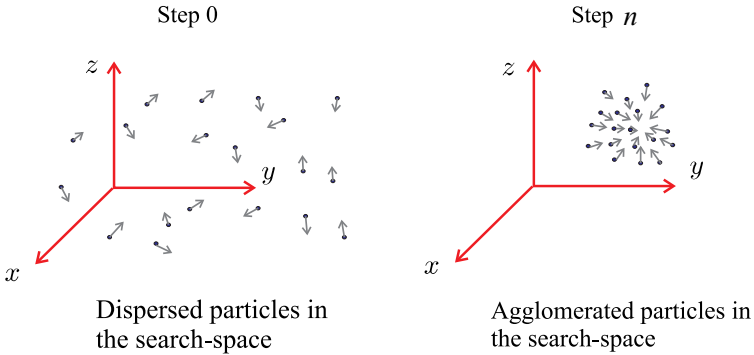
The particle swarm optimization method (PSO) is originally attributed to Kennedy, Eberhart and Shi (2001) and is inspired in the way groups behave (SHI; EBERHART, 1998; KENNEDY; EBERHART, 1995), for instance, fish school, flock birds or insects swarm².

Basically, the PSO method proposes to solve an optimization problem where the candidate solutions are called particles and the set formed by them is known as swarm. These particles are moved around in the search-space where the movements of each particle are guided by its own best known position in the search-space (the position that comes closest to the optimum point for the considered particle) and the entire swarm's best known position (defined by the position that comes closest the optimal point among the positions of all particles) (BAI, 2010). This process is repeated until a stop criterion be met, so that the swarm must be led towards to the optimal solution (see Fig. 22). Each iteration is named generation, such that this method is classified as evolutionary.

PSO is also considered an heuristic method as it makes few or no assumptions about the problem that is being optimized and can search very large spaces of candidate solutions. In spite of that as this type of algorithm does not employ guaranties, it cannot ensure that a satisfactory solution will be discovered (BAI, 2010). As PSO does not use gradients, it does not require that the optimization problem be differentiable, and for this rea-

² In the work of Kennedy, Eberhart and Shi (2001) aspects around the origin of the PSO are substantially discussed.

Figure 22 – PSO behavior after n iterations in a three-dimensional space.



son, it is extensively used in optimization problems that are partially irregular, noisy, change over time, and so forth.

According to Vaz and Cardoso (2014), the PSO termination criteria can be a preset number of generations n_g , the difference between the best and worst particles or the difference between the best fitness of consecutive generations, among other alternative criteria found in the literature. In this work, a preset number of generations is adopted, namely $n_g = 200$.

In order to formally describe the canonical PSO problem, it is considered the objective function

$$\text{Minimize } f : \mathbb{R}^n \rightarrow \mathbb{R}. \quad (4.4)$$

The goal is to find a solution \mathbf{a} such that

$$f(\mathbf{a}) \leq f(\mathbf{a}_s) \quad \forall \quad \mathbf{a}_s \in X, \quad (4.5)$$

being $X \subset \mathbb{R}^n$ the search space where the upper and lower limiting are respectively \mathbf{b}_{\min} and \mathbf{b}_{\max} , according to Eq. 4.2.

Let n_p be the number of particles in the swarm, each having a position $\mathbf{x}_i \in X, i = 1, \dots, n_p$ and a velocity $\mathbf{v}_i \in V$, where

$V \subset \mathbb{R}^n$ is the search space of the velocities associated to each particle. It is also considered that \mathbf{p}_i is the best known position of particle i and \mathbf{g} the best known position of the entire swarm. Thereat, the description of the classical PSO is done considering the following steps:

1. For each particle $i = 1, \dots, n_p$:

(i) The initial position \mathbf{x}_i is randomly generated and

$$\mathbf{p}_i \leftarrow \mathbf{x}_i.$$

(ii) Initialize the particle's best known position \mathbf{g} to its initial position:

$$\mathbf{g} \leftarrow \mathbf{p}_i,$$

where

$$f(\mathbf{p}_i) \leq f(\mathbf{p}_j) \quad \forall \quad j = 1, \dots, n_p.$$

In other words, \mathbf{g} receives the value \mathbf{p}_i with best approximate the minimum of f among the considered particles.

(iii) The velocity of each particle is also randomly initialized:

$$\mathbf{v}_i \in V.$$

After that, the following steps are iterated until the termination criterion.

2. For each particle $i = 1, \dots, n_p$:

(i) For each dimension $d = 1, \dots, n$ ($n =$ number of design variables)

* The values $r_p, r_g \in (0, 1)$ are generated randomly;

* Update the particle's velocity:

$$\mathbf{v}_{i,d} \leftarrow \omega \mathbf{v}_{i,d} + \varphi_p r_p (\mathbf{p}_{i,d} - \mathbf{x}_{i,d}) + \varphi_g r_g (\mathbf{g}_d - \mathbf{x}_{i,d}),$$

where $\mathbf{v}_{i,d}$ and $\mathbf{x}_{i,d}$ are respectively the particle i velocity and position associate with the dimension, and the control parameters ω, φ_p and φ_g are constants heuristically chosen

(ii) Update the particle's position:

$$\mathbf{x}_i \leftarrow \mathbf{x}_i + \mathbf{v}_i$$

(iv) If $f(\mathbf{x}_i) < f(\mathbf{p}_i)$ then

* Update the particle's best known position:

$$\mathbf{p}_i \leftarrow \mathbf{x}_i.$$

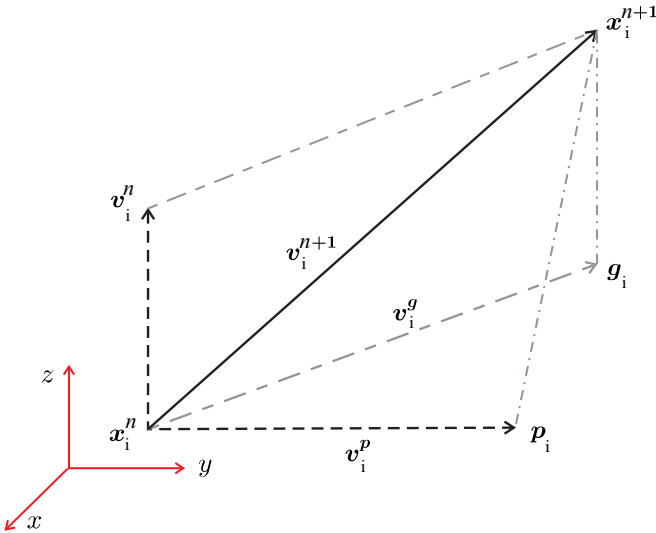
* If $f(\mathbf{p}_i) < f(\mathbf{g})$ update the swarm's best known position:

$$\mathbf{g} \leftarrow \mathbf{p}_i$$

3. In this moment \mathbf{g} holds the best found solution (see Fig. 23).

Many techniques have been proposed to refine or com-

Figure 23 – PSO updating of the best positions towards to the optimum value in a three-dimensional space.



plement the original canonical PSO algorithm described above (PIRES; MACHADO; OLIVEIRA, 2009), namely regarding it tuning parameters and by considering hybridization with other evolutionary techniques. In this work, the PSO is employed in association with fractional derivatives. Such combination has achieved satisfactory results in many recent works, as can be seen in the paper of Lewandowski and Choraśyczewski (2010) and Pires, Machado and Oliveira (2009).

4.2.2 Optimization Procedure

The identification of the material parameters, for the fractional Zener model at each experimental group of stress levels, is done via PSO method in two different ways, according to the following description:

Case 1. Initially, only lateral constraints are used, namely $[0, 10^6]$ for p , E_0 and E_1 , and $[0.00001, 0.99999]$ for α . It is important to emphasize that the range chosen for the parameters p , E_0 and E_1 is based on the default values for such elements found in the literature, and the range for α is based on the duality of the viscoelastic behavior (elastic + viscous), as explained in section 3.1.

Case 2. In a second step, additional constraints are imposed. Following Cheng, Polak and Pendolis (2011) formulation, E_0 is taken as the ratio between the applied stress and the strain measured in the first 60 seconds of the experimental test, i.e.

$$E_0 = \frac{\sigma}{\varepsilon(t = 60s)}. \quad (4.6)$$

Furthermore, the other parameters are restricted to the condition: if $b_1 < b_2$ then $b_i < b_{i+1}$, otherwise $b_i > b_{i+1}$. These constraints are defined aiming at a monotonic behavior of the material parameters when the stress levels are monotonically increased. The need for enforcement of these complementary constraints are further enlightened.

In both of these cases, the adopted PSO parameters are: $n_g = 200$, $n_p = 200$, $\omega = 0.5$, $\varphi_p = \varphi_g = 1$. Such values were extracted from previous works found in the literature [see Vaz and Cardoso (2014) for more details]. Moreover, the convergence of this method was tested performing the optimization procedure four times for each stress level. The implications and results obtained are presented next.

5 APPLICATIONS, RESULTS AND DISCUSSIONS

This chapter presents fitting and interpolation results for experimental measurements provided by Liu, Polak and Penlidis (2008) and Kühn (2014). Moreover the application of the MSP, in association with the fractional derivatives formulation, is employed for some cases of stress which change over the time. The chapter additionally compares the outcome of numerical schemes used in the fractional derivatives modeling: G1, P2 and SG.

5.1 CURVE FITTING

Fitting results for the two groups of experimental data considered in this work, as well as some comparisons between them, are presented in this section.

5.1.1 Curve Fitting for Experimental Data Obtained by Liu, Polak and Penlidis (2008)

The HDPE creep-compliance curves in Liu, Polak and Penlidis (2008) are converted into strain curves and used as data for testing the fractional derivative modeling given by Eq (3.33).

A parameter identification for the fractional Zener model at each experimental stress level is carried out using Eq. (4.2) for two different cases, as explained in Section 4.2.2. The five material parameters of the fractional model are identified in terms of a non-linear optimization using PSO.

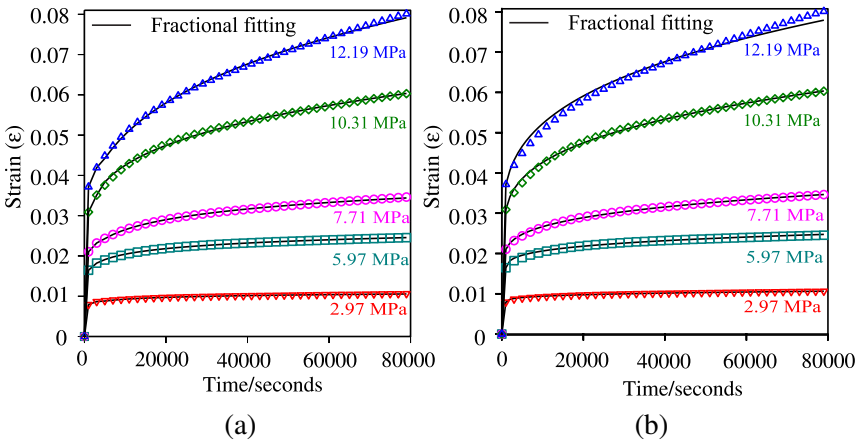
For Case 1, the identified parameters at each stress level are given in Tab. 3, and the resulting fitting, is compared to the experimental measurements in Fig. 24(a). It may be noticed in

Tab. 3 that the material parameters do not grown monotonically for increasing stress levels.

Table 3 – Identified fractional parameters for Liu’s experimental data (Case 1).

Stress level (MPa)	Fractional parameters			
	α	$p(\text{Ns}^\alpha / \text{m}^2)$	$E_0(\text{N}/\text{m}^2)$	$E_1(\text{N}/\text{m}^2)$
2.97	0.2045122	848.5291	207.48341	90249.023
5.97	0.1811692	916.3561	136.51704	83515.193
7.71	0.1879511	1321.9562	81.837660	16119.714
10.31	0.3231736	6047.9332	62.467066	555.29249
12.19	0.2898247	4870.4281	10.278508	1102.2502

Figure 24 – Fractional fitting obtained for Liu’s experimental data in Case 1 (a) and in Case 2 (b).



On the other hand, due to the additional constraints imposed in Case 2, the identified parameters showed in Tab. 4, present monotonic increase, as expected. The resulting curves in such a case are shown in Fig. 24(b).

Table 4 – Identified fractional parameters for Liu’s experimental data (Case 2).

Stress level (MPa)	Fractional parameters			
	α	$p(\text{Ns}^\alpha/\text{m}^2)$	$E_0(\text{N/m}^2)$	$E_1(\text{N/m}^2)$
2.97	0.2399289	42663.205	44.972408	1124.7627
5.97	0.2427847	56433.302	42.295203	2415.4409
7.71	0.2679076	69850.315	38.795354	3682.9055
10.31	0.2999991	89512.823	28.264060	4749.9521
12.19	0.318479	112322.31	17.797184	5932.9533

Table 5 shown the ℓ^2 norm of the relative error regarding the experimental strain for Cases 1 and 2.

Table 5 – ℓ^2 norm of the relative error between the experimental strains and the fractional fitting in Case 1 and 2.

Stress Level (MPa)	ℓ^2 norm of the relative error ($\times 10^{-8}$)	
	Case 1	Case 2
2.97	1.5368382	6.3396940
5.97	3.5057297	47.063782
7.71	1.9053371	104.431551
10.31	19.97574	217.16936
12.19	14.987934	265.7170

For this group of experimental data, the fractional fitting obtained with the material parameters in Case 1 is better than that obtained in Case 2, although the difference found is in the order of 10^{-8} . Furthermore, it was verified that the imposition of constraints (Case 2) is fundamental for finding acceptable results when using linear interpolation, as shown in Section 5.2.1.

5.1.2 Curve Fitting for Experimental Data obtained by Kühl (2014)

The results below are based on creep experimental tests made in HDPE samples by Kühl (2014). The identification of the fractional material parameters in Case 1 for each stress level is shown in Tab. 6. The resulting curves are compared to the experimental data and to the fitting given by Prony series (obtained with the parameters given in Tab. 2) in Fig. 25.

Table 6 – Identified fractional parameters obtained for Kühl’s experimental data (Case 1).

Stress level (MPa)	Fractional parameters			
	α	$p(\text{Ns}^\alpha / \text{m}^2)$	$E_0(\text{N}/\text{m}^2)$	$E_1(\text{N}/\text{m}^2)$
3.6	0.2564222	10000.000	22.314933	512.71663
5.5	0.1533441	831.05537	96.170401	6529.9876
7.2	0.2165844	1482.6964	100.00000	6948.6585
9.1	0.2178070	803.22324	99.010042	62681.855
11	0.2898683	2021.0274	87.693405	90990.084
13	0.2852317	1537.5904	75.510188	33541.788

In this group of measurements, the application of additional constraints to obtain a monotonic behavior of the parameters, led to frustrated attempts for good matching results.

Figure 25 – Fractional Zener and generalized Kelvin fittings for Kühl’s experimental data.

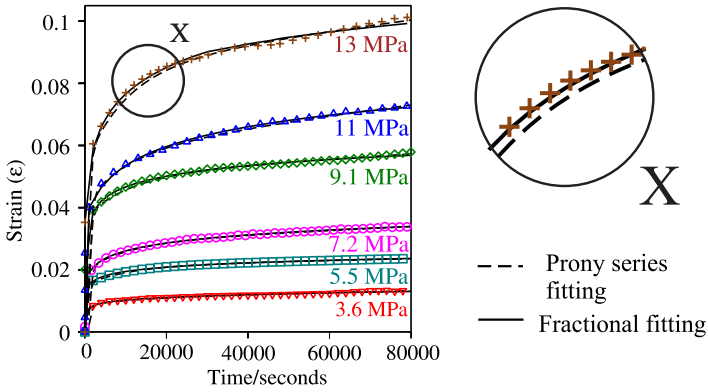


Table 7 shows the ℓ^2 norm of the relative error for both, the fractional Zener and the generalized Kelvin models, with respect to the experimental strain. It is worth noting that for all the stress levels, the ℓ^2 norm of the relative error is lower for fractional derivatives than that for Prony series modeling. Furthermore, the errors presented correspond to one and two rheological blocks for the fractional Zener and the traditional Kelvin models, respectively. It must be remarked, however, that the G1 algorithm [Eq. (2.17)] demands the storage of variables at each step of the implementation. This fact, combined to the use of the PSO, where the computation of the fractional derivative is performed for each generation, results in a very high computational cost. Conversely, modeling using Prony series requires minimal computational effort, because at each time increment, the strain is calculated with the simple evaluation of Eq. (3.5). In this regard, aiming at a reduction of computation time for the fractional derivatives approach, a comparison between the computational economic schemes P2, SG and the referential algorithm G1 is presented in Section 5.4.

Table 7 – ℓ^2 norm of the relative error between the experimental strains and both, the fractional fitting and the Prony series fitting.

Nível de tensão (Pa)	ℓ^2 norm of the relative error.	
	Fractional derivative	Prony series
3.6	0.1116343	0.1238776
5.5	0.0499800	0.0634855
7.2	0.0608742	0.1499886
9.1	0.0414798	0.0991086
11	0.0371300	0.0420484
13	0.0485603	0.0977726

5.2 CREEP AT INTERMEDIATE STRESS LEVELS

In order to estimate the creep behavior of HDPE at stress levels in the range, but different from the ones which were used to calibrate the model, the linear interpolation of the material parameters (Section 3.4.1) and the TSEP (Section 3.4.2) are compared. Such comparison is carried out for the two cases presented in Section 4.2.2. The comparison provides information on how the proposed schemes work for the nonlinear behavior of HDPE. Again, the G1 algorithm is considered as referential in the applications that involve fractional derivatives.

5.2.1 Results for Linear Interpolation

The linear interpolation procedure, Eqs. (3.41), (3.42) and (3.43) is employed for the two groups of experimental data presented in Section 4.1, as described below.

5.2.1.1 Liu's data

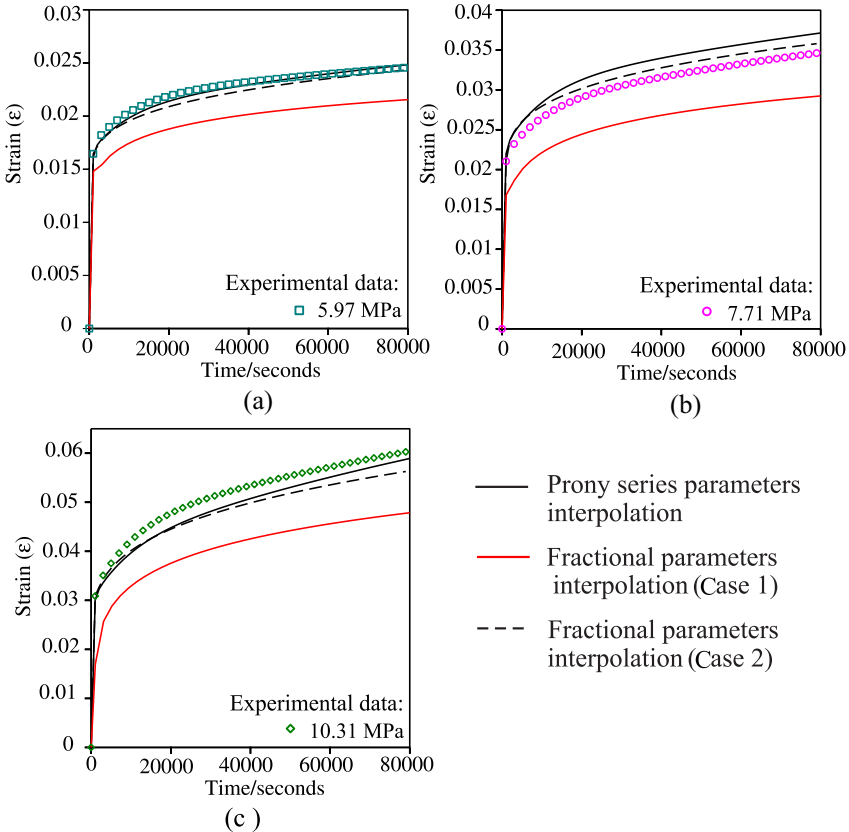
The linear interpolation scheme presented in Eq. (3.43) is employed to the fractional parameters shown in Tab. 3 (Case 1) and Tab. 4 (Case 2). The same procedure is applied to the Prony series parameters shown in Tab 1, this time employing Eqs. (3.41) and (3.42). Figure 26 shows the results for each considered stress level: (a) 5.97 MPa, (b) 7.71 MPa and (c) 10.31 MPa, which are the intermediate levels in the Liu's measurements. It is import to emphasize that the interpolated result is obtained taking the intermediate value σ with $\sigma_n \leq \sigma \leq \sigma_m$ (see Section 3.4.1).

It can be seen from Fig. 26 that the results provided in Case 1 demonstrate unsatisfactory approximations. This is expected due to the behavior of the parameters in Tab. 3. On the other hand, the additional constraints imposed in Case 2 showed up to be vital for obtaining successful approximation results in the linear interpolation for the fractional parameters. In this case, the results are comparable to those obtained by Prony series parameters interpolation. Nonetheless, this procedure does not correspond to the best possible fit for each individual stress level (Fig. 24) and, in addition, it is totally dependent on well behaved parameters.

5.2.1.2 Kühl's data

The results of the parameters linear interpolation in Case 1 for Kühl's experimental data is presented in Fig. 27 for the intermediate stress levels: (a) 5.5, (b) 7.2, (c) 9.1 and (d) 11 MPa. As explained previously in Section 5.1.2, the application of constraints to obtain a monotonic behavior of the parameters (Case 2) led to frustrated attempts for good matching results, hindering

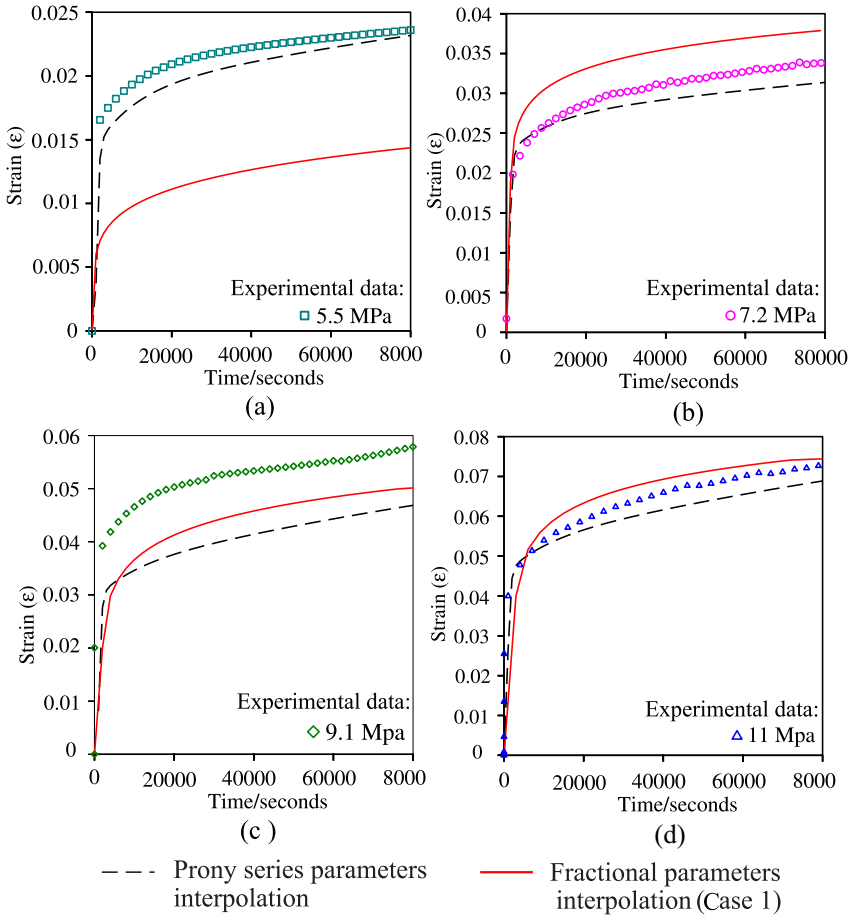
Figure 26 – Linear interpolation approach for Liu’s experimental data: (a) 5.97 MPa; (b) 7.71 MPa; (c) 10.31 MPa.



linear interpolations.

Once again, the outcome obtained using linear interpolation in Case 1 does not yield a good approximation, as consequence of the non-monotonic behavior of the identified parameters. The approximation for 11 MPa [Fig. 27(d)] seems to be somewhat close to the measured data, but this result is unsubstantiated since the reasonable outcome in this case was due to

Figure 27 – Linear interpolation approach for Kühl’s experimental data: (a) 5.5 MPa; (b) 7.2 MPa; (c) 9.1 MPa; (d) 11 MPa.



coincidence and not to the robustness of the employed method. This problem can be avoided using the TSEP, as shown in the next section.

5.2.2 Results for Time-Stress Equivalence Principle

The TSEP, described in the Section 3.4.2, is employed in association with fractional derivatives as an alternative to approximate strains at non-experimentally measured stress levels. The identified parameters used here were those obtained in Case 1 for the two groups of experimental data. The results for both of these groups are present in this section.

5.2.2.1 Liu's data

The procedure to obtain the approximations using the TSEP, starts with the time shift search for some experimentally measured stress levels. It must be performed to relate the individual compliances to a master curve defined at a reference stress. In other words, the resulting master curve is valid over the time scale at one stress level by shifting and superposing creep compliance data provided at other stress levels in a short term test (BRINSON; BRINSON, 2015) (see Section 3.4.2).

For Liu's experimental data, shift values are: $\phi_{2.97} = 1$, $\phi_{5.97} = 0.22380$, $\phi_{7.71} = 0.10471$, $\phi_{10.31} = 0.03162$, $\phi_{12.19} = 0.00800$, $\delta_{2.97} = 1$, $\delta_{5.97} = 0.90021$, $\delta_{7.71} = 0.80100$, $\delta_{10.31} = 0.55101$ and $\delta_{12.19} = 0.37001$. The shift values $\phi_{2.97}$ and $\delta_{2.97}$ are equal to unity, so that 2.97 MPa is the reference stress level.

Figure 28(a) shows the master curve and its fitting in log-log scale and Figure 28(b) gives the same graph in linear scale. Both are obtained using the horizontal and vertical shifts given by Eqs. (3.53) and (3.55) and plotted in Fig. 29(a) and 29(b), respectively.

Figure 28 – Master curve fitting in the TSEP for Liu’s data: (a) log-log scale; (b) linear scale.

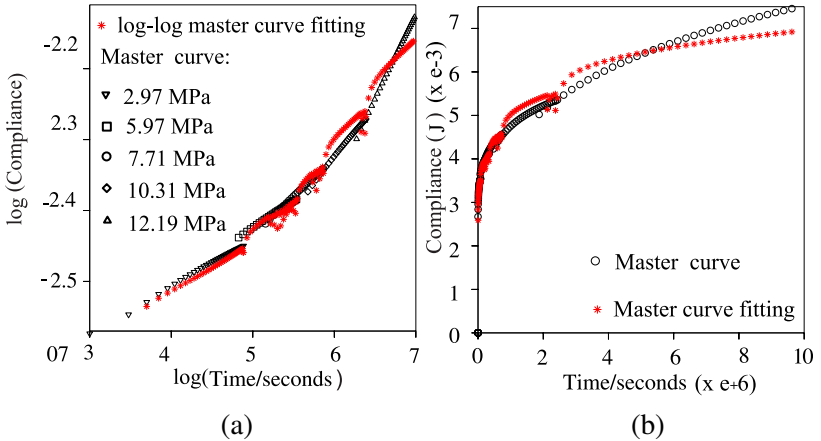


Figure 29 – Fitting of the shifts values for Liu’s data: (a) horizontal shift (ϕ_σ); (b) vertical shift (δ_σ).

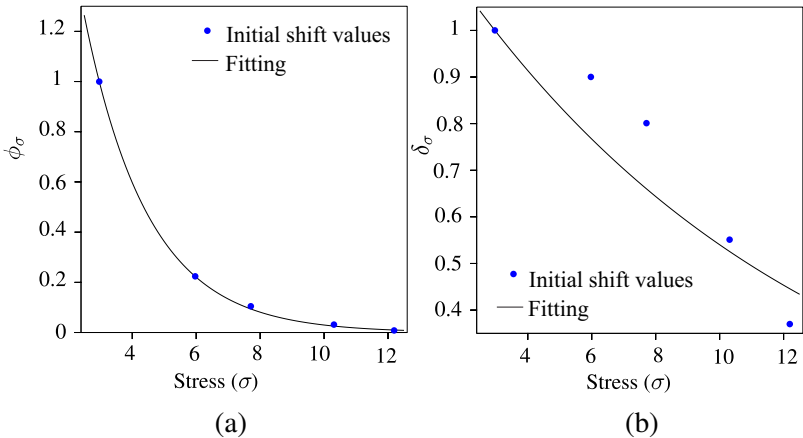


Figure 30 shows some approximations obtained by the TSEP which evince the accuracy of the approach for (a) 2.97, (b) 5.97, (c) 7.7, (d) 10.31 and (e) 12.19 MPa. The results are

visually better than those obtained by linear interpolation.

5.2.2.2 *Kühl's data*

The same procedure described in the previous section is employed for Kühl's experimental data. In this case there is no need of to use the vertical shifts δ_σ , since the use of horizontal shifts already results in good approximations. The considered stress levels for constructing the master curve are: 3.6, 7.2, 11 and 13 MPa; and the respective horizontal shifts found are: $\phi_{3.6} = 1$, $\phi_{7.2} = 0.1379288$, $\phi_{11} = 0.0194110$, and $\phi_{13} = 0.0050468$. Here, 3.6 MPa is the reference stress level. Figure 31(a) shows the resulting master curve fitting for this data in a log-log scale and Fig. 31(a) gives the same curve in a linear scale.

The horizontal shift curve is shown in Fig. 32 and the resulting approximations for some stress levels are plotted in Fig. 33.

A substantial improvement in the approximation accuracy can be observed in Fig. 33. Moreover, for the data studied in this work the TSEP provided excellent approximations irrespective of the material parameters behavior.

5.3 RESPONSE TO MULTIPLE LOADING STEPS

In addition to the creep tests at constant stresses, Liu, Polak and Penlidis (2008) studied the strain response of HDPE samples to step varying loadings. They performed experimental tests and tried to reproduce the strain response based on their linear interpolation scheme together with the MSP. In this section, (i) the fractional derivative approach is employed using the TSEP (procedure proposed in this work); (ii) the Prony series formulations is used with an interpolation of the material parameters (procedure proposed by Liu, Polak and Penlidis (2008)). Both

Figure 30 – TSEP results for Liu’s experimental data.

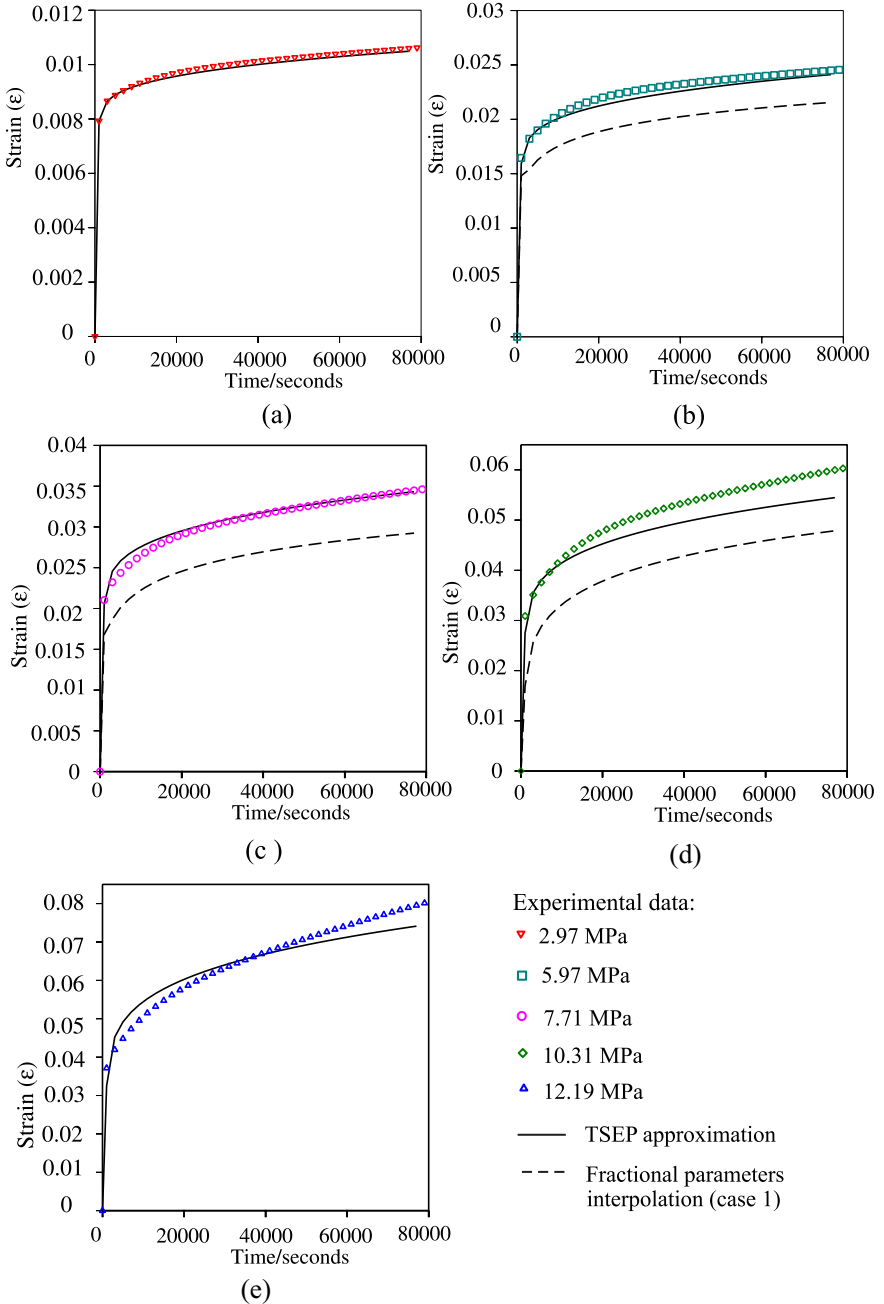


Figure 31 – Master curve fitting in the TSEP for Kühl's data: (a) log-log scale; (b) linear scale.

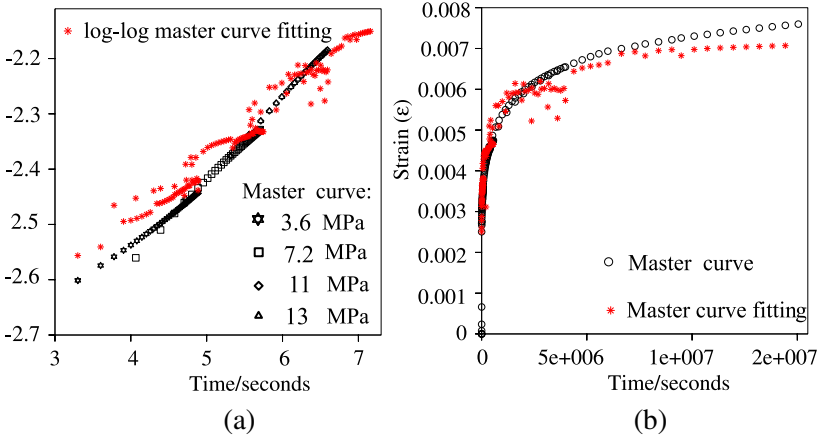


Figure 32 – Fitting of the shifts values for Kühl's data.

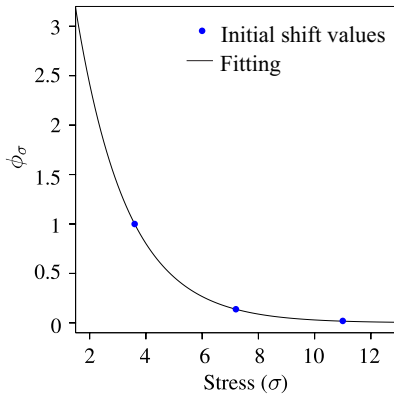
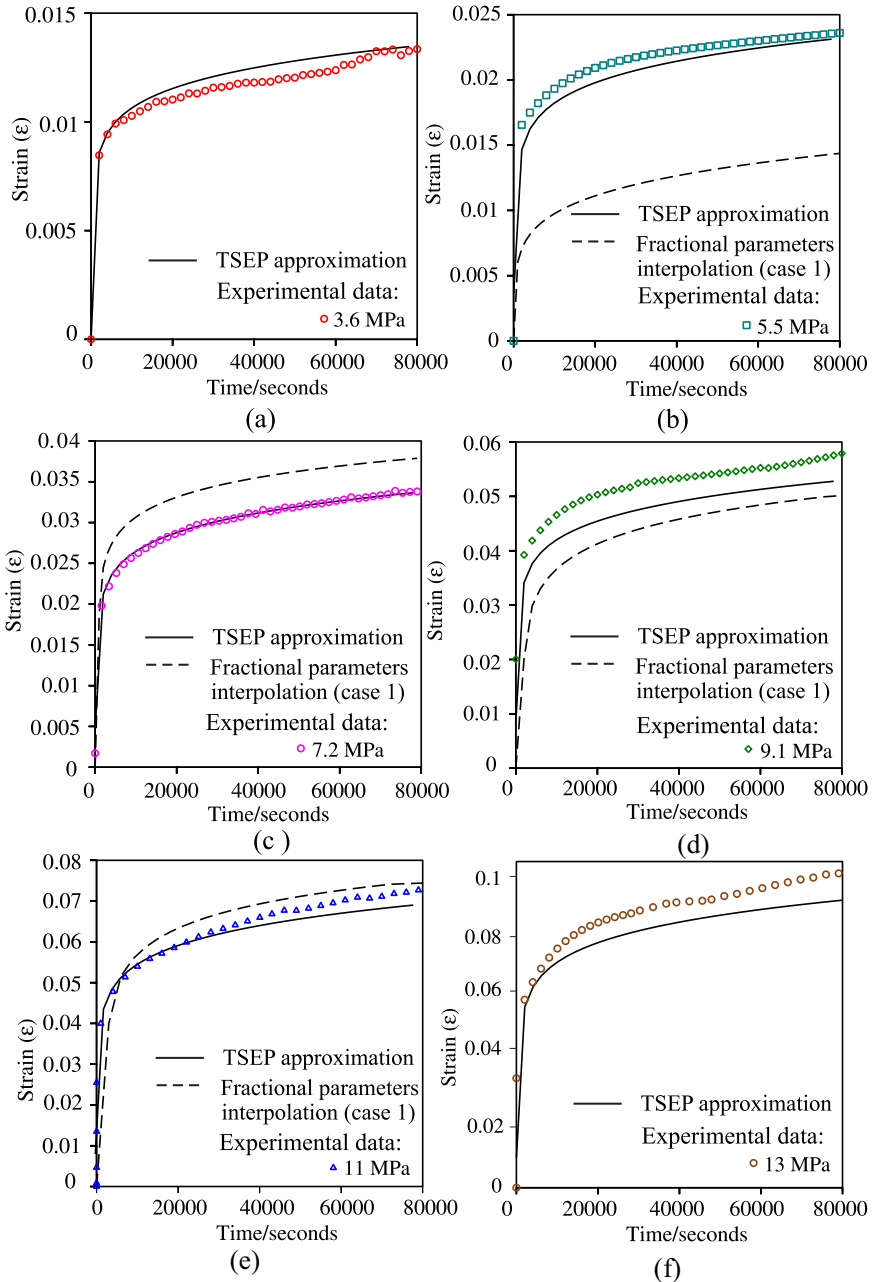


Figure 33 – TSEP results for Küh1's experimental data.



formulations are associated with the MSP (see Section 3.5) to approximate Liu's experimental data.

Figure 34 shows the comparison of simulated and experimental results for increasing and decreasing two-step loading cases. Again, the approach used in this work yields visually better results than those presented by Liu, Polak and Penlidis (2008), especially in the decreasing step loading¹.

5.4 LONG-TERM CREEP TESTS

An evaluation of different concepts for reducing the computation time and storage requirements in the fractional derivatives evaluation is presented in this section. It is performed by calculating long-term creep tests for HDPE in the stress level $\sigma = 2.97$. The algorithms P2 and SG are compared to the referential algorithm G1. The overall simulation time was $1e + 8s$ with $\Delta t = 2000s$, resulting in $N = 50000$ time steps. The material parameters considered for $\sigma = 2.97$ are shown in the Tab. 3.

5.4.1 Results for the P2 algorithm

The evaluation of the P2 algorithm is carried out by just inserting Eq. (2.18) into Eq. (3.23), where the resulting equation is similar to Eq. (3.33). The HDPE creep in the stress level 2.97 MPa is simulated for different values of N_{\max} . Figure 35(a) depicts some of these fittings in contrast with the numerical fitting by using the G1 algorithm and Fig. 35(a) shows emphasis in the interest region X.

¹ Additional quantitative comparisons regarding the accuracy of the employed method cannot be performed since the experimental data in this case was obtained through a software to extract some points in Liu's graph.

Figure 34 – Increasing two-step loading: (a) changing from 5.25 to 8.31 MPa at $t_1 \approx 16000$ s; (b) changing from 5.33 to 10.55 MPa at $t_1 \approx 18000$ s. Decreasing two-step loading: (c) changing from 10.59 to 5.35 MPa at $t_1 \approx 17000$ s; (d) changing from 8.36 to 5.29 MPa at $t_1 \approx 13000$ s.

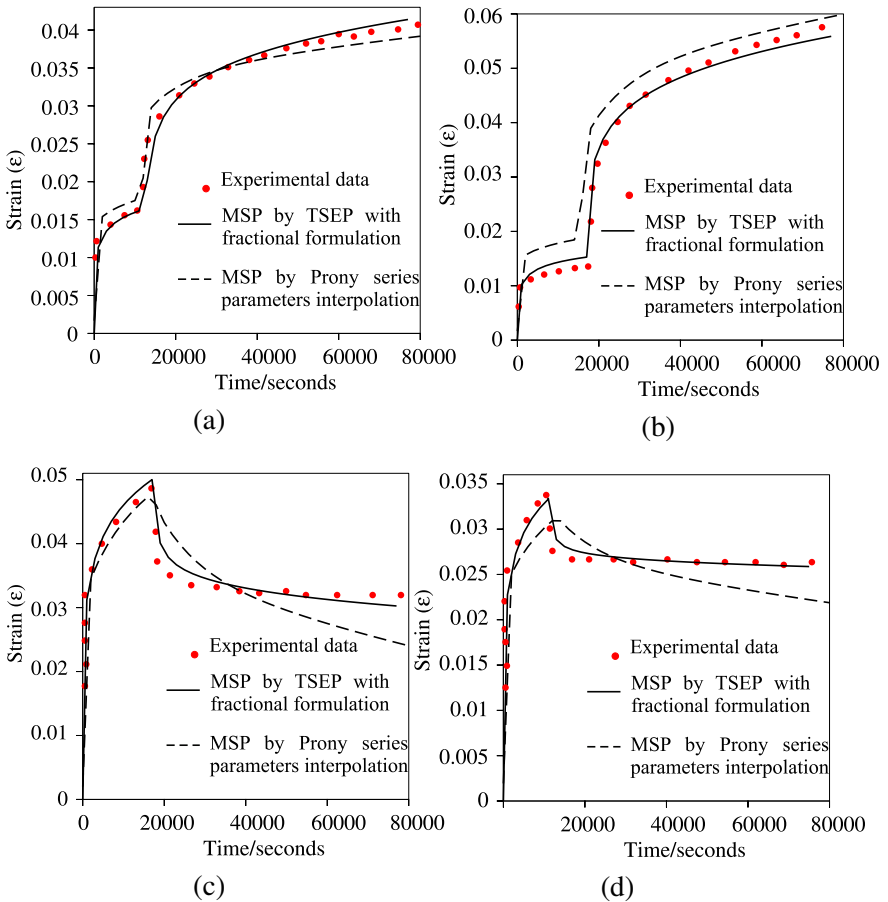
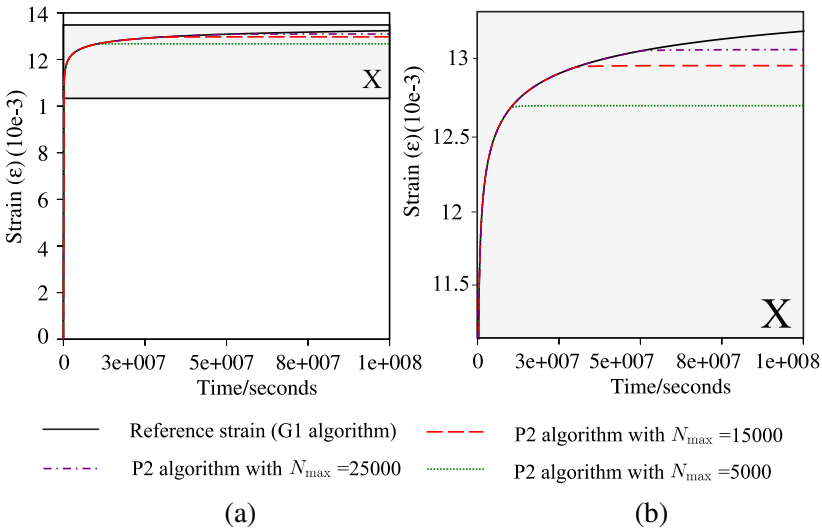


Figure 35 shows that as N_{\max} increases, the fitting becomes closer to the reference curve. This is expected, since the reference fitting is equivalent to truncation with $N_{\max} = 50000$ and there are 50000 experimental points. Figure 36(a) plot the ℓ_2 norm of the difference between algorithm G1 and the fittings provided by algorithm P2 for some truncation times N_{\max} . The same figure additionally shows the CPU time spent in each computation. Figure 36(b) presents the graph of Fig. 36(a) plotted in a logarithm scale. Although the savings could be considerably increased by reduction the factor N_{\max} , it can be observed in Fig. 35 that the underlying creep would stabilize too soon, thus increasing the calculation error. Fig. 37 shows the rate of time changing with the error (Δ time/ Δ error) for a given truncation value N_{\max} .

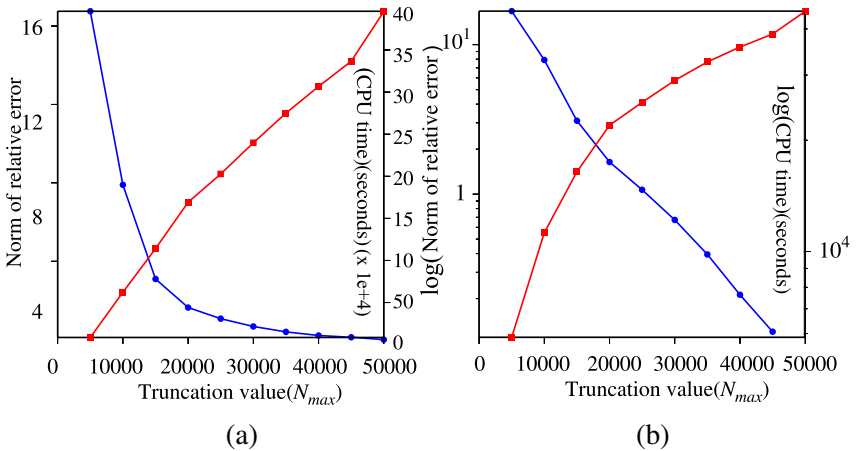
Figure 35 – (a) Application of P2 algorithm in contrast with the G1 algorithm for some values of N_{\max} ; (b) Emphasis on the interest region X.



The difference between the time required by the P2 and

the G1 algorithms is considerably large. If this tests were considered in the material parameters identification, including the PSO calculations, a much larger difference of time could be verified, since in this case the fractional derivative must be evaluated several times. Hence, although the P2 algorithm is able to reduce the numerical effort and the storage requirements, a high value of N_{\max} is needed to get an acceptable norm value. For instance, if $N_{\max} \geq 25000$ the norm verified is much lower than for values $N_{\max} \leq 25000$. On the other hand, if $N_{\max} \geq 25000$ the computational time and storage requirements increase substantially.

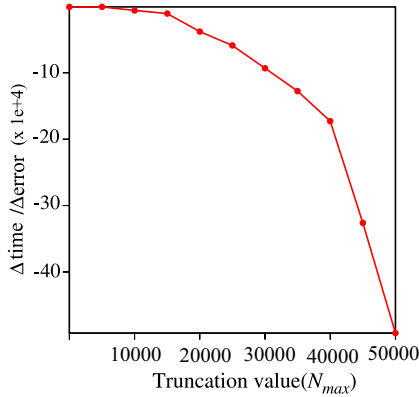
Figure 36 – ℓ^2 norm of the relative error for P2 algorithm in contrast with the CPU time: (a) linear scale; (b) logarithm scale.



5.4.2 Results for the SG algorithm

The SG algorithm is also compared to the referential algorithm. For this purpose, Eq. (2.26) is inserted into Eq. (3.23). Some values of $i = k$ (see Section 2.2.2) are adopted for evaluation, and the graphical result for three of these values is shown in Fig. 38(a). Figure 38(b) shows a detail of the interest region.

Figure 37 – Ratio (Δ time/ Δ error) of P2 algorithm in relation to the truncation value.



The actual creep behavior resulting from the reference calculation is better matched by the SG than by the P2 algorithm, since in the latter case, the creeping process unrealistically stabilizes after some time.

Figures 39(a) and (b) show the ℓ_2 norm of the relative error between the G1 and the SG, contrasting with the CPU time spent for the evaluation of the creep response using the SG algorithm in linear scale and logarithmic scales, respectively. The graph in Fig. 40 displays the rate of time changing with the error (Δ time/ Δ error) in this case.

Clearly, the ℓ_2 norm for the SG calculation is lower than that achieved with the P2 implementation. Furthermore, the CPU time spent in the computation is also smaller.

Based on the graph of Fig. 39, it can be noticed that for $500 \leq i = k \leq 1000$ the accuracy becomes much higher than if $i = k \leq 500$. Moreover, the CPU time spent in the same interval also shows great advantage compared to the time spent at the reference calculation. The SG algorithm shows good perfor-

Figure 38 – (a) Application of the SG algorithm in contrast with the G1 algorithm for some values of $i = k$; (b) Emphasis on the interest region X.

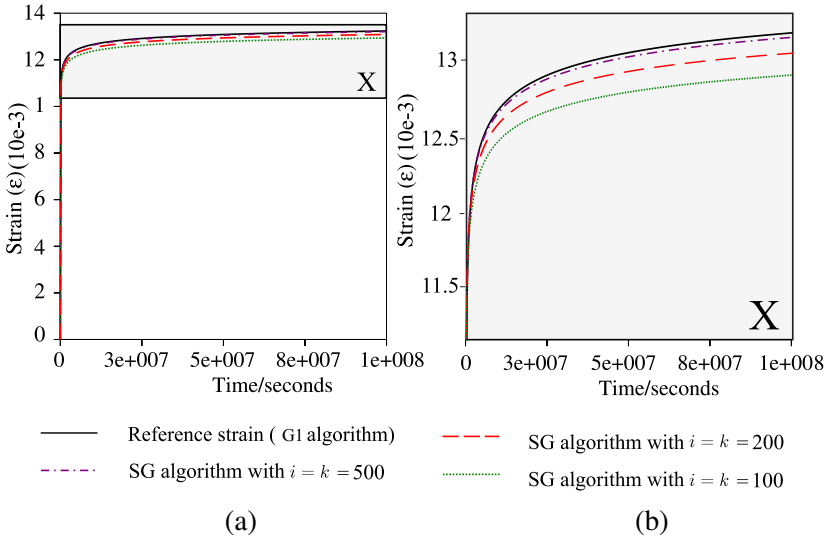


Figure 39 – ℓ_2 norm of the relative error for SG algorithm in contrast with the CPU time: (a) linear scale; (b) logarithm scale.

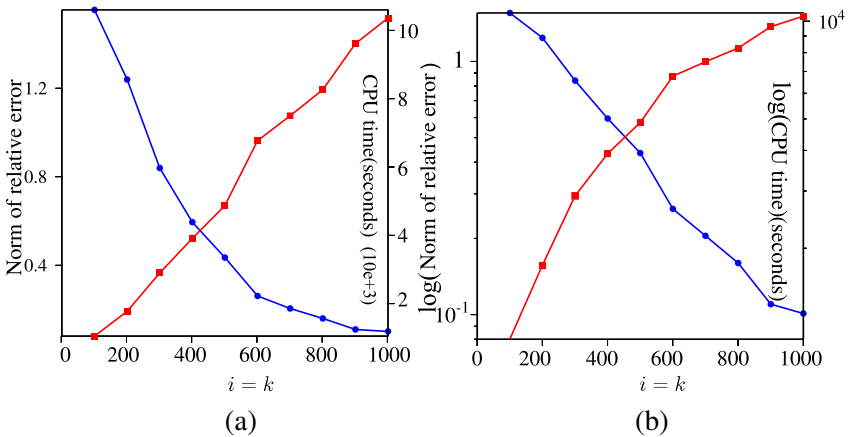
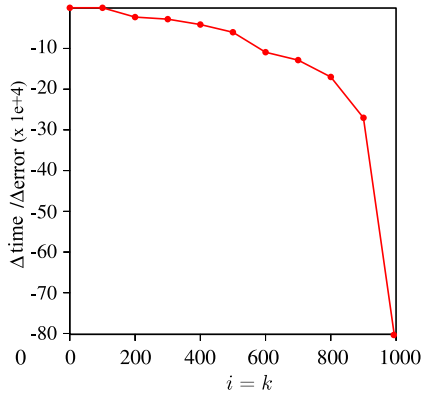


Figure 40 – Ratio (Δ time/ Δ error) of SG algorithm in relation to the parameters $i = k$.



mance, although the parameters i and k used in the simulation are chosen somewhat arbitrarily and could be optimized for further reduction of the numerical costs.

6 CONCLUSIONS

In this work, Grünwald Letnikov (GL) fractional derivative was used in conjunction with the Zener viscoelastic model. Such approach was employed aiming to model both time and nonlinear effects in a creep analysis for high density polyethylene (HDPE).

The fractional Zener model demands only four material parameters which were identified by fitting creep tests at different stress levels. In this regard, an inverse constrained optimization problem was solved using the particle swarm optimization method (PSO) in two different ways: (1) firstly, lateral constraints related to the PSO implementation were imposed; (2) secondly, additional constraints were defined to achieve a monotonic behavior of the material parameters when the stress levels are monotonically increased.

Some curves fitted by Liu, Polak and Penlidis (2008), were used to generate points in corroboration of a formulation based on the numerical fractional G1 algorithm for the two cases previously mentioned. A comparison regarding the accuracy in such cases was performed in relation to the collected sampled points. Moreover, a linear interpolation of the identified parameters and the time-stress equivalence principle (TSEP), were applied in order to estimate the creep behavior at intermediate non-experimentally measured stress levels. It was found that the additional constraints, in Case 2, lead to less accurate results in the individual fittings than in Case 1, but the observed difference between them was just around 10^{-8} . Apart from that, only in Case 2 the application of the fractional parameters interpolation for estimating the creep behavior at intermediate stresses, provides results comparable to other interpolation schemes suggested in the literature. Such fact means that, while no significant loss of accuracy is found in the fitting with the introduction of the

additional constraints, it is mandatory to include them if linear interpolation schemes are to be used. On the other hand, monotonicity of the material parameters was not required for the TSEP implementation in any the problems tested.

The fractional derivatives modeling was also compared with the traditional Kelvin model described by Prony series to fit actual experimental creep data obtained by Kühl (2014). In this group, the application of additional constraints to obtain a monotonic behavior of the parameters in Case 2, led to frustrated attempts for good matching results. Therefore, the results were disregarded for this case. The linear interpolation of the material parameters and the TSEP were once again applied and compared for this data. It was noticed that the fractional procedure presents better matching and less material parameters to describe the creep behavior in relation to the traditional Kelvin model. However, the linear interpolation of the fractional parameters for this group, lead to unsatisfactory approximations. The latter result was expected due to the parameters obtained in this case. Conversely, the TSEP application resulted in remarkably accurate intermediate creep approximations for most cases tested in this work.

In addition to the fittings and interpolation procedures described above, the modified superposition principle (MSP) was used to predict the strain response of HDPE samples when subjected to stress levels that change in a stepwise pattern from time to time. An approach based on the TSEP in association with fractional derivatives was proposed and compared with the formulation developed by Liu, Polak and Penlidis (2008). In all cases analyzed the method suggested in this work showed better agreement with the experimental data.

Although the fractional derivatives method presents accurate results with less material parameters to account the viscoelastic phenomenon, the involved computational effort is much

higher when compared to the traditional Kelvin model. In order to cope with this issue, two approximate but faster algorithms, P2 and SG, are implemented and their time/accuracy performance is evaluated in relation to the referential algorithm G1. It is verified that the P2 procedure shows a high CPU time reduction but a significant accuracy loss when compared to the reference algorithm. The CPU time reduction achieved with the SG is even higher and the relative error much lower, in agreement with the statements of Schmidt and Gaul (2002). In other words, the SG algorithm was shown to maintain the benefits of accuracy provided by fractional derivatives, while reducing drastically the underlying numerical effort. Clearly the numerical analyses performed evince a general trend in the comparative behavior of the algorithms. However, quantitative conclusions regarding the trade-off between cost and accuracy would require a deeper investigation.

This study showed that the fractional derivatives formulation is a very helpful tool to perform calculation specifically dealing with viscoelastic problems. This matter can unfold in different directions. In this sense, continuity workflow suggestions are summarized below:

1. To implement the Caputo fractional derivative for the same applications proposed in this research and compare the results provided by such method with those showed in the present study;
2. To extend the proposed fractional formulation to bidimensional models of viscoelasticity in conjunction with finite element method;
3. To implement other economy schemes proposed in the literature for the fractional derivatives;

4. To extend the fractional formulation to viscoelastoplastic behavior;
5. To improve the parameters identification including relaxation and dynamic tests.

REFERENCES

AKIL, K. A. K.; MUNIANDY, S. V.; LIM, E. Fractional reaction-diffusion equations for modelling complex biological patterns. *Malaysian Journal of Fundamental and Applied Sciences*, v. 8, n. 3, 2012. Cited on page 42.

AKLONIS, J.; MACKNIGHT, J. *Introduction to Polymer Viscoelasticity*]. Wiley-Interscience Publication, 1983. Available from Internet: <<https://books.google.com.br/books?id=YdTkPPqsL6sC>>. Cited on page 69.

ARTIN, E.; BUTLER, M. *The Gamma Function*. Dover Publications, 2015. (Dover Books on Mathematics). ISBN 9780486803005. Available from Internet: <<https://books.google.com.br/books?id=c3R2BgAAQBAJ>>. Cited on page 128.

AYOUB, G.; ZAÏRI, F.; NAÏT-ABDELAZIZ, M.; GLOAGUEN, J. Modelling large deformation behaviour under loading–unloading of semicrystalline polymers: application to a high density polyethylene. *International Journal of Plasticity*, Elsevier, v. 26, n. 3, p. 329–347, 2010. Cited on page 53.

BAGLEY, R. L.; TORVIK, P. J. Fractional calculus. a different approach to the analysis of viscoelastic damped structures. *AIAA Journal*, p. 741–748, 1983. Cited on page 61.

BAGLEY, R. L.; TORVIK, P. J. A theoretical basic for the application of fractional calculus to viscoelasticity. *Journal of Rheology*, v. 27, n. 3, p. 201–210, 1983. Cited 3 times on pages 33, 59, and 60.

BAI, Q. Analysis of particle swarm optimization algorithm. *Computer and information science*, 2010. Cited on page 82.

BARBERO, E. Time-temperature-age superposition principle and its application to linear viscoelastic materials. 2010. Cited on page 72.

BRINSON, H.; BRINSON, L. *Polymer Engineering Science and Viscoelasticity: An Introduction*. Springer US, 2015. (SpringerLink : Bücher). ISBN 9781489974853. Available from Internet: <<https://books.google.com.br/books?id=kmpnBgAAQBAJ>>. Cited 3 times on pages 70, 72, and 98.

CAPUTO, M. Linear models of dissipation whose q is almost frequency independent. *Annali di Geofisica*, 1966. Cited on page 59.

CAPUTO, M. Linear models of dissipation whose q is almost frequency independent. *Geophys. J. R. Astr. Soc.*, 1967. Cited on page 59.

CAPUTO, M.; MAINARDI, F. Linear models of dissipation in inelastic solids. *Riv. Nuovo Cimento*, p. 161–198, 1971. Cited on page 59.

CAPUTO, M.; MAINARDI, F. A new dissipation model based on memory mechanism. *Pure Appl. Geophys*, 1971. Cited on page 59.

CHENG, J.; POLAK, M.; PENDILIS, A. An alternative approach to estimating parameters in creep models of high-density polyethylene. *Polymer engineering and science*, 2011. Cited on page 87.

COOK, R.; MALKUS, D.; PLESHA, M. *Concepts and Applications of Finite Element Analysis*. Wiley, 1989. ISBN 9780471503194. Available from Internet: <<https://books.google.com.br/books?id=irZHPgAACAAJ>>. Cited on page 144.

Costa Haveroth, T. *Estudo da Viscoelasticidade com Modelos Reológicos Fracionários*. [S.l.], 2015. Cited 2 times on pages 50 and 142.

Costa Haveroth, T.; MUÑOZ-ROJAS, P.; KUHL, A.; SASSE, F. D. Modeling hdpe nonlinear viscoelastic behavior using fractional derivatives: parameters interpolation and economy schemes. In: *Fifth International Symposium on Solid Mechanics*. [S.l.: s.n.], 2015. Cited on page 68.

DASAPPA, P.; LEE-SULLIVAN, P.; XIAO, X. Development of viscoplastic strains during creep in continuous fibre gmt composites. *Composites Part B: Engineering*, Elsevier, v. 41, n. 1, p. 48–57, 2010. Cited on page 52.

DAVIS, H. *The Theory of Linear Operators*. Read Books, 2008. ISBN 9781443731492. Available from Internet: <<https://books.google.com.br/books?id=yW2NWFcWkgMC>>. Cited on page 39.

DEALY, J.; WISSBRUN, K. *Introduction to Nonlinear Viscoelasticity*. [S.l.]: Springer Netherlands, 1999. Cited on page 32.

DENG, W. Short memory principle and a predictor-corrector approach for fractional differential equations. *Journal of Computational and Applied Mathematics*, v. 206, n. 1, p. 174–188, 2007. Cited on page 44.

ELLEUCH, R.; TAKTAK, W. Viscoelastic behavior of hdpe polymer using tensile and compressive loading. *Journal of Materials Engineering and Performance*, 2006. Cited on page 32.

FINDLEY, W. K.; LAI, J. S. Y. A modified superposition principle applied to creep of nonlinear viscoelastic material under abrupt changes in state of combined stress. *TRANSACTIONS OF*

THE SOCIETY OF RHEOLOGY, 1967. Cited 3 times on pages 72, 73, and 74.

FINDLEY, W. N.; DAVIS, F. A. *Creep and Relaxation of Non-linear Viscoelastic Materials*. Dover Publications, 2013. (Dover Civil and Mechanical Engineering). ISBN 9780486145174. Available from Internet: <<http://books.google.com.br/books?id=AZuNioxH\i4C>>. Cited on page 54.

FRIEDRICH, C.; SCHISSEL, H.; BLUMEN, A. Constitutive behavior modeling and fractional derivatives. *Advances in the Flow and Rheology of non-Newtonian Fluids- Part*, p. 429–466, 1999. Cited 2 times on pages 33 and 59.

GAUL, L.; SCHMIDT, A. Experimental determination and modeling of material damping. *VDI-Berichte*, p. 17–40, 2007. Cited 5 times on pages 49, 61, 133, 141, and 142.

GEMANT, A. A method of analyzing experimental results obtained from elastiviscous bodies. *Physics* 7, 1936. Cited on page 59.

GEMANT, A. On fractional differentials. *Phil. Mag.*, 1938. Cited on page 59.

GERASIMOV, A. A generalization of linear laws of deformation and its applications to problems of internal friction. *Prikl. Matem. i Mekh. (PMM)*, 1948. Cited on page 59.

GLOCKLE, W. G.; NONNENMACHER, T. F. Fractional integral operators and fox functions in the theory of the viscoelasticity. *Macromolecules*, 1991. Cited 2 times on pages 33 and 59.

HODGE, I. M.; HUVARD, G. S. Effects of annealing and prior history on enthalpy relaxation in glassy polymers. 3. experimental and modeling studies of polystyrene. *Macromolecules*, ACS Publications, v. 16, n. 3, p. 371–375, 1983. Cited on page 53.

JIA, J. H.; SHEN, X. Y.; HUA, H. X. Viscoelastic behavior analysis and application of the fractional derivative maxwell model. *Journal of vibration and control*, 2007. Cited on page 60.

KENNEDY, J.; EBERHART, R. Particle swarm optimization. In: *Proceedings of IEEE International Conference on Neural Networks*. [S.l.: s.n.], 1995. Cited on page 82.

KENNEDY, J.; EBERHART, R.; SHI, Y. *Swarm Intelligence*. Morgan Kaufmann Publishers, 2001. (Evolutionary Computation Series). ISBN 9781558605954. Available from Internet: <<https://books.google.com.br/books?id=vOx-QV3sRQsC>>. Cited on page 82.

KÜHL, A. *Uma Formulação Viscoelastoplástica Não linear Aplicada ao Polietileno de Alta Densidade*. Dissertação (Mestrado) — UNIVERSIDADE DO ESTADO DE SANTA CATARINA, 2014. Cited 13 times on pages 14, 17, 28, 33, 35, 58, 78, 79, 80, 81, 89, 92, and 112.

KOELLER, R. C. Application of fractional calculus to the thory of viscoelasticity. *Appl. Mech.*, n. 51, p. 299–307, 1984. Cited on page 60.

KOLOWANKAR, K. M.; GANGAL, A. D. Fractional diferentiability of nowhere diferentiable functions and di- mensions. *CHAOS*, American Institute of Phycis, 1996. Cited on page 38.

KRISHNASWAMY, R. K.; LAMBORN, M. J.; SUKHADIA, A. M.; REGISTER, D. F.; MAEGER, P. L.; LEEBERS, P. S. Rapid crack propagation failures in hdpe pipes: Structure–property investigations. *Polymer Engineering and Science*, 2006. Cited on page 32.

LAI, J.; BAKKER, A. Analysis of the nonlinear creep of high-density polyethylene. *Polymer*, 1995. Cited 2 times on pages 32 and 72.

LEWANDOWSKI, R.; CHORAŚYCZEWSKI, B. Identification of parameters of the fractional rheological model of viscoelastic dampers. In: *Symposium Vibrations in Physical Systems*. [S.l.: s.n.], 2010. Cited on page 86.

LION, A. On the thermodynamics of fractional damping elements. *Continuum Mechanics and Thermodynamics*, v. 9, n. 2, p. 83–96, 1997. Cited 2 times on pages 33 and 59.

LIU, H.; POLAK, M. A.; PENLIDIS, A. A. A practical approach to modeling time-dependent nonlinear creep behavior of polyethylene for structural applications. *Polymer Engineering and Science*, 2008. Cited 16 times on pages 17, 28, 32, 33, 35, 51, 52, 67, 75, 77, 78, 89, 100, 104, 111, and 112.

LOVERRO, A. Fractional calculus: history, definitions and applications for the engineer. *Rapport technique, Univeristy of Notre Dame: Department of Aerospace and Mechanical Engineering*, 2004. Cited 3 times on pages 37, 38, and 127.

LUO, W.; YANG, T.; AN, Q. Time-temperature stress equivalence and its application to nonlinear viscoelastic materials. *Acta Mechanica Solida Sinica*, 2001. Cited 5 times on pages 51, 68, 69, 71, and 72.

MAINARDI, F. *Fractional Calculus and Waves in Linear Viscoelasticity: An Introduction to Mathematical Models*. World Scientific Publishing Company Pte Limited, 2010. ISBN 9781848163300. Available from Internet: <<http://books.google.com.br/books?id=3DZ9RuBTHo0C>>. Cited 2 times on pages 59 and 60.

MAINARDI, F. An historical perspective on fractional calculus in linear viscoelasticity. *Fractional Calculus and Applied Analysis*, 2012. Cited on page 59.

MAINARDI, F.; SPADA, G. Creep, relaxation and viscosity properties for basic fractional models in rheology. *The European Physical Journal*, 2011. Cited on page 60.

MEYERS, M.; CHAWLA, K. *Mechanical Behavior of Materials*. Cambridge University Press, 2009. ISBN 9780521866750. Available from Internet: <<https://books.google.com.br/books?id=LXcjEAZ9tX4C>>. Cited on page 52.

MUI, J. Viscoelastic-viscoplastic model to predict creep in a random chopped mat thermoplastic composite. 2008. Cited 2 times on pages 52 and 53.

MUÑOZ-ROJAS, P.; KÜHL, A. Modeling nonlinear viscoelastic behavior of high density polyethylene (hdpe): Application of stress-time equivalence versus interpolation of rheological properties. In: *International Symposium on Solid Mechanics*, 2011. Cited 2 times on pages 32 and 71.

NISHIMOTO, K. An essence of nishimoto's fractional calculus (calculus in the 21st century): integrations and differentiations of arbitrary order. *Koriyama, Japan*, 1991. Cited on page 37.

OLDHAM, K. B.; SPANIER, J. *The fractional calculus*. New York-London: Academic Press, 1974. Cited 3 times on pages 40, 44, and 145.

OLIVEIRA, E. C. de; MACHADO, J. A. T. A review of definitions for fractional derivatives and integral. *Mathematical Problems in Engineering*, 2014. Cited on page 38.

ORTIGUEIRA, M. D. *Fractional Calculus for Scientists and Engineers*. Springer Science and Business Media, 2011. (Lec-

ture Notes in Electrical Engineering). Available from Internet: <<https://books.google.com.br/books?id=YdTkPPqsL6sC>>. Cited 2 times on pages 125 and 145.

PADOVAN, J. Computational algorithms for fe formulations involving fractional operators. *Comp. Mech.*, 1987. Cited 2 times on pages 33 and 46.

PARK, S.; SCHAPERY, R. Methods of interconversion between linear viscoelastic material functions. part i—a numerical method based on prony series. *International Journal of Solids and Structures*, Elsevier, v. 36, n. 11, p. 1653–1675, 1999. Cited on page 58.

PETERS, M. Multifunctional polymer hybrid nanoparticles for biomedical applications. tUL, 2013. Cited on page 68.

PIRES, E.; MACHADO, J.; OLIVEIRA, P. Particle swarm optimization: Dynamical analysis through fractional calculus. In: _____. *Particle Swarm Optimization*. [S.l.: s.n.], 2009. Cited on page 86.

PODLUBNY, I. *Fractional Differential Equations*. San Diego-Boston-New York-London-Tokyo-Toronto: Academic Press, 1999. Cited on page 44.

RABOTNOV, Y. N. Equilibrium of an elastic medium with after effect. *Prikl. Matem. i Mekh. (PMM)*, 1948. Cited on page 59.

RAO, S. *Vibration of Continuous Systems*. Wiley, 2007. ISBN 9780471771715. Available from Internet: <<https://books.google.com.br/books?id=kWja9NTH0bEC>>. Cited on page 136.

RIANDE, E.; DIAZ-CALLEJA, R.; PROLONGO, M.; MASEGOSA, R.; SALOM, C. *Polymer Viscoelasticity: Stress and Strain in Practice*. Taylor & Francis, 1999. (Plastics Engineering). ISBN 9780824779047. Available from Internet:

<http://books.google.com.br/books?id=-dpOEMX76GwC>.
Cited on page 51.

ROSSIKHIN, Y. A.; SHITIKOVA, M. V. Applications of fractional calculus to dynamic problems of solid mechanics: novel trends and recent results. *Appl. Mech.*, 2010. Cited on page 60.

SAMKO, S. G.; KILBAS, A. A.; MARICHEV, O. I. *Fractional integrals and derivatives - theory and applications*. 1a. ed. New York: Gordon and Breach Science Publishers, 1987. Cited on page 38.

SCHAPERLY, R. A. On the characterization of nonlinear viscoelastic materials. *Polymer Engineering and Science*, 1969. Cited on page 32.

SCHIESSEL, H.; METZLER, R.; BLUMEN, A.; NONNEN-MACHER, T. Generalized viscoelastic models: their fractional equations with solutions. *Journal of physics A: Mathematical and General*, IOP Publishing, v. 28, n. 23, p. 6567, 1995. Cited on page 56.

SCHMIDT, A.; GAUL, L. Implementation of viscoelastic constitutive stress-strain relation involving fractional time derivatives. *Proceedings of the 2nd European Conference on Constitutive Models for Rubber*, p. 79–89, 2001. Cited on page 60.

SCHMIDT, A.; GAUL, L. Finite element formulation of viscoelastic constitutive equations using fractional time derivatives. *Nonlinear Dynamics*, 2002. Cited 6 times on pages 42, 45, 46, 47, 113, and 129.

SCHMIDT, A.; GAUL, L. On the numerical evaluation of fractional derivatives in multi-dof systems. *Signal processing*, 2006. Cited 2 times on pages 135 and 142.

SCOTT-BLAIR, G. W. Analytical and integrative aspects of the stress-strain-time problem. *J. Scientific Instruments*, 1944. Cited on page 59.

SCOTT-BLAIR, G. W. *Survey of General and Applied Rheology*. [S.l.]: Isaac Pitman and Sons, 1944. Cited on page 59.

SHI, Y.; EBERHART, R. A modified particle swarm optimizer. In: *Evolutionary Computation Proceedings of IEEE World Congress on Computational Intelligence*. [S.l.: s.n.], 1998. Cited on page 82.

SOUSA, E. How to approximate the fractional derivative of order $1 < \alpha \leq 2$. *International Journal of Bifurcation and Chaos*, World Scientific, v. 22, n. 04, p. 1250075, 2012. Cited on page 42.

TALLA, P.; ALABEWEH, F.; FOGUE, M.; FOADIENG, E. Time stress equivalence principle applied to nonlinear creep of bibolo. *Acta Mechanica Solida Sinica*, 2014. Cited on page 69.

TSCHOEGL, N. T. *The Phenomenological Theory of Linear Viscoelastic Behavior*. 2. ed. [S.l.]: Springer-Verlag, 1989. Cited on page 32.

VAZ, M.; CARDOSO, E. Aspects of identification of elastic-plastic parameters using heuristic algorithms. In: *World Congress on Computational Mechanics*. [S.l.: s.n.], 2014. Cited 2 times on pages 83 and 87.

WELCH, S. W. J.; RORRE, R. A. L.; DUREN, R. G. J. Application of time-based fractional calculus methods to viscoelastic creep and stress relation of materials. *Mechanic 423s of time-Dependent Materials*, v. 3, p. 279–303, 1999. Cited on page 59.

WINEMAN, A. S.; RAJAGOPAL, K. R. *Mechanical Response of Polymers: An Introduction*. [S.l.]: Cambridge University, 2000. Cited 2 times on pages 32 and 62.

APPENDIX A – SOME DEFINITIONS OF FRACTIONAL DERIVATIVES

The following definitions for $\alpha >$ are originally found in the work of Ortigueira (2011).

Left side Riemann–Liouville:

$$D_{-}^{\alpha} f(t) = \frac{1}{\Gamma(n - \alpha)} \frac{d^n}{dt^n} \int_a^t f(\tau) \cdot (t - \tau)^{n-\alpha-1} d\tau, \quad (\text{A.1})$$

with $n \in \mathbb{N}$ and the derivative defined in the interval $[a, t]$.

Right side Riemann–Liouville:

$$D_{+}^{\alpha} f(t) = \frac{(-1)^n}{\Gamma(n - \alpha)} \frac{d^n}{dt^n} \int_t^b f(\tau) \cdot (\tau - t)^{n-\alpha-1} d\tau, \quad (\text{A.2})$$

with $n \in \mathbb{N}$ and the derivative defined in the interval $[t, b]$.

Left side Caputo:

$$D_{-}^{\alpha} f(t) = \frac{1}{\Gamma(n - \alpha)} \int_a^t f^{(n)}(\tau) \cdot (t - \tau)^{n-\alpha-1} d\tau, \quad t > 0, \quad (\text{A.3})$$

with $n \in \mathbb{N}$ and the derivative defined in the interval $[a, t]$.

Right side Caputo:

$$D_{+}^{\alpha} f(t) = \frac{1}{\Gamma(n - \alpha)} \int_t^b f^{(n)}(\tau) \cdot (\tau - t)^{n-\alpha-1} d\tau, \quad (\text{A.4})$$

with $n \in \mathbb{N}$ and the derivative defined in the interval $[t, b]$.

Marchaud:

$$D_{+}^{\alpha} f(t) = c \cdot \int_0^{\infty} \frac{\Delta_{\tau}^k f(t)}{\tau^{1+\alpha}} d\tau, \quad (\text{A.5})$$

with c a constant, Δ_{τ}^k the time step and the derivative defined in the interval $[0, \infty)$.

Generalized function:

$$D^\alpha f(t) = \frac{1}{\Gamma(-\alpha)} \int_{-\infty}^t f(\tau) \cdot (t - \tau)^{-\alpha-1} d\tau \quad (\text{A.6})$$

Left Grünwald–Letnikov:

$$D_-^\alpha f(t) = \lim_{\Delta t \rightarrow 0^+} \frac{1}{\Delta t^\alpha} \sum_{k=0}^{\infty} (-1)^k \binom{\alpha}{k} f(t - k\Delta t), \quad (\text{A.7})$$

with Δt the time step.

Right Grünwald–Letnikov:

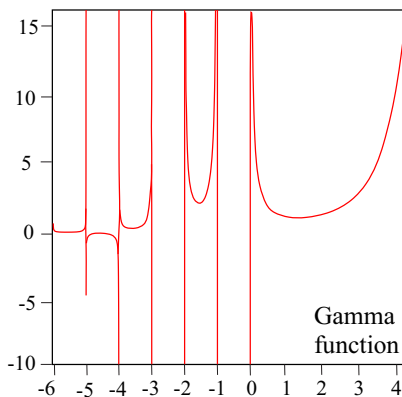
$$D_+^\alpha f(t) = \lim_{\Delta t \rightarrow 0^+} \frac{1}{\Delta t^\alpha} \sum_{k=0}^{\infty} (-1)^k \binom{\alpha}{k} f(t + k\Delta t), \quad (\text{A.8})$$

with Δt the time step.

APPENDIX B – GAMMA FUNCTION

According to Loverro (2004), the interpretation of the Gamma function is simply the extension of the factorial for all real numbers, except for negative integers and zero, as can be seen in Fig. 41.

Figure 41 – Gamma function, $\Gamma(x)$.



In general, the most extensively used definition for the Gamma function is known as Euler integral, and is given by

$$\Gamma(x) = \int_0^{\infty} t^{x-1} e^{-t} dt, \quad (\text{B.1})$$

where $x \in \mathbb{C}$ such that $\text{Re}(x) > 0$.

The Gamma function also satisfies the functional equation

$$\Gamma(x + 1) = x\Gamma(x). \quad (\text{B.2})$$

Equation (B.2) is obtained calculating $\Gamma(x + 1)$ in the form

$$\Gamma(x + 1) = \int_0^{\infty} t^x e^{-t} dt.$$

Using integration by parts, one can rewrite

$$\int_0^{\infty} t^x e^{-t} dt = x \int_0^{\infty} t^{x-1} e^{-t} dt. \quad (\text{B.3})$$

The left side of Eq. B.3 is $\Gamma(x + 1)$, and the right side is $x\Gamma(x)$. In this way, a recursive relationship can be observed:

$$\begin{aligned} \Gamma(x + 1) &= x\Gamma(x), \\ \Gamma(x) &= (x - 1)\Gamma(x - 1), \\ \Gamma(x - 1) &= (x - 2)\Gamma(x - 2), \\ &\vdots \end{aligned} \quad (\text{B.4})$$

Obviously $\Gamma(1) = 1$, and using (B.2) it comes out that

$$\begin{aligned} \Gamma(2) &= 1\Gamma(1) = 1 = 1! \\ \Gamma(3) &= 2\Gamma(2) = 2 \cdot 1! = 2! \\ \Gamma(4) &= 3\Gamma(3) = 3 \cdot 2! = 3! \\ &\vdots \\ \Gamma(n + 1) &= n\Gamma(n) = n(n - 1)! = n! \end{aligned} \quad (\text{B.5})$$

with $n \in \mathbb{N}$. Equation (B.5) is also commonly referred as a definition for the Gamma function and is used in this work.

There are some alternative definitions for this special function. For instance

$$\Gamma(x) = \int_0^1 (\ln y)^{x-1} dy. \quad (\text{B.6})$$

and

$$\Gamma(x) = \int_{-\infty}^{+\infty} e^{xz} e^{-e^z} dz. \quad (\text{B.7})$$

The latter two equations are obtained from Eq. (B.1), just taking $y = e^{-t}$ e $z = \ln t$, respectively. In the book of Artin and Butler (2015) the above definitions are discussed in the pure mathematics framework.

APPENDIX C – ANALYSIS OF THE SG ALGORITHM

The validation of Eq. (2.24) is illustrated in Fig. 42(a), (b), (c) and (d), where the ratio

$$R_f = \frac{T_n - T_0}{T_\infty - T_0} \approx R_1 = \frac{T_n^1 - T_0^1}{T_\infty^1 - T_0^1} \xrightarrow{t \rightarrow \infty} 1, \quad (\text{C.1})$$

is plotted for each elementary function showed below:

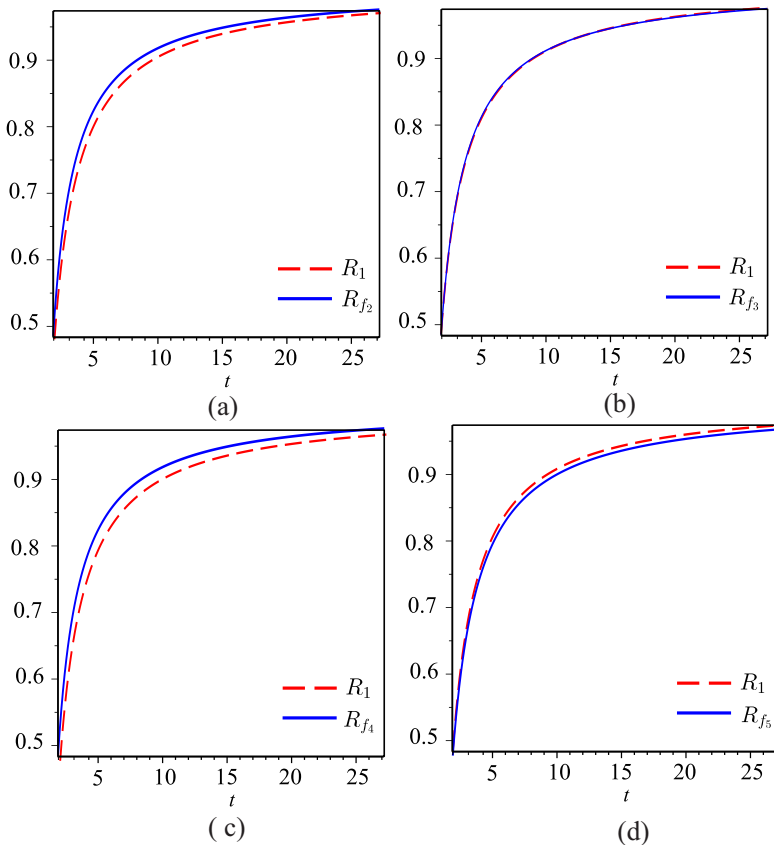
$$\begin{aligned} f_1(t) &= 1, \\ f_2(t) &= t, \\ f_3(t) &= \sin(\pi t), \\ f_4(t) &= e^t, \\ f_5(t) &= \frac{1}{t}. \end{aligned} \quad (\text{C.2})$$

The considered time interval is $[2, 27]s$ and the additional data are: $\alpha = 0.5$, $i = k = 20$ and $t_a = 2$, as suggested by Schmidt and Gaul (2002).

The accuracy of the approximation of Eq. (2.25) is also demonstrated using the same elementary functions given in Eq. (C.2). The transfer function T_n is evaluated in the interval $[2, 27]$ with $t_a = 2$. The time step is $t_a/n = \Delta t = 0.05s$, where $n = (t - t_a)/\Delta t$ is the number of elapsed time steps until t_a . The overall simulation time demanded 500 steps. In Fig. 43(a), (b), (c) and (d), T_n is plotted according to Eqs. (2.23) and (2.25).

Obviously, for f_1 the approximation T_n results in the referential function itself, since $f_1 = 1$ is the test function. In the other cases, f_2 , f_3 , f_4 and f_5 , the approximation provides the same result of the actual T_n function when $t \rightarrow \infty$. This can be clearly noticed in Fig. 44(a), (b), (c) and (d), where the relative errors for each analyzed function are shown in the considered interval.

Figure 42 – Ratio R_{f_r} , $r = 2, \dots, 5$ in comparison with R_1 according to Eq. (2.24).



Both, Fig. 42 and 43, show good results for the proposed approximations with respect to the original ones.

Figure 43 – Transfer function T_n in relation to the Eqs. (2.25) and (2.23).

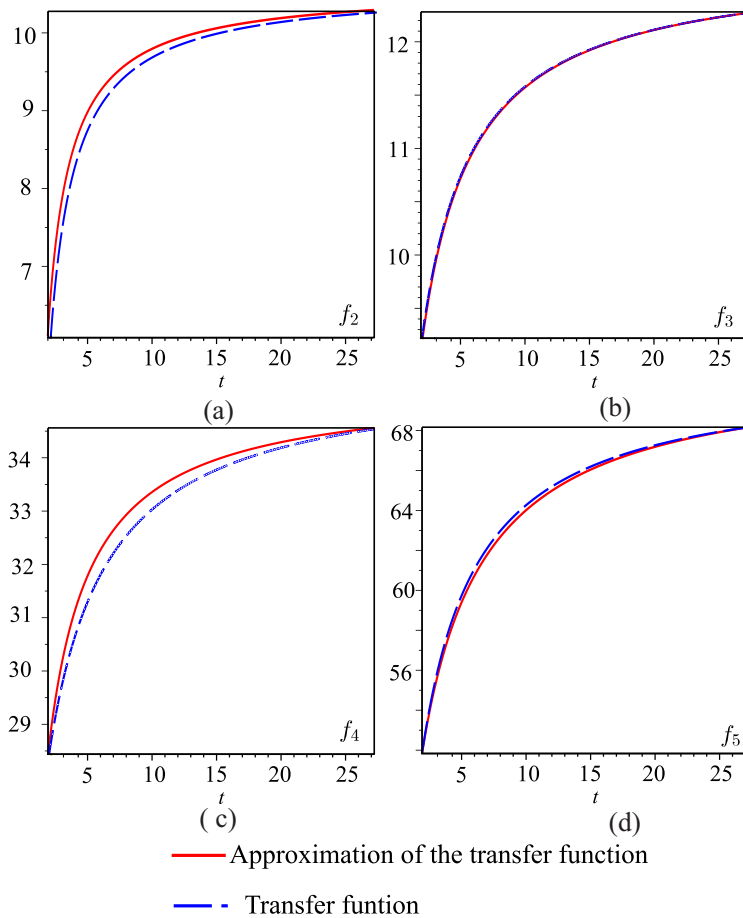
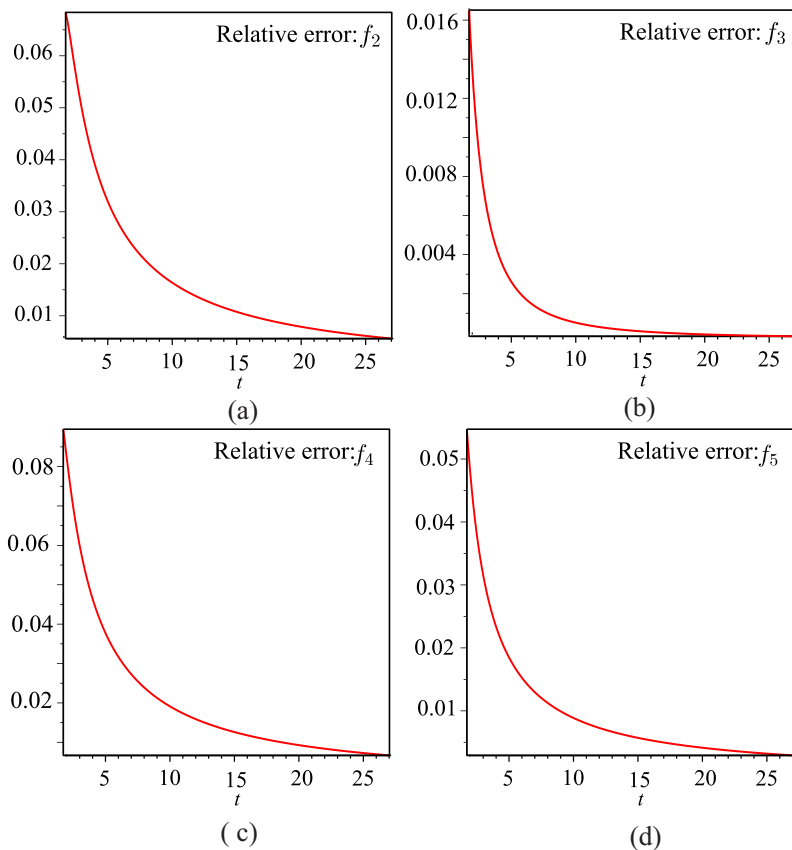


Figure 44 – Relative error in T_n given by Eq. (2.25) and the actual T_n given by Eq. (2.23).



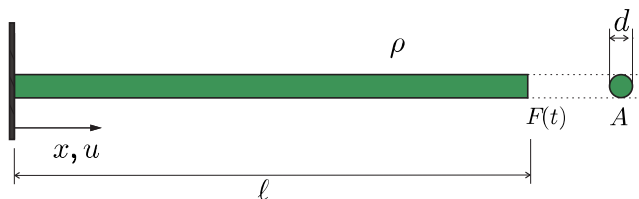
APPENDIX D – AN EXAMPLE FOR VALIDATION OF THE FRACTIONAL VISCOELASTIC IMPLEMENTATION

A polyacetal homogeneous rod (see Fig. 45), with density ρ and constant cross-section area A , is fixed at $x = 0$ and is subjected to an external force $F(t)$ at $x = \ell$, where ℓ is the length of the rod¹, as show in Fig. 46.

Figure 45 – Rods of polyoxymethylene (POM), also known as polyacetal.



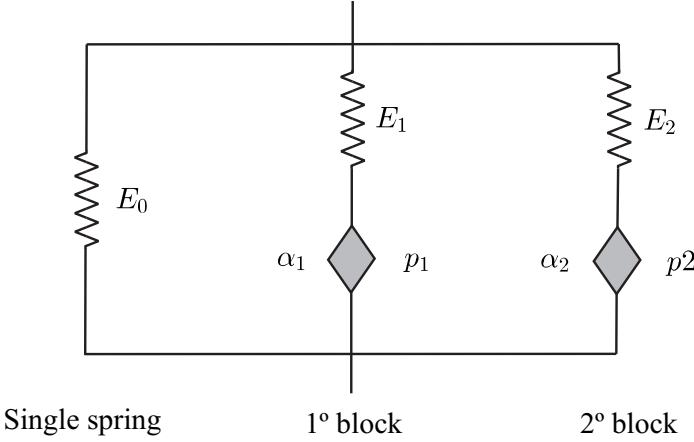
Figure 46 – Schematized polyacetal rod.



As polyacetal presents viscoelastic properties, its behavior can be described using fractional rheological models. According to Gaul and Schmidt (2007), a five parameters structure (see Fig. 47) is able to characterize such behavior.

¹ This problem is based on the study of Gaul and Schmidt (2007), and was used to validate the fractional derivatives for viscoelastic problems.

Figure 47 – Fractional viscoelastic model for polyacetal: two fractional Maxwell models and a spring in parallel.



Since the proposed rheological arrangement presents two Maxwell models and a spring in parallel, one can use Eqs. (3.3) and (3.13) to find a strain/stress relationship:

$$\varepsilon = \frac{\sigma}{E_0} \quad (\text{Single spring}), \quad (\text{D.1})$$

$$D_t^{\alpha_1} \varepsilon = \frac{\sigma}{p_1} + \frac{D_t^{\alpha_1} \sigma}{E_1} \quad (1^\circ \text{ block}), \quad (\text{D.2})$$

$$D_t^{\alpha_2} \varepsilon = \frac{\sigma}{p_2} + \frac{D_t^{\alpha_2} \sigma}{E_2} \quad (2^\circ \text{ block}). \quad (\text{D.3})$$

Applying the Laplace transform (see Appendix E) in the above equations, and using the relations

$$\mathcal{L}[\varepsilon_0] = \mathcal{L}[\varepsilon_1] = \mathcal{L}[\varepsilon_2] = \mathcal{L}[\varepsilon], \quad (\text{D.4})$$

and

$$\mathcal{L}[\sigma_0] + \mathcal{L}[\sigma_1] + \mathcal{L}[\sigma_2] = \mathcal{L}[\sigma], \quad (\text{D.5})$$

it comes out that

$$\mathcal{L}[\sigma] = E_0 \mathcal{L}[\varepsilon] + \frac{s \mathcal{L}[\varepsilon]}{(1/p_1 + s/E_1)} + \frac{s \mathcal{L}[\varepsilon]}{(1/p_2 + s/E_2)}. \quad (\text{D.6})$$

After some algebraic manipulations in Eq. (D.6), one obtains

$$\begin{aligned} & \left[\frac{1}{p_1 p_2} + s \left(\frac{1}{E_2 p_1} + \frac{1}{E_1 p_2} \right) + s^\alpha \frac{1}{E_1 E_2} \right] \mathcal{L}[\sigma] = \\ & \mathcal{L}[\varepsilon] \left\{ \left[\frac{1}{E_1 E_2} + s \left(\frac{1}{E_2 p_1} + \frac{1}{E_1 p_2} \right) + s^\alpha \frac{1}{E_1 E_2} \right] E_0 \right. \\ & \left. + s \left[\left(\frac{1}{p_1} + \frac{1}{p_2} \right) + s \left(\frac{1}{E_1} + \frac{1}{E_2} \right) \right] \right\}. \quad (\text{D.7}) \end{aligned}$$

Applying the inverse Laplace transform in the above equation, one has the sought relationship:

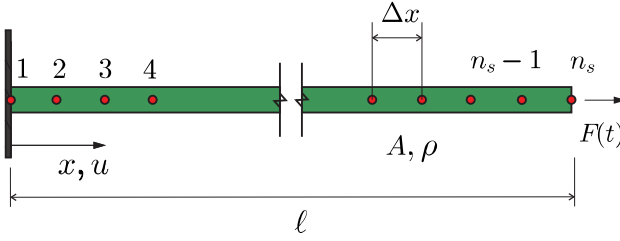
$$\begin{aligned} & \sigma + \frac{p_1}{E_1} D_t^{\alpha_1} \sigma + \frac{p_2}{E_2} D_t^{\alpha_2} \sigma + \frac{p_1 p_2}{E_1 E_2} D_t^{\alpha_1 + \alpha_2} \sigma \\ & = E_0 \varepsilon + p_1 \frac{E_0 + E_1}{E_1} D_t^{\alpha_1} \varepsilon + p_2 \frac{E_0 + E_2}{E_2} D_t^{\alpha_2} \varepsilon + \\ & + p_1 p_2 \frac{E_0 + E_1 + E_2}{E_1 E_2} D_t^{\alpha_1 + \alpha_2} \varepsilon. \quad (\text{D.8}) \end{aligned}$$

In order to solve this fractional differential equation, pertinent fractional-order initial conditions have to be defined. Following Schmidt and Gaul (2006), all initial conditions are assumed to be zero, referring to a material that is completely relaxed at $t = 0$. The approach proposed to describe the displacement u and the strain ε in the rod is detailed in the next section.

D.1 FINITE DIFFERENCE SCHEME

Consider the mentioned polyacetal rod discretized by n_s spatial nodes with a regular spacing $\Delta x = \ell / (n_s - 1)$ (see Fig.

Figure 48 – Discretized viscoelastic rod.



48). From the bars theory (RAO, 2007), the equation that describes the motion due to the external force $F(t)$ in this case, is given by

$$\rho D_t^2 u(x, t) = D_x^1 \sigma(x, t), \quad (\text{D.9})$$

where $u(x, t)$ is the displacement depending on the space x and the time t that must be calculated for each node. The stress σ has to be evaluated from the viscoelastic constitutive equation (D.8). Replacing G1 approximation, shown in Eq. (2.17), in (D.8) yields

$$\begin{aligned} \sigma + \frac{p_1}{E_1} \Delta t^{-\alpha_1} \sum_{k=0}^{N-1} A_{k+1}^{\alpha_1} \sigma_k + \frac{p_2}{E_2} \Delta t^{-\alpha_2} \sum_{k=0}^{N-1} A_{k+1}^{\alpha_2} \sigma_k + \\ + \frac{p_1 p_2}{E_1 E_2} \Delta t^{-(\alpha_1 + \alpha_2)} \sum_{k=0}^{N-1} A_{k+1}^{\alpha_1 + \alpha_2} \sigma_k = E_0 \varepsilon + \\ + \frac{p_1}{E_1} (E_0 + E_1) \Delta t^{-\alpha_1} \sum_{k=0}^{N-1} A_{k+1}^{\alpha_1} \varepsilon_k + \\ + \frac{p_2}{E_2} (E_0 + E_2) \Delta t^{-\alpha_2} \sum_{k=0}^{N-1} A_{k+1}^{\alpha_2} \varepsilon_k + \\ \frac{p_1 p_2}{E_1 E_2} (E_0 + E_1 + E_2) \Delta t^{-(\alpha_1 + \alpha_2)} \sum_{k=0}^{N-1} A_{k+1}^{\alpha_1 + \alpha_2} \varepsilon_k, \quad (\text{D.10}) \end{aligned}$$

where the coefficients A_{k+1}^α are defined in Eq. (2.10), $\varepsilon_k = \varepsilon(t_a - k\Delta t)$ and $\sigma_k = \sigma(t_a - k\Delta t)$ with t_a the actual time in the analysis. Using gamma function definition in the GL coefficients and opening the summations in Eq. (D.10) for the first term, yields

$$\begin{aligned} \sigma(t)[1 + a_1 + a_2 + a_3] &= \varepsilon(t)[E_0 + b_1 + b_2 + b_3] - \\ &- a_1 S_{1\sigma} - a_2 S_{2\sigma} - a_3 S_{3\sigma} + b_1 S_{1\varepsilon} + b_2 S_{2\varepsilon} + b_3 S_{3\varepsilon}, \end{aligned} \quad (\text{D.11})$$

being,

$$a_1 = \frac{p_1}{E_1} \Delta t^{-\alpha_1}, \quad a_2 = \frac{p_2}{E_2} \Delta t^{-\alpha_2}. \quad (\text{D.12 - D.13})$$

$$a_3 = \frac{p_1 p_2}{E_1 E_2} \Delta t^{-\alpha_3}, \quad b_1 = a_1 (E_0 + E_1). \quad (\text{D.14 - D.15})$$

$$b_2 = a_2 (E_0 + E_1), \quad b_3 = a_3 (E_0 + E_1 + E_2). \quad (\text{D.16 - D.17})$$

$$S_{m\sigma} = \sum_{k=1}^{N-1} A_{k+1} \sigma_k, \quad S_{m\varepsilon} = \sum_{k=1}^{N-1} A_{k+1} \varepsilon_k. \quad (\text{D.18 - D.19})$$

with $m = 1, 2, 3$, and

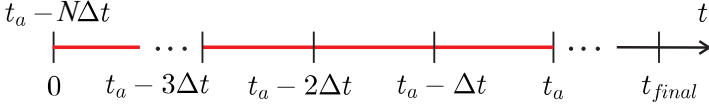
$$\alpha_3 = \alpha_1 + \alpha_2. \quad (\text{D.20})$$

An equation analogue to Eq. (D.8) is found, but this time using the fractional derivatives definition G1. It is import to emphasize that the values $S_{m\varepsilon}$, with $m = 1, 2, 3$, have to be calculated and stored for all nodes, since they are needed in the sums for the next integration step, i.e.

$$\begin{aligned} S_{m\varepsilon} &= \sum_{k=1}^{N-1} A_{k+1} \varepsilon_k \\ &= A_2 \varepsilon_1 + A_3 \varepsilon_2 + \dots + A_n \varepsilon_{n-1} \\ &= A_2 \varepsilon(t_a - \Delta t) + A_3 \varepsilon(t_a - 2\Delta t) + \dots + \\ &+ A_{Nt} \varepsilon[t_a - (N-1)\Delta t]. \end{aligned}$$

For $S_{m\sigma}$, the meaning can be interpreted in a similar way. Figure 49 illustrates this situation.

Figure 49 – Evaluation of the $S_{m\varepsilon}$ and $S_{m\sigma}$. The actual time calculation uses the overall variable history.



Solving for $\sigma(t)$ in Eq. (D.11) one obtains,

$$\sigma(t) = c_1\varepsilon(t) - \sum_{i=1}^3 \left[\frac{a_i}{c_2} S_{i\sigma} - \frac{b_i}{c_2} S_{i\varepsilon} \right], \quad (\text{D.21})$$

where

$$c_1 = \frac{E_0 + b_1 + b_2 + b_3}{c_2}, \quad (\text{D.22})$$

$$c_2 = 1 + a_1 + a_2 + a_3, \quad (\text{D.23})$$

and the strain $\varepsilon(t)$ is given by the displacement derivative in relation to the space x :

$$\varepsilon = D_x^1 \mathbf{u}. \quad (\text{D.24})$$

Equation (D.24) can be rewritten by central finite differences for each node $2 \leq i \leq n_s$. $\varepsilon(t) = 0$ for the first node, since the latter stays on the collet and does not suffer strain. In order to keep second-order accuracy, a “ghost” point n_{s+1} is needed to evaluate the strain and its derivative at node n_s :

$$\varepsilon_{n_s}^j = \frac{u_{n_{s+1}} - u_{n_{s-1}}}{2\Delta t}.$$

Since there cannot be any change in strain with respect to the spatial coordinate x at the free end of the rod, we obtain

$$\varepsilon_{n_{s+1}} = \frac{u_{n_{s+1}} - u_{n_s}}{\Delta t} = \frac{u_{n_s} - u_{n_{s-1}}}{\Delta t} = \varepsilon_{n_{s-1}}, \quad (\text{D.25})$$

or, simply

$$u_{n_s+1} = 2u_{n_s} - u_{n_s-1}. \quad (\text{D.26})$$

Using Eq. (D.24) and replacing Eq. (D.21) into (D.9), it comes out that

$$\begin{aligned} \rho D_t^2 u(x, t) &= D_x^1 \left[c_1 \varepsilon - \sum_{i=1}^3 \left(\frac{a_i}{c_2} S_{i\sigma} - \frac{b_i}{c_2} S_{i\varepsilon} \right) \right] \\ &= D_x^1 \left[c_1 D_x^1 u - \sum_{i=1}^3 \left(\frac{a_i}{c_2} S_{i\sigma} - \frac{b_i}{c_2} S_{i\varepsilon} \right) \right] \\ &= c_1 D_x^2 u - \sum_{i=1}^3 \left(\frac{a_i}{c_2} D_x^1 S_{i\sigma} - \frac{b_i}{c_2} D_x^1 S_{i\varepsilon} \right). \end{aligned} \quad (\text{D.27})$$

Replacing the second derivatives with respect to time and space by a central-difference quotient in Eq. (D.27), it results in

$$\begin{aligned} \rho \frac{(u_i^{j+1} - 2u_i^j + u_i^{j-1}))}{\Delta t^2} &= c_1 \frac{(u_{i+1}^j - 2u_i^j + u_{i-1}^j)}{\Delta x^2} - \\ &\quad - \sum_{i=1}^3 \left[\frac{a_i}{c_2} D_x^1 S_{i\sigma} - \frac{b_i}{c_2} D_x^1 S_{i\varepsilon} \right]. \end{aligned} \quad (\text{D.28})$$

In Eq. (D.28) the upper index at the displacements u_i^j denotes the time increment (time discretization) and the lower index denotes the node number (spatial discretization). Rearrangement of the terms finally leads to

$$\begin{aligned} u_i^{j+1} &= \frac{\Delta t^2}{\rho} \left\{ 2 \left(\frac{\rho}{\Delta t^2} - \frac{c_1}{\Delta x^2} \right) u_i^j + \frac{c_1}{\Delta x^2} u_{i+1}^j - \frac{c_1}{\Delta x^2} u_{i-1}^j - \right. \\ &\quad \left. - \frac{\rho}{\Delta t^2} u_i^{j-1} - \sum_{i=1}^3 \left[\frac{a_i}{c_2} D_x^1 S_{i\sigma} - \frac{b_i}{c_2} D_x^1 S_{i\varepsilon} \right] \right\}, \end{aligned} \quad (\text{D.29})$$

for each node $2 \leq i \leq n_s - 1$.

The boundary conditions provide the two missing equations for the nodes $i = 1$ and $i = n_s$. At the Dirichlet boundary, the displacement

$$u_1^{j+1} = 0, \quad (\text{D.30})$$

is prescribed, whereas at the Neumann boundary the condition

$$\sigma_n S^j = \frac{F^j}{A}. \quad (\text{D.31})$$

is given. If one inserts Eq. (D.21) into Eq. (D.31) and uses a second-order accurate central difference, it comes out that

$$\begin{aligned} \frac{F^j}{A} &= c_1 \varepsilon(t) - \sum_{i=1}^3 \left[\frac{a_i}{c_2} S_{i\sigma} - \frac{b_i}{c_2} S_{i\varepsilon} \right] \\ &= \frac{c_1}{2\Delta x} (u_{n_s+1}^j - u_{n_s-1}^j) - \sum_{i=1}^3 \left[\frac{a_i}{c_2} S_{i\sigma} - \frac{b_i}{c_2} S_{i\varepsilon} \right]. \end{aligned} \quad (\text{D.32})$$

In order to eliminate the ghost point displacement $u_{n_s+1}^j$, Eq. (D.29) is used for node n_s , finally yielding

$$\begin{aligned} u_{n_s}^{j+1} &= \frac{\Delta t^2}{\rho} \left\{ 2 \left(\frac{\rho}{\Delta t^2} - \frac{c_1}{\Delta x^2} \right) u_n S^j + \frac{c_1}{\Delta x^2} u_{n_s+1}^j - \right. \\ &\quad \left. - \frac{c_1}{\Delta x^2} u_{n_s-1}^j - \frac{\rho}{\Delta t^2} u_n S^{j-1} - \right. \\ &\quad \left. - \sum_{i=1}^3 \left[\frac{a_i}{c_2} D_x^1 S_{n_s\sigma} - \frac{b_i}{c_2} D_x^1 S_{n_s\varepsilon} \right] \right\}, \end{aligned} \quad (\text{D.33})$$

or

$$\begin{aligned}
 u_{ns}^{j+1} = & \frac{\Delta t^2}{\rho} \left\{ \frac{2F^j}{A\Delta x} + 2 \left(\frac{\rho}{\Delta t^2} - \frac{c_1}{\Delta x^2} \right) u_{ns}^j + \frac{2c_1}{\Delta x^2} u_{ns-1}^j - \right. \\
 & - \frac{\rho}{\Delta t^2} u_{ns}^{j-1} - \frac{2}{\Delta x} \sum_{i=1}^3 \left[\frac{a_i}{c_2} S_{i\sigma} - \frac{b_i}{c_2} S_{i\varepsilon} \right] - \\
 & \left. - \sum_{i=1}^3 \left[\frac{a_i}{c_2} D^1 S_{i\sigma} - \frac{b_i}{c_2} D^1 S_{i\varepsilon} \right] \right\}.
 \end{aligned}
 \tag{D.34}$$

Equations (D.29), (D.30) and (D.34) provide a system of ns equations for u_i^{j+1} to perform the next integration step. Subsequently, the spatial derivatives of the actual stresses have to be calculated and stored for all nodes since they are needed in the sums $D_x^1 S_{i\sigma}$ in the next integration step. Similarly, the stress itself is needed for the node ns . These calculations are performed using the constitutive equation (D.21) and its first derivative with respect to time. Note that due to the fractional derivatives of strains and stresses in the constitutive equation, not only the displacement history has to be stored but also the strain, stress and their spatial derivatives.

The parameters identification in Eq.(D.8) for polyacetal is done by Gaul and Schmidt (2007). Such identification is described in Tab. 8 and is employed in the next subsection to solve the rod problem.

Table 8 – Identified fractional parameters to model the polyacetal rod.

$E_0 \left[\frac{N}{m^2} \right]$	$E_1 \left[\frac{N}{m^2} \right]$	$E_2 \left[\frac{N}{m^2} \right]$	$p_1 \left[\frac{Ns^\alpha}{m^2} \right]$	$p_2 \left[\frac{Ns^\alpha}{m^2} \right]$	α_1	α_2
0.0	1430.1×10^6	3681.3×10^6	214.6×10^6	20011.8×10^6	0.0794	0.0202

Font: (GAUL; SCHMIDT, 2007).

D.2 DISCUSSION AND RESULTS

The load in the free end for the considered rod is

$$F(t) = \begin{cases} 0 & \text{if } t = 0 \\ 100N & \text{if } t > 0 \end{cases}. \quad (\text{D.35})$$

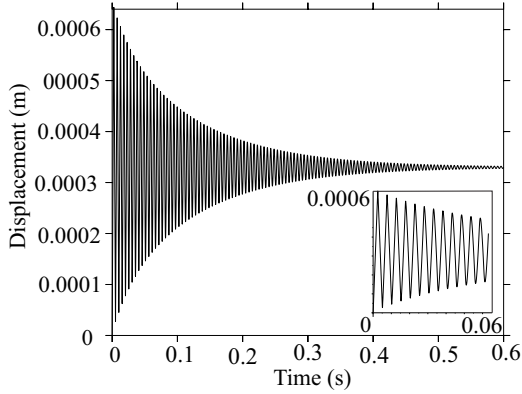
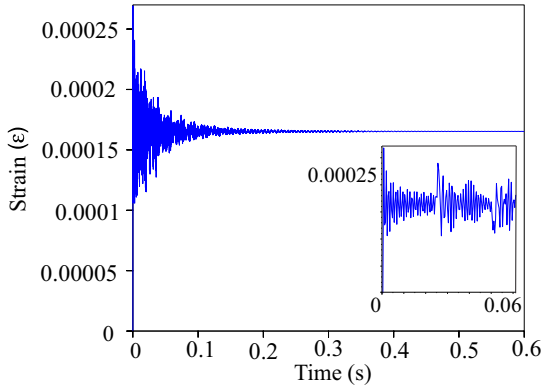
To find the displacement the finite difference scheme presented in the previous section is employed. The rod with $\ell = 2$ is discretized in $n_s = 30$ spatial nodes. The constitutive behavior is described by the parameters in Tab. 8.

Since the time integration is performed by the explicit central-difference method, there is a critical time-step size Δt_{cr} that must not be exceeded. Following Gaul and Schmidt (2007) suggestion, the critical time step size was found to be $4.0 \times 10^{-5} \leq \Delta t_{cr} \leq 5.0 \times 10^{-5}$ s.

In order to obtain a stable scheme along with limited numerical costs, the time step size was chosen to be $\Delta t = 4.0 \times 10^{-5}$. The overall simulation time was 6s resulting in 15000 time steps. The area of the cross sections is $A = \pi(0.00075)^2 \text{ m}^2$. Moreover, the nodal distance is $\Delta x = 0.06897$ and the polyacetal density is $\rho = 1420 \text{ kg/m}^3$.

Since the identified material model accounts for the time-dependent creep behavior and the decaying behavior of an oscillation, the resulting motion of the rod is expected to be a free oscillation that dies away superimposed to a creep process of its neutral position (SCHMIDT; GAUL, 2006). In Fig. 50 this behavior is verified in the interval $[0s, 0.6s]$ to the reference algorithm G1. The strain and stress behavior are shown in Figs. 51 and 52, respectively.

The displacement in other nodes can be seen in the work of Costa Haveroth (2015). If the loading of Eq. (D.35) is re-

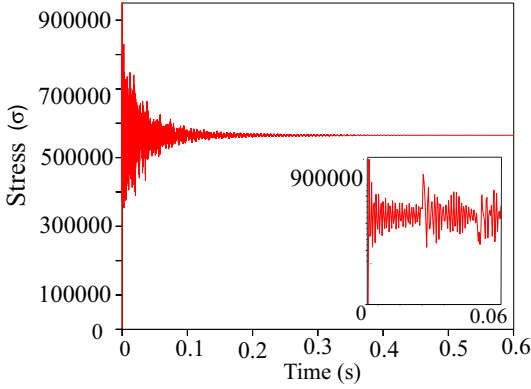
Figure 50 – Displacement in the node $i = 30$ for the polyacetal rod.Figure 51 – Strain in the node $i = 30$ for the polyacetal rod.

placed by

$$F(t) = \begin{cases} 100 & \text{if } t = 0 \\ 0 & t > 0 \end{cases}, \quad (\text{D.36})$$

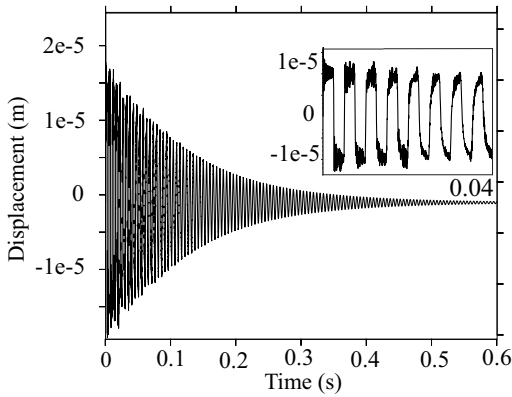
then the resulting displacements change their behavior, as shown in Fig. 53. Such behavior is in agreement with Cook, Malkus

Figure 52 – Stress in the node $i = 30$ for the polyacetal rod.



and Plesha (1989) statements.

Figure 53 – Displacement in the node $i = 30$ for an instantaneous initial load.



APPENDIX E – LAPLACE TRANSFORM OF THE FRACTIONAL DERIVATIVE

The Laplace transform is defined by

$$\mathcal{L}[D^\alpha f(t)] = \int_0^\infty e^{-st} D^n f(t) dt, \quad (\text{E.1})$$

with $\alpha \in \mathbb{R}$ (OLDHAM; SPANIER, 1974). It is possible generalize the well known relation between natural order derivatives and the Laplace transform for any alpha value:

$$\mathcal{L}[D^\alpha f(t)] = s^\alpha \mathcal{L}[f] = \sum_{k=0}^{n-1} s^k D^{\alpha-1-k}(0), \quad \alpha \in \mathbb{R}, \quad (\text{E.2})$$

when n is an integer and $n - 1 < \alpha \leq n$. The summation in Eq. E.2 is empty and vanishes when $q \leq 0$. According to Ortigueira (2011), in a simplified form, the Laplace transform can be given by

$$\mathcal{L}[D^\alpha f(t)] = s^\alpha \mathcal{L}[f(t)], \quad \alpha \in \mathbb{R}. \quad (\text{E.3})$$

For more details regarding this subject see Oldham and Spanier (1974) or Ortigueira (2011).

Among the wide range of structural polymers currently available in the market, this work is concerned particularly with high density polyethylene. The typical nonlinear viscoelastic behavior presented by this material is not trivial to model, and has already been investigated by many authors in the past. Aiming at a further contribution, this work proposes modeling this material behavior using an approach based on fractional derivatives. This formulation produces fractional constitutive equations that result in good curve-fitting properties with less parameters to be identified when compared to traditional methods. In this regard, experimental creep results of high density polyethylene evaluated at different stress levels are fitted by this scheme.

Advisor: Pablo Andrés Muñoz-Rojas

Co-advisor: Fernando Deeke Sasse

Joinville, 2015